STTR: Utilize Cementitious High Carbon Fly Ash (CHCFA) to Stabilize Cold In-Place Recycled (CIR) Asphalt Pavement as Base Course

Phase II Report to the U.S. Department of Energy

Award Number: DE-FG02-05EG86238

Submitted by

Haifang Wen, PhD, PE, Assistant Professor
Xiaojun Li, Research Assistant
Washington State University
Pullman, WA

Tuncer Edil, PhD, PE, D.GE Professor
Jonathan O'Donnell, Research Assistant
University of Wisconsin
Madison, WI

and

Swapna Danda
Bloom Companies,
LLC
Milwaukee, WI

February 5, 2011

SUMMARY

The purpose of this study was to evaluate the performance of cementitious high carbon fly ash (CHCFA) stabilized recycled asphalt pavement as a base course material in a real world setting. Three test road cells were built at MnROAD facility in Minnesota. These cells have the same asphalt surface layers, subbases, and subgrades, but three different base courses: conventional crushed aggregates, untreated recycled pavement materials (RPM), and CHCFA stabilized RPM materials. During and after the construction of the three cells, laboratory and field tests were carried out to characterize the material properties. The test results were used in the mechanistic-empirical pavement design guide (MEPDG) to predict the pavement performance. Based on the performance prediction, the life cycle analyses of cost, energy consumption, and greenhouse gasses were performed. The leaching impacts of these three types of base materials were compared.

The laboratory and field tests showed that fly ash stabilized RPM had higher modulus than crushed aggregate and RPM did. Based on the MEPDG performance prediction, the service life of the Cell 79 containing fly ash stabilized RPM, is 23.5 years, which is about twice the service life (11 years) of the Cell 77 with RPM base, and about three times the service life (7.5 years) of the Cell 78 with crushed aggregate base. The life cycle analysis indicated that the usage of the fly ash stabilized RPM as the base of the flexible pavement can significantly reduce the life cycle cost, the energy consumption, the greenhouse gases emission.

Concentrations of many trace elements, particularly those with relatively low water quality standards, diminish over time as water flows through the pavement profile. For many elements, concentrations below US water drinking water quality standards are attained at the bottom of the pavement profile within 2-4 pore volumes of flow.

TABLE OF CONTENTS

TABLE OF TABLES

TABLE OF FIGURES

CHAPTER 1: INTRODUCTION

1.1 Background

Due to the increasingly stringent environmental policy stipulated by the Environmental Protection Agency (EPA) and/or local authority, the power generation industry must take measures to reduce the emission of nitrogen oxides (NOx), sulfur oxides (SOx), and Mercury (Hg). Low-NOx burners reduced emissions by changing the combustion characteristics of coal boilers, but increased the amount of residual unburned carbon in ash. Additionally, activated carbon is injected to reduce mercury emission, which also increases the carbon level in fly ash. In 2002, approximately 76.5 million tons of fly ash was produced in the U.S. and about 49.8 million tons of that was placed in landfills (ACAA, 2003), resulting in significant land purchase and energy costs, and potential environmental issues. Increased carbon levels in fly ash make air-entrained concrete production more difficult (Ramme and Tharaniyil 2000). These issues transform ash from a revenue generating commodity to the third-greatest operating cost (behind fuel and labor) at coal-based power plants. It would also take commercial products away from ash marketers, concrete producers, cement manufacturers, construction contractors, plastics manufacturers and others who depend on using coal combustion products. Consumption of fly ash, especially off-spec fly ash (e.g. high carbon fly ash), will greatly relieve the pressure on the power industry by beneficially utilizing the fly ash. Even though some measures exist to beneficiate high carbon fly ash, such as carbon/ash separation and reburning ash as a fuel for coal boilers, there are disadvantages to these technologies. The carbon/ash separation process consumes energy and ash reburning needs a burner capable of producing marketable fly ash. Therefore, direct utilization of high carbon fly ash without treatment is still the best possible scenario to consume high carbon fly ash.

Simultaneously, most of highways in the United States were built in 1950s and 1960's and have deteriorated significantly to date. More than 96 percent of the current highways consist of asphalt pavements. Quarrying virgin aggregates for highway construction also results in environmental problems and energy consumption. An alternative to quarrying virgin materials is in-place recycling of asphalt pavement. This recycling process is relatively inexpensive and contributes towards sustainable pavement rehabilitation. Existing hot mix asphalt (HMA) layer is pulverized and blended with some of or the entire base course to form a broadly graded material referred to as recycled pavement material (RPM) (Li et al. 2008). There is an increasing trend towards recycling existing asphalt pavement and using as base course for the new pavement (FHWA 1995). However, there are concerns on the load-carrying capacity and deformability of a base layer made of RPM.

In general, within-spec fly ash is referred to as Class C and Class F fly ash. Combustion of bituminous or anthracite coal produces Class F (low calcium) fly ash and combustion of lignite or sub-bituminous coal produces Class C (high calcium) fly ash. Class F fly ash is pozzolanic while Classs C fly ash is both self-cementitious and pozzolanic. According to ASTM C-618, the top limit of loss on ignition (LOI) for both Class C and F fly ash, mostly due to carbon, is 6%. The majority of within-spec fly ash is used as a mineral admixture in concrete to improve the durability of concrete. As stated above, the measures taken to reduce emission of NOx and mercury from power plant make it difficult to produce within-spec fly ash. Cementitious high carbon fly ash (CHCFA) has self-hardening properties in the presence of moisture, similar to the property of Class C fly ash. However, the high carbon content in CHCFA eliminates CHCFA from being used in concrete, because the carbon in fly ash absorbs the air-entraining admixture in concrete, affecting the durability of concrete. Unlike concrete which

needs air void (generally 6%), air void is not desired in a base course of an asphalt pavement. A base course with maximum density and minimal air void lasts longer than a loose base course. Therefore, the high carbon content in CHCFA presumably does not affect the performance of a base course. At the same time, the cementitious property of CHCFA will produce a strong base course to support the loads, compared to untreated base course. Stabilization of RPM with CHCFA could create a strong base course, which improves the long term performance of asphalt pavement and beneficially utilizes the high carbon fly ash, which would otherwise be landfilled.

1.2 Objectives

In order to comparatively evaluate the performance of CHCFA stabilized RPM base course material in a real world setting, three test cells were built, with the same asphalt surface layers, subbases, and subgrades, but three different base courses: conventional crushed aggregates, untreated RPM, and CHCFA stabilized RPM materials. The three test cells were subjected to a high volume of loads, which can discriminate the performance of the three pavements within the period of this study. The results demonstrated the effectiveness of incorporating CHCFA stabilized RPM in real highway construction. The pavement design parameters, pavement life, and cost effectiveness of such a base course were obtained in realistic field setting, including actual traffic loads and environmental conditions. Along with the demonstrated performance of such a base course as evidenced by the real construction, the economic and environmental analysis of such a technology was analyzed to provide a basis to promote this technology.

CHAPTER 2: CONSTRUCTION

Laboratory testing has limitations to evaluate performance of a material, largely because the laboratory scale of specimen and testing conditions do not simulate those of pavement in the field. Therefore, full-scale field evaluation can realistically evaluate the performance of a material. In this study, three test cells of flexible pavements with different base materials were constructed at MnROAD test facility to evaluate the effectiveness of RPM with and without fly ash addition and to compare it with traditional crushed aggregate base course. The crushed aggregate is a Class 6 granite aggregate widely used by the Minnesota Department of Transportation (MnDOT) (Clyne and Palek 2008). The MnROAD test facility is a two-lane pavement test track located 64.4 km (40 miles) northwest of Minneapolis. The construction started on August 30th, 2007. A 150 mm (5 in.) thick layer of clay subgrade material was placed in Cells 77, 78 and 79 and compacted over existing subgrade soils after the pulverization and removal of the existing bituminous pavement and underlying granular base course material.

The RPM base course was placed in Cell 77. The field density results were compared to the maximum dry density obtained during laboratory testing. The test results showed that a compaction density of 95.1% to 98.0% of maximum dry density achieved by the Proctor tests in the laboratory was achieved on the untreated RPM base course material. The Class 6 aggregate base course was placed in Cell 78. The test results showed that a compaction level of 95.5% to 101.1% of maximum dry density was achieved. The fly ash stabilized RPM base course was placed in Cell 79. The contractor added 14% of fly ash within the RPM. The RPM was mixed with fly ash and water, before the compaction. Field density tests were performed on the stabilized base course material utilizing a Troxler 3440 Nuclear Gauge. The field density results

were compared to the maximum dry density obtained from laboratory testing. The test results showed that a compaction level of 94.5% to 95.1% of maximum dry density was achieved.

About two weeks after the completion of placement of subgrade and base course materials in Cell 79, placement of bituminous concrete wearing course was completed. The bituminous concrete wearing course was to be placed in 2 lifts of 50 mm (2 inches) each. When the placement of the wearing course was initiated in Cells 77 and 78, the base material appeared to be unstable under the weight of the paving machine and other construction traffic. Paving operations in these two cells was temporarily abandoned. The placement of wearing course in Cell 79 was accomplished in 2 lifts – each of 50 mm (2 inches) thickness. Field density tests were performed on both lifts of the compacted wearing course material utilizing a Troxler 3440 Nuclear Gauge. The test results showed that a compaction level of 93.2% to 100.9% of maximum dry density was achieved.

After further investigation by MnROAD personnel, it was discovered that the subgrade material in Cells 77 and 78 had become very wet possibly due to the excess precipitation following the placement of the base course materials. The subgrade material in Cell 79 was protected from excessive seepage of rain water probably due to the presence of the fly ash. Therefore, the base course material from Cells 77 and 78 was removed. The subgrade clay material was disked to dry it out and then compacted to the required density. Following the compaction of subgrade material, the RPM and Class 6 aggregate base courses were placed in Cell 77 and Cell 78, respectively. Two lifts of hot mix asphalt wearing course were placed and compacted. Field density tests were performed on both lifts of the wearing course material in Cells 77 and 78. The tests were performed based on the theoretical maximum density value obtained from the batch plant. The test results showed that a compaction level of 91.0% to 95.5%

of theoretical maximum density was achieved in Cell 77, a compaction of 91.0% to 101.7% was achieved in Cell 78. The Cell 79 was completed in September 2007 and Cells 77, 78 were completed in October 2007. Samples of the subgrade, subbase, base, and wearing course material were taken in the field and transported to laboratory for further testing. The final pavement structures of Cells 77, 78, and 79 are shown in Figure 2.1.

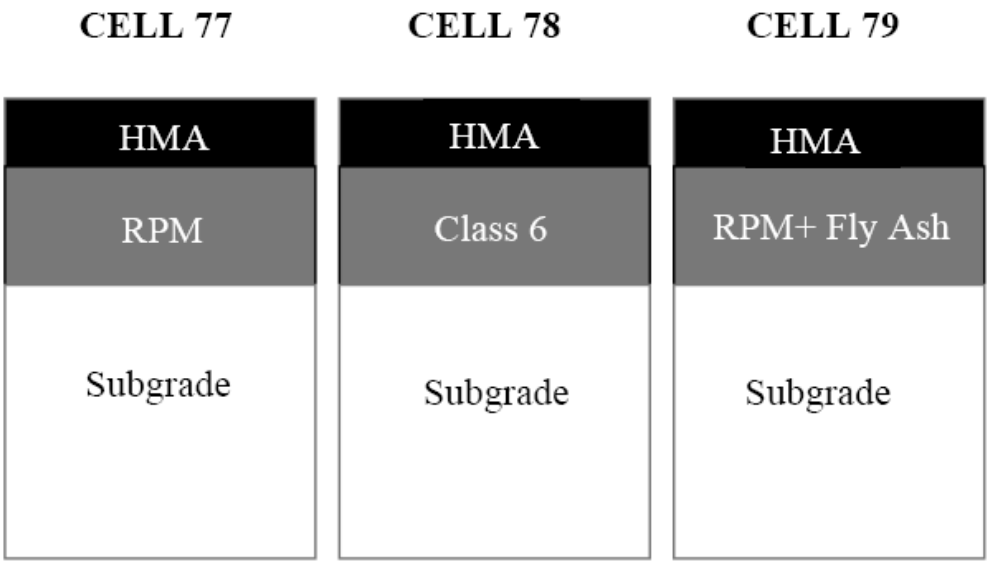

Figure 2.1: The Pavement Structure of Cells 77, 78, and 79.

CHAPTER 3: LABORATORY TEST RESULTS

The field performance of pavement and materials may need many years of service which may be longer than the duration of study. Therefore, the performance of pavements needs to be predicted by the MEPDG in which various laboratory testing results are needed. The laboratory test was carried out to determine the material properties of asphalt binder, hot mix asphalt, crushed aggregate and treated/untreated RPM base. The test samples were taken in the construction field.

3.1 Asphalt Concrete Material

3.1.1 Binder

The PG-grade analysis of the Elvaloy/PPA binder used in this research was carried out by Mathy Technology & Engineering Services, Inc (MTE). The binder meets PG 64-34 requirements. The Dynamic Shear Reometer (DSR) test results of the binder after rolling thin film oven (RTFO) aging were shown in Table 3.1.

Table 3.1: DSR Test Results ob the Elvaloy/PPA Binder

Temp. ^{0}C	G*/SINδ (Pa)	Phase Angle (δ)	G* (Pa)
64	3900	69.0	3640.962
58	7700	66.2	7045.186
52	15000	63.7	13447.29

3.1.2 Hot Mixed Asphalt

The laboratory testing of the properties of the HMA was run at the University of Illinois at Urbana-Champaign (UIUC), including low temperature mechanical property characterization testing for two asphalt mixtures. The characterization was carried out at the Advanced

Transportation Research and Engineering Laboratory (ATREL), located in Rantoul, IL to determine the creep compliance, tensile strength, and dynamic modulus of asphaltic materials.

Two different sets of loose HMA mixtures, Cell 77 & 78 and Cell 79, were sampled at the MnROAD facility. Table 3.2 summarizes maximum theoretical density (G_{mm}) of received loose mixture from two different sources (i.e., MnROAD Cell #79 and Cell #77 & 78). G_{mm} testing was carried out in accordance with ASTM D2041-03. In order to achieve the target air void of actual testing specimens, an air void level of 7.5 % was targeted for gyratory compacted specimens.

Table 3.2: Maximum theoretical density of received materials

Mixture	Rep 1	Rep 2	Average
Cell # 79	2.497	2.486	2.491
Cell # 77 & 78	2.499	2.487	2.493

G_{mb} testing was conducted using an InstroTek Corelok^{TM} device (vacuum sealed plastic bag method) after specimen fabrication to the appropriate test dimensions following ASTM D2726. Table 3.3 summarizes the bulk density and air voids for each of the test specimens. Averages were within 0.7% of the target void level of 7.0%.

3.1.2.1 IDT Creep Test Results

Creep compliance and stiffness tests were performed at three low temperatures, namely: -36, -24, and -12 ^{o}C considering the cold climate presented at the MnROAD facility in St. Cloud, Minnesota. The results summarized in Table 3.4 are the trimmed average of 3 replicate specimens following the analysis method recommended in AASHTO T 322, except the Cell #79 material at -24 ^{o}C. One of the three replicate specimens of this material was damaged during the testing due to a power outage caused by inclement weather and could not be included in the data

analysis. Thus, data from the two remaining specimens were averaged without trimming the highest and lowest values.

Table 3.3: Volumetric information for test specimens

Material	Test	Batch ID	G_{mb}	Air voids (%)
Cell #79	Dynamic Modulus	79-2	2.337	6.2
		79-3	2.329	6.5
		79-4	2.337	6.2
		Average	**2.334**	**6.3**
	Creep & Strength	79-5T*	2.323	6.7
		79-5M*	2.318	6.9
		79-5B*	2.300	7.7
		Average	**2.314**	**7.1**
Cell #77 & 78	Dynamic Modulus	77-1	2.330	6.5
		77-2	2.327	6.7
		Average	**2.328**	**6.6**
	Creep & Strength	77-3T*	2.308	7.4
		77-3M*	2.324	6.8
		77-3B*	2.320	6.9
		Average	**2.317**	**7.0**

*: T, M, and B refer to Top, Middle, and Bottom portions of a gyratory specimen

Figure 3.1 graphically presents the creep compliance test results at three low temperatures and master curves at a reference temperature of -36 ^{o}C. It appeared that the material from Cell #77 and #78 is slightly more compliant than the material from Cell #79. However, the difference between these two mixtures is not considerably large. Therefore, it may be suspected that the thermal cracking performances of pavement sections of these two mixtures are not significantly different.

Table 3.4 Creep compliance and stiffness of tested materials

Temp. (^{o}C)	Time, t (sec)	Cell #79		Cell #77 & 78	
		D(t) (1/GPa)	S(t) (GPa)	D(t) (1/GPa)	S(t) (GPa)
-36	1	3.71E-02	26.98	4.29E-02	23.30
	2	3.72E-02	26.87	4.34E-02	23.05
	5	3.91E-02	25.56	4.47E-02	22.38
	10	4.01E-02	24.93	4.64E-02	21.56
	20	4.11E-02	24.33	4.76E-02	21.03
	50	4.27E-02	23.45	5.00E-02	20.01
	100	4.44E-02	22.54	5.23E-02	19.12
	200	4.58E-02	21.82	5.42E-02	18.44
	500	4.85E-02	20.60	5.76E-02	17.37
	1000	5.07E-02	19.73	5.92E-02	16.90
-24	1	5.12E-02	19.52	6.19E-02	16.15
	2	5.19E-02	19.28	6.37E-02	15.69
	5	5.20E-02	19.21	6.68E-02	14.98
	10	5.68E-02	17.60	7.15E-02	13.99
	20	6.12E-02	16.35	7.78E-02	12.86
	50	6.87E-02	14.55	8.77E-02	11.40
	100	7.58E-02	13.19	9.73E-02	10.27
	200	8.39E-02	11.91	1.09E-01	9.19
	500	9.68E-02	10.33	1.25E-01	7.98
	1000	1.08E-01	9.25	1.39E-01	7.18
-12	1	7.90E-02	12.66	9.25E-02	10.81
	2	8.74E-02	11.44	1.01E-01	9.87
	5	1.01E-01	9.91	1.17E-01	8.55
	10	1.18E-01	8.46	1.34E-01	7.45
	20	1.36E-01	7.33	1.56E-01	6.42
	50	1.70E-01	5.87	1.95E-01	5.12
	100	2.08E-01	4.80	2.36E-01	4.23
	200	2.55E-01	3.92	2.90E-01	3.45
	500	3.42E-01	2.92	3.79E-01	2.64
	1000	4.37E-01	2.29	4.85E-01	2.06

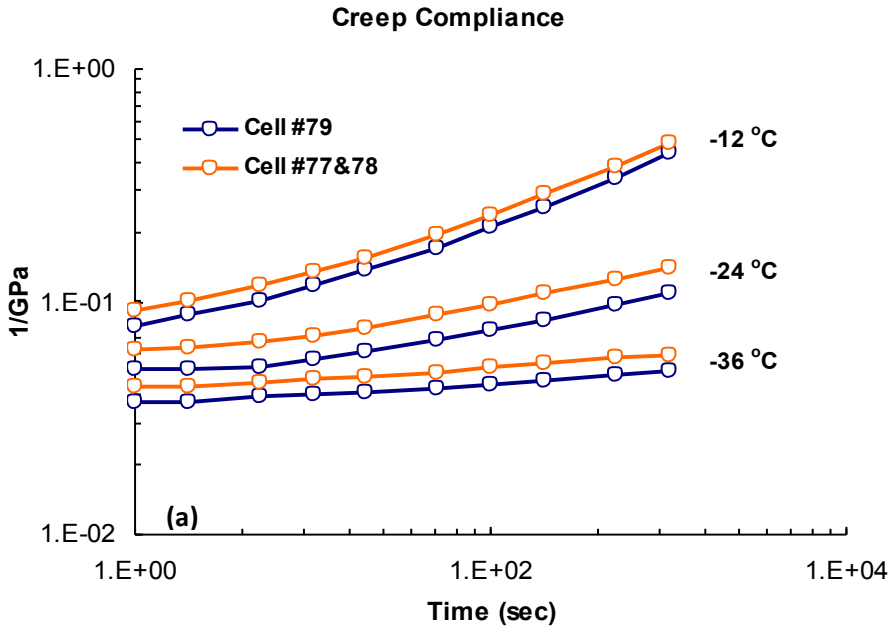

(a)

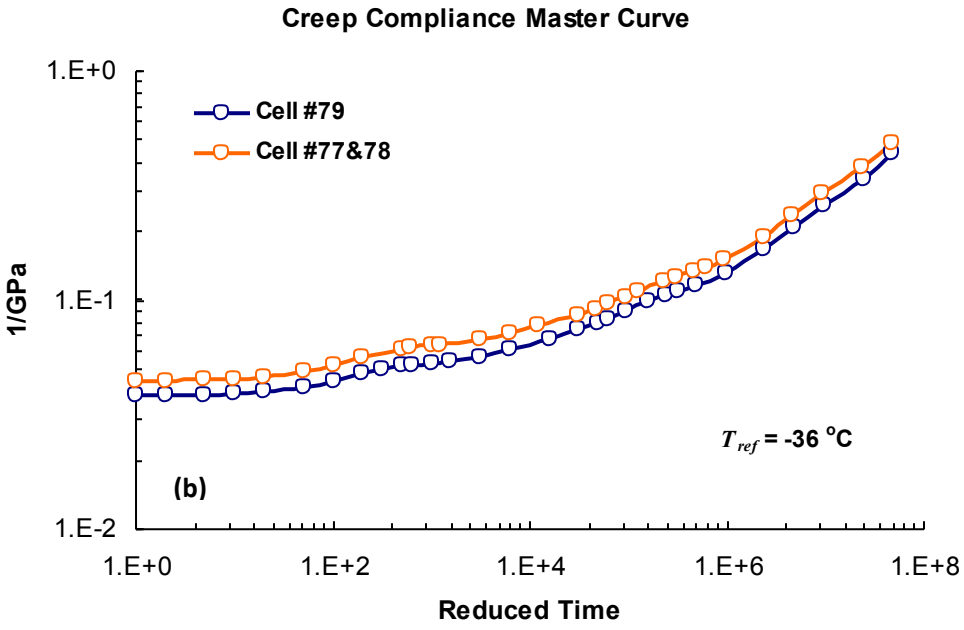

(b)

Figure 3.1: Creep compliance test result: (a) Creep compliance at three low temperatures and (b) Creep compliance master curves.

3.1.2.2 IDT Strength Test Results

The indirect tension (IDT) strength test was performed at -24 °C. Table 3.5 and Figure 3.2 present the IDT strength test results of two materials. Only two replicate specimens of the material from Cell #79 were tested since one replicate specimen was damaged during the creep compliance testing at -24 °C as mentioned in the previous section. The strength test data were analyzed and the instances of the first failure were determined following the data analysis procedure recommended in the AASHTO T 322.

Table 3.5: IDT tensile strength of tested materials

Strength	Cell #79				Cell #77 and 78				
	Rep #1	Rep #2	Mean	COV (%)	Rep #1	Rep #2	Rep #3	Mean	COV (%)
First failure	4.27 (619.5)	3.05 (442.1)	3.66 (530.8)	24	3.07 (445.0)	4.10 (594.3)	3.74 (542.5)	3.64 (527.2)	14
Ultimate failure	4.27 (619.5)	4.27 (619.7)	4.27 (619.6)	0	3.55 (514.8)	4.41 (638.9)	4.35 (631.1)	4.10 (594.9)	12

Unit: MPa; numbers shown in ( ) are in **psi**

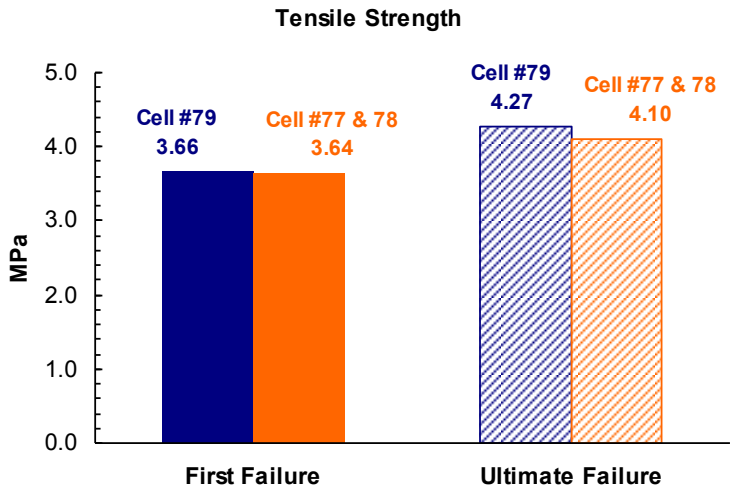

Figure 3.2: Tensile strength test result.

In Figure 3.2, it can be observed that the tensile strengths of the two materials are almost identical in terms of the first failure strength. The ultimate failure strength of the material from

Cell #79 was found to be modestly higher than that of the Cell #77 and #78 material. But again, the difference was not deemed to be significant.

3.1.2.3 Dynamic Modulus Test Results

Table 3.6 summarizes the dynamic modulus (|E*|) test results of the two materials. As mentioned in the previous section regarding materials received, due to the lack of loose mixture from Cell #77 & #78, only two replicate specimens were produced and tested for this material. Test results were analyzed according to the AASHTO TP62-03 and the averaged dynamic moduli of the two materials at three temperatures (i.e., -10, 4, and 21 ^{o}C) are graphically presented in Figure 3.3. Table 3.7 summarizes the phase angle (δ) measurements for the two materials. Finally, Figure 3.4 presents master curves of dynamic modulus (|E*|) and phase angle (δ) at a reference temperature of -10 ^{o}C.

Table 3.6: Dynamic modulus (|E*|) of tested materials (MPa)

Temp. (^{o}C)	*f* (Hz)	Cell #79					Cell #77 & 78			
		Rep #1	Rep #2	Rep #3	Mean	COV (%)	Rep #1	Rep #2	Mean	COV (%)
-10	25	15,330	14,413	13,615	14,453	6	17,286	15,973	16,629	6
	10	13,618	13,257	12,513	13,129	4	15,226	14,355	14,790	4
	5	12,423	12,324	11,384	12,043	5	13,928	13,202	13,565	4
	1	9,752	9,967	8,949	9,556	6	11,210	10,597	10,904	4
	0.5	8,690	9,024	7,948	8,554	6	10,055	9,512	9,784	4
	0.1	6,378	6,862	5,851	6,364	8	7,571	7,154	7,363	4
4	25	9,740	11,799	10,871	10,803	10	11,166	10,487	10,826	4
	10	8,114	10,367	9,305	9,262	12	9,760	8,762	9,261	8
	5	6,969	9,212	8,237	8,140	14	8,664	7,593	8,128	9
	1	4,752	6,725	5,936	5,804	17	6,291	5,274	5,783	12
	0.5	3,986	5,787	5,086	4,953	18	5,423	4,420	4,922	14
	0.1	2,644	3,914	3,456	3,338	19	3,766	2,901	3,333	18
21	25	3,550	3,889	3,204	3,548	10	4,359	3,344	3,852	19
	10	2,583	2,873	2,368	2,608	10	3,315	2,475	2,895	21
	5	2,051	2,290	1,897	2,079	10	2,697	1,980	2,339	22
	1	1,287	1,421	1,173	1,294	10	1,719	1,241	1,480	23
	0.5	1,053	1,163	1,000	1,072	8	1,420	1,011	1,216	24
	0.1	1,036	787	695	839	21	961	679	820	24

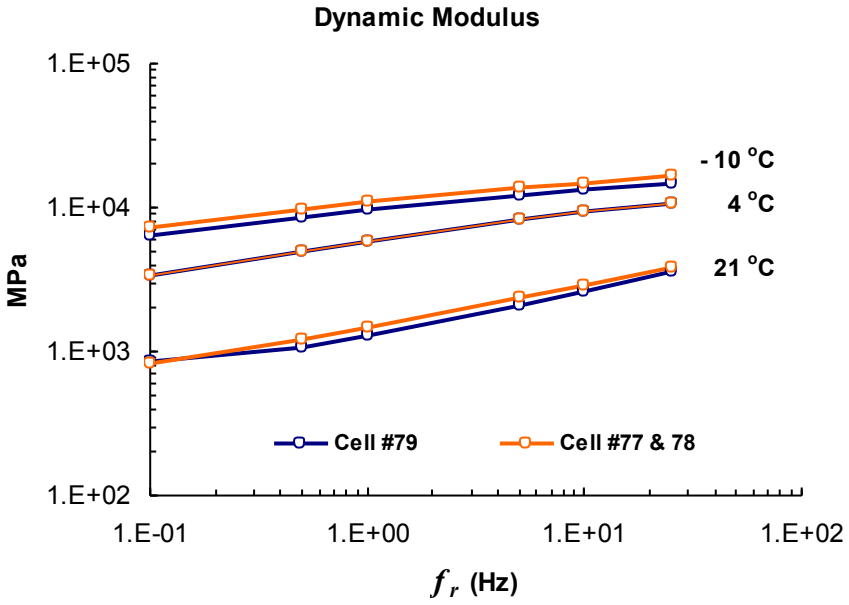

Figure 3.3: Dynamic modulus test results.

Table 3.7: Phase angle (θ) of tested materials (degree)

Temp. (°C)	f (Hz)	Cell #79					Cell #77 & 78			
		Rep #1	Rep #2	Rep #3	Mean	COV (%)	Rep #1	Rep #2	Mean	COV (%)
-10	25	12.0	10.3	11.6	11.3	8	10.1	10.6	10.3	3
	10	12.9	11.3	12.3	12.2	7	10.7	11.0	10.8	2
	5	13.3	12.1	13.2	12.9	5	11.5	11.7	11.6	1
	1	16.8	14.8	16.0	15.9	6	13.9	14.1	14.0	1
	0.5	18.3	16.3	17.6	17.4	6	15.2	15.4	15.3	1
	0.1	22.2	20.3	21.4	21.3	5	18.7	18.9	18.8	1
4	25	18.6	15.2	14.7	16.2	13	15.6	16.9	16.2	6
	10	19.4	16.1	16.3	17.3	11	16.2	18.2	17.2	8
	5	20.6	17.3	17.7	18.5	10	17.1	19.6	18.4	10
	1	24.2	21.2	21.6	22.3	7	20.3	23.8	22.1	11
	0.5	25.4	23.0	23.3	23.9	5	21.9	25.6	23.7	11
	0.1	27.0	27.0	26.6	26.9	1	24.9	28.3	26.6	9
21	25	28.8	27.8	27.6	28.0	2	28.2	27.8	28.0	1
	10	28.5	28.2	27.7	28.1	1	29.0	28.0	28.5	2
	5	28.3	28.3	27.6	28.1	2	29.7	28.2	29.0	4
	1	27.0	27.1	27.2	27.1	0	30.4	27.8	29.1	6
	0.5	26.2	26.1	25.5	25.9	1	29.8	27.2	28.5	7
	0.1	21.8	22.1	22.3	22.1	1	26.8	24.0	25.4	8

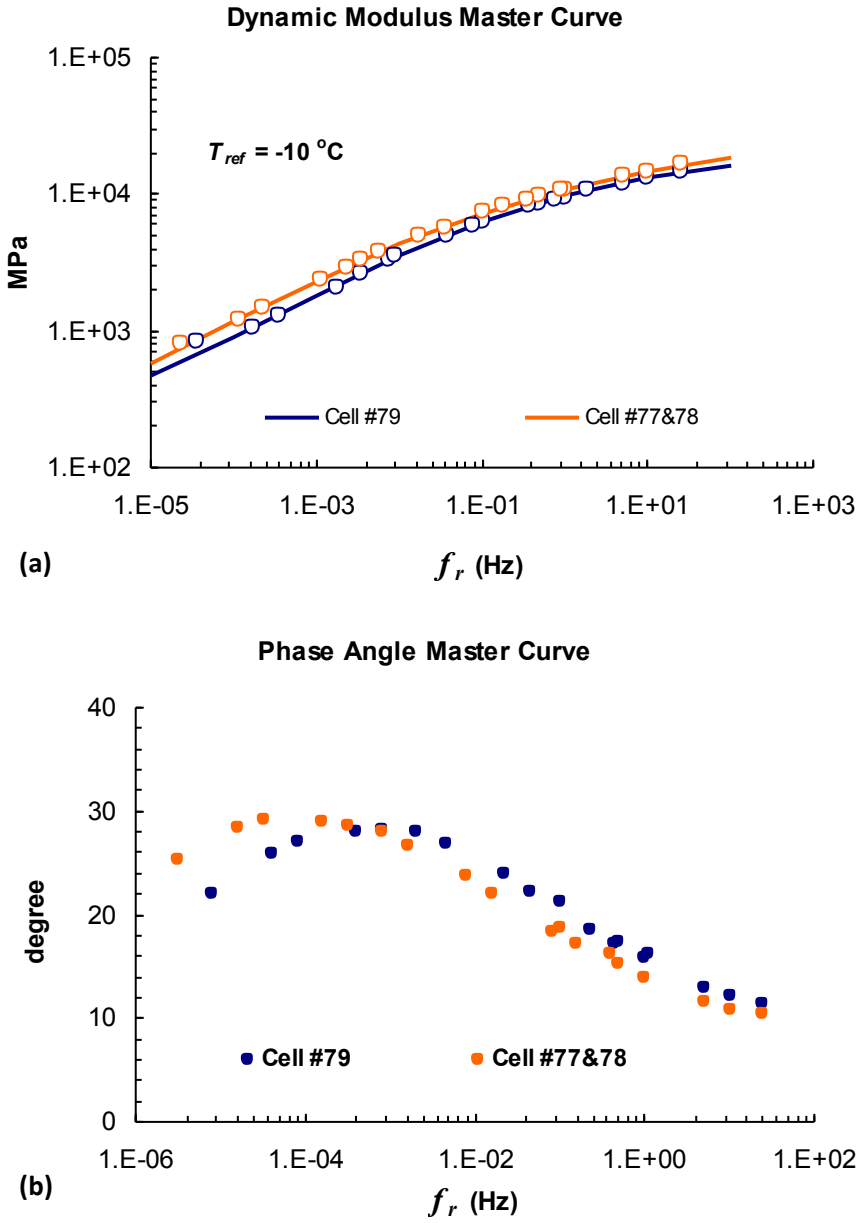

Figure 3.4: Master curves at a reference temperature of -10 °C: (a) Dynamic modulus and (b) phase angle.

Unlike the creep compliance test result, which was presented at much lower reference temperature of -36 °C, the material from Cell #77 and #78 appears to be slightly stiffer than the material from Cell #79 at the reference temperature of -10 °C. Again, however, the difference between the two materials was not found to be significant.

3.1.2.4 Summary of HMA Properties

IDT creep compliance, strength, and dynamic modulus testing was conducted to determine the low temperature mechanical properties of two MnROAD HMA mixtures (i.e., Cell #79 and Cell #77 & 78). According to an observation from the creep compliance master curves, Cell #77 & 78 material appeared to be slightly more compliant at a reference temperature of -36 ^{o}C than the material from Cell #79. On the other hand, the tensile strength of the same material at -24 ^{o}C was found to be slightly lower than that of Cell #79. However, the differences in both creep compliance and tensile strength between these two mixtures is not considerably large. Thus, it can be expected that these two materials will perform very similarly in resisting low temperature thermal cracking. The dynamic modulus test results also confirm that these two materials are very similar to each other in terms of their viscoelastic properties at low temperatures.

3.2 Base Course Materials

During construction, the base course materials were sampled and stored for laboratory testing. The fly ash stabilized RPM specimens were fabricated in the laboratory. The moisture-density relationship of RPM, fly ash stabilized RPM, and Class 6 were obtained in accordance with ASTM D 1557. Resilient modulus (M_r), were also characterized in accordance with the National Highway Research Program (NCHRP) 1-28A test protocol (Witczak, 1997). During the construction, the field density and moisture contents of base materials on site were measured using a nuclear density gauge. The field densities and moisture contents were used to fabricate laboratory specimens for testing.

3.2.1 Fly Ash

Fly ash obtained from Unit 8 of the Riverside Power Plant in Minneapolis, MN (operated by Xcel Energy) was used to stabilize the RPM. This fly ash has a calcium oxide (CaO) content of 22.37% and a carbon content of 16.35%. Riverside Unit 8 fly ash is a cementitious high-carbon fly ash. A fly ash application rate of 14% by weight of dry mix was used to stabilize RPM as base course.

3.2.2 RPM and Class 6 Aggregate

3.2.2.1 Gradation

The RPM was produced by pulverizing the in-situ asphalt pavement at MnROAD. The RPM consisted of 50% of recycled asphalt pavement and 50% of existing crushed aggregate base course. The Class 6 aggregate is a granite base course material used by MnDOT. The gradations of the RPM and Class 6 are shown in Table 3.8.

Table 3.8: Gradation of RPM and Class 6

Sieve Opening	Percent Finer	
	RPM	Class 6
(mm)	(%)	(%)
37.5	100	100
25	99	100
19	96	98
12.7	86	73
9.5	77	55
4.75	60	32
2	39	11
0.425	13	4
0.075	6	2

3.3.3.2 Density and Moisture Property

The maximum dry density and optimum moisture content values obtained in the laboratory tests are presented in Table 3.9. It can be seen from Table 3.9 that the Class 6 crushed

aggregate has higher maximum dry density than fly ash stabilized RPM, followed by untreated RPM.

Table 3.9: The Moisture Density Properties of Base Material

Type of Material	Maximum Dry Density, kg/m^3	Optimum Moisture Content, %
Reclaimed Asphalt base course	2044	4.9
Reclaimed Asphalt base course + 14% King Fly Ash base course	2111	6.5
Crushed Aggregate base course	2220	5.2

3.3.3.3 Resilient Modulus

The resilient modulus model in the Mechanistic-Empirical Pavement Design Guide (MEPDG) is shown by Equation (3.1) (Witczak et al., 2004). The parameters for different base materials were resolved by fitting the test data with the model and were shown in Table 3.10. The resilient moduli reported in Table 3.11 was predicted by the resolved model at the peak cyclic stress of 103 kPa and confining stress of 45 kPa for aggregate base, and peak cyclic stress of 41 kPa and confining stress of 14 kPa for subgrade. Table 3.11 indicates that the fly ash stabilized RPM has much higher resilient modulus at 28 days curing age than that at 7 days of curing age, and has much higher resilient modulus than untreated RPM and Class 6 aggregate.

$$M_r = k_1 * P_a \left(\frac{\sigma_b - 3k_6}{P_a}\right)^{k_2} * \left(\frac{\tau_{oct}}{P_a} + k_7\right)^{k_3} \qquad (3.1)$$

where: M_r =resilient modulus, psi,

k_1, k_2, k_3, k_6, and k_7 = regression constants (obtained by fitting resilient modulus test data to equation),

σ_b =bulk stress = $\sigma_1+\sigma_2+\sigma_3$,

σ_1, σ_2, and σ_3= the major, intermediate and minor principal stress, respectively,

P_a =normalizing stress (atmospheric pressure),

τ_{oct} = octahedral shear stress.

Table 3.10: Parameters in the Resilient Modulus Model

Base Type	k1	k2	k3	k6	k7
Clay	2380.4971	0.8451	-5.4203	-9.4677	1.0317
Class 6	376.4932	1.4858	-0.7325	-67.4420	1.0000
RPM	764.7781	1.2642	-1.0341	-55.4167	1.0000
RPM+Fly Ash 7D	31194.3790	0.1545	-0.4353	-8.9163	1.0301
RPM+Fly Ash 28D	50966.4110	0.1424	-0.6308	0.0000	1.0000

Table 3.11: Summary of Resilient Modulus Test Results of Field Sampled Materials

Materials	Curing Time (days)	Mr (kPa)
Clay	n/a	105,711
Class 6	n/a	218,257
RPM	n/a	268,685
RPM+Fly Ash	7	3,084,597
	28	4,686,837

CHAPTER 4: FIELD TEST RESULTS

In order to analyze the field performance of the base materials in Cells 77, 78, and 79, various field test procedures were carried out at different times, including Dynamic Cone Penetrometer (DCP), Lightweight Deflectometer (LWD), Falling Weight Deflectometer (FWD), and Soil Stiffness Gauge (SSG). During the construction at MnROAD, various sensors were placed in the pavement to monitor the responses of materials to traffic and weather. The field tests results can be used to characterize material properties and predict the pavement performance.

4.1 Tests Methods

1. Dynamic Cone Penetrometer (DCP)

DCP is an instrument designed to provide a measure of the in-situ strength of subgrade, subbase, and base materials. A 7.9-kg weight is raised to a height of 57.4 cm and then dropped, driving the 60-degree 20-mm-diameter cone into the soil or aggregate base. The penetration depth per blow is used to calculate the strength or stiffness of the subject materials.

2. Lightweight Deflectometer (LWD)

LWD device is hand-operated and takes measurements of the deflection of compacted soil that is impacted by a falling weight. The LWD has one sensor directly below the falling weight. The device measures the resulting deflection and estimates a modulus value based on the force required to generate a given deflection for that soil type.

3. Falling Weight Deflectometer (FWD)

FWD tests were conducted directly on the base courses during the construction. Prior to the placement of HMA, the base course had one month of curing. FWD tests were also conducted on several curing days to monitor the change of the properties of fly ash stabilized

RPM. After the placement of HMA surface, FWD tests were conducted on HMA to backcalculate the modulus of base materials.

4. Soil Stiffness Gauge (SSG)

A Humboldt H-4140 SSG was used in this study. The soil stiffness gauge (SSG) is a non-destructive testing device, which measures the stiffness (and or modulus) of surficial materials in place. The SSG directly measures in-situ stiffness of materials in a zone lying 125 mm ~ 380 mm below the surface. The SSG stiffness measurements were made in accordance with ASTM D6758.

4.2 Test Results

4.2.1 Results of Field Tests on Base Courses

During the construction, after the base courses were finished, field tests were conducted directly on the base courses. The field test results were analyzed to obtain the modulus of base materials. For the DCP measurement, 15 readings were taken in each test location. From these readings, the first two and the last two reported readings were not used in the calculation of DPI (DCP Penetration Index) (DeBeer, M. 1991). The DPI is calculated using Equation (4.1).

$$DPI_i = \frac{\mathrm{Re}\,ading_{i+5} - \mathrm{Re}\,ading_i}{5} \tag{4.1}$$

With the calculated DPI in mm per blow, the modulus (E) in MPa can be estimated using Equation (4.2).

$$\log(E_i) = 3.05 - 1.06\log(DPI_i) \tag{4.2}$$

For each test section, there were 5 estimated modulus values.

For the LWD tests, 3 deflection readings were taken for each section with a load level of approximately 6.0 kN and a plate radius of 0.1 m. These readings were then used to estimate the base modulus using Equation (4.3) (Fleming et al., 2007).

$$E = \frac{2k(1-\nu^2)P\ r}{A\delta_c} \tag{4.3}$$

Where E = modulus, MPa,

P/A = stress, MPa,

r = plate radius, m,

A = area, m^2,

ν = poisson's ratio,

k = shape and rigidity factor (0.79 for rigid, 1.0 for flexible circular plate),

δ_c = center deflection, m.

For FWD analysis, there are 2 equations used in the calculation of modulus from FWD data, depending on the distance of the sensor from the loading plate (George et al 2004). Equation (4.4) is for the sensor directly below the loading plate, while Equation (4.5) is for a sensor at a distance r from the loading plate.

$$E = \frac{2P}{A}(1-\nu^2)RaD_o \tag{4.4}$$

$$E = \frac{P}{A}(1-\nu^2)\frac{R^2}{r}D_r \tag{4.5}$$

Where E = modulus, MPa,

P/A = stress, MPa,

R = plate radius, mm (small = 150 mm, large = 225 mm),

A = area, m^2,

ν = poisson's ratio,

a = shape and rigidity factor (0.79 for rigid, 1.0 for flexible circular plate),

D_o = deflection below plate (m),

D_r = deflection at distance r from center of plate (m),

Table 4.1 summarizes the direct measurements on the base layer, based on Equation (4.4). It can be seen that for any of M_r and field test methods, fly ash stabilized RPM had higher modulus than RPM, followed by crushed aggregate, as shown in Figure 4.1 in which the number after the test method indicates the days after the construction of base courses. The resilient modulus was always higher than moduli from field tests. The Mr of RPM was 257 MPa, while the highest modulus for RPM from field tests, DCP in this case, was 104.58MPa. The difference between Mr and backcalculated moduli for stabilized materials was significant. The Mr of 28-day stabilized RPM was 4,334 MPa, while the highest modulus from field tests was 364 MPa. The M_r from the laboratory testing is more than ten times higher than moduli form field the tests. In the field tests, DCP tests resulted in higher modulus than LWD, SSG, and FWD. The moduli from SSG were higher than those from LWD and FWD tests, except for stabilized RPM. Between LWD and FWD tests, LWD generated higher moduli. This might be related to the stress/strain-dependence of these materials. Each of these test methods applies different load levels to the materials. The stress/strain-dependence will affect the modulus backcalculated from the response of materials. Peterson et al. (2006) attributed this variation of modulus from different field tests to sensing depth, soil heterogeneity, and vertical stress levels. However, the sensing depth and vertical stress level might be related to each other, as larger vertical stress can impact deeper soils. These heterogeneities are also affected by the volume of soil impacted by the loads and also depend on the vertical stress levels. Therefore, it is believed that load levels are most important factors for the variation of modulus from different field tests.

Table 4.1: Comparison Between Laboratory M_r and Field measurement Moduli

Curing Days	Test Method	Fly Ash+RPM	RPM	Class 6
		Average Moduli, MPa		
7	M_r	2984	257	220
28	M_r	4334		
8	DCP	3634	105	67
8	LWD	182	42	15
22	DCP	328	83	63
22	FWD	134	36	22
22	SSG	159	70	59
26	FWD	112		

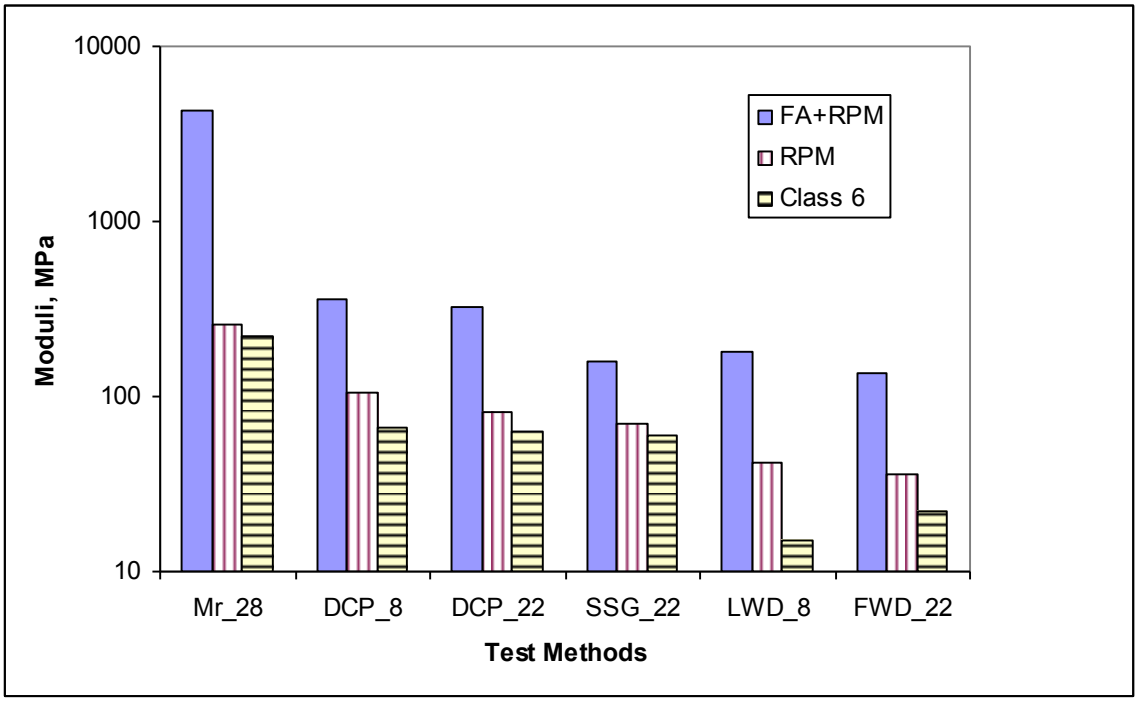

Figure 4.1: Comparison of Moduli from Different Tests Methods.

Another observation was that with the increase of time after the placement of the base courses, the moduli of base materials dropped slightly, as shown in Figure 4.2. For all three base

materials, the 8-day DCP moduli were higher than 22-day moduli. For FWD tests, the 22-day moduli also were higher than the 28-day moduli. It is believed that moisture infiltrated into the base courses and weakened the materials. However, this finding is unexpected for the fly ash stabilized RPM, as the continuous hydration of fly ash would result in an increase of moduli with the increase of curing time. This indicated that, after the construction of base courses, surface layers should be constructed promptly, even for the stabilized layers, to prevent the weakening of base course materials, mostly due to precipitation.

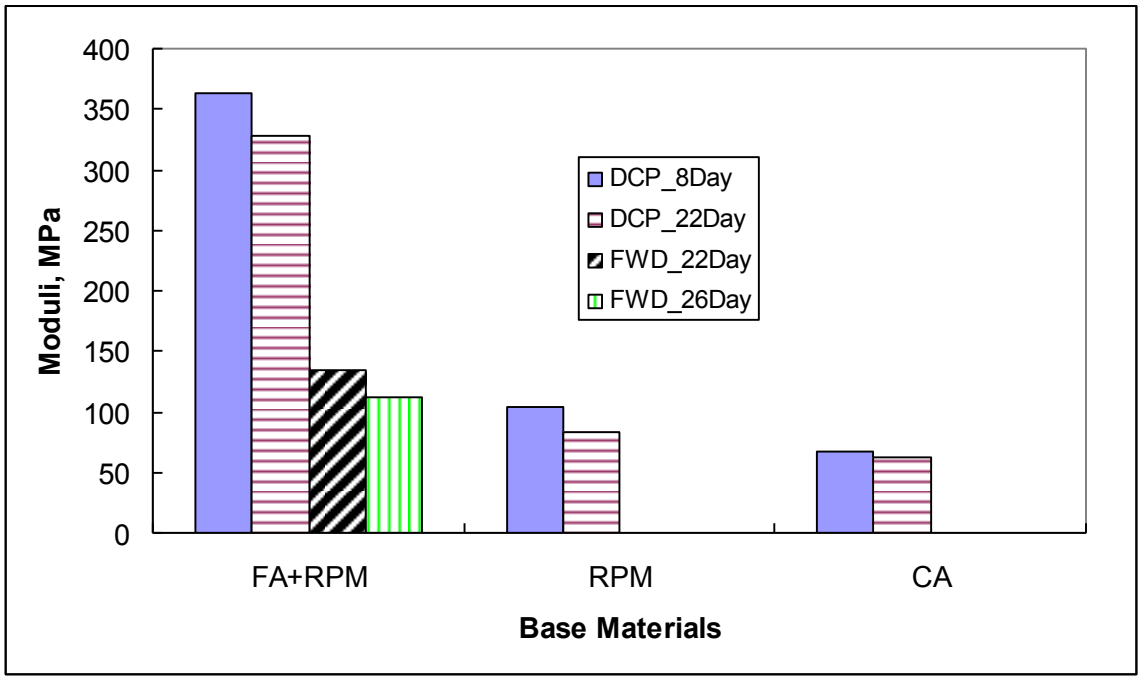

Figure 4.2: Modulus from Field Tests as Function of Curing Days.

4.2.2 Back-calculated Modulus from FWD Tests on HMA

After the HMA layer was finished, the FWD tests were conducted on the HMA layer surface using a 40 kN (9,000 lbf) load level. The load level of 40 kN was selected for this comparison considering it represents the load level exerted by a dual-wheel load. For the

modulus back-calculation, the Texas Transportation Institute (TTI) software MODULUS (TTI, 2001*)* was used.

Table 4.2 summarized the averaged back-calculated modulus at different testing date using MODULUS. The backcalculated moduli of base materials from FWD tests performed on the HMA confirmed the results of FWD performed on the base courses before HMA placement. The fly ash stabilized RPM had higher moduli than unstabilized RPM, followed by Class 6, as shown in Figure 4.3. The backcalculated moduli of the base courses from FWD tests were extremely higher for the winter season when the base course materials were frozen (as indicated by the temperature gages placed in the base course). The moduli of base courses were lower in Spring than the moduli in other seasons, indicating the weakening of materials by spring thaw. The backcalculated moduli of base materials from the FWD tests on HMA surface were higher than that directly performed on base course during construction. One unexpected result is that the backcalculated moduli of fly ash stabilized RPM did not show significant increase with the increase of curing age. This might be due to the micro shrinkage crack within fly ash stabilized RPM layer which compensated the strength increase. However, this assumption need further study. The loading center deflections in FWD test of these 3 Cells are shown in Figure 4.4. It can be seen that the deflections on Cell 79 with fly ash stabilized RPM base were much smaller than that on Cell 77 and 78, with RPM and Class 6 base, respectively. It should be noted that although the backcalculated moduli of fly ash stabilized RPM are higher than the other two base materials, the difference is not as significant as the difference between the laboratory tested resilient moduli, as shown in Table 3.11.

Table 4.2: Summary of Back-calculated Modulus from FWD Tests

Test Date	RPM (kPa)	Class 6 (kPa)	RPM+Fly Ash (kPa)
22Day	35,998	22,001	134,000
26Day	n/a	n/a	111,998
10/31/07	193,053	137,895	216,495
11/01/07	215,806	158,579	344,048
01/28/08	3,652,842	2,392,481	4,637,414
03/13/08	426,096	395,070	783,934
03/20/08	288,201	139,274	342,669
04/16/08	127,553	102,732	198,569
05/21/08	109,627	81,358	215,806
06/26/08	86,874	66,190	250,280
07/02/08	89,632	75,153	307,506
07/14/08	103,421	76,532	268,896
08/14/08	109,627	95,148	377,143
08/20/08	n/a	n/a	292,338
09/04/08	n/a	n/a	342,669
04/08/09	139,274	127,553	177,885
04/13/09	227,527	221,322	499,180
05/11/09	111,006	104,800	195,811
06/17/09	137,206	127,553	207,532
07/21/09	117,211	95,837	238,559
09/15/09	153,753	134,448	264,759
10/15/09	267,517	244,764	315,090
10/27/09	204,085	168,232	238,559
10/15/09	316,469	248,901	288,201
10/27/09	176,506	157,200	226,838
11/17/09	204,085	188,916	226,148
02/18/10	4,904,241	5,339,989	4,616,040
03/08/10	151,685	156,511	272,343
03/17/10	110,316	127,553	168,922
04/06/10	139,964	142,032	170,300
06/07/10	86,874	83,427	202,706
07/28/10	122,727	111,006	228,216
09/16/10	176,506	166,164	246,832
10/29/10	244,764	203,395	n/a

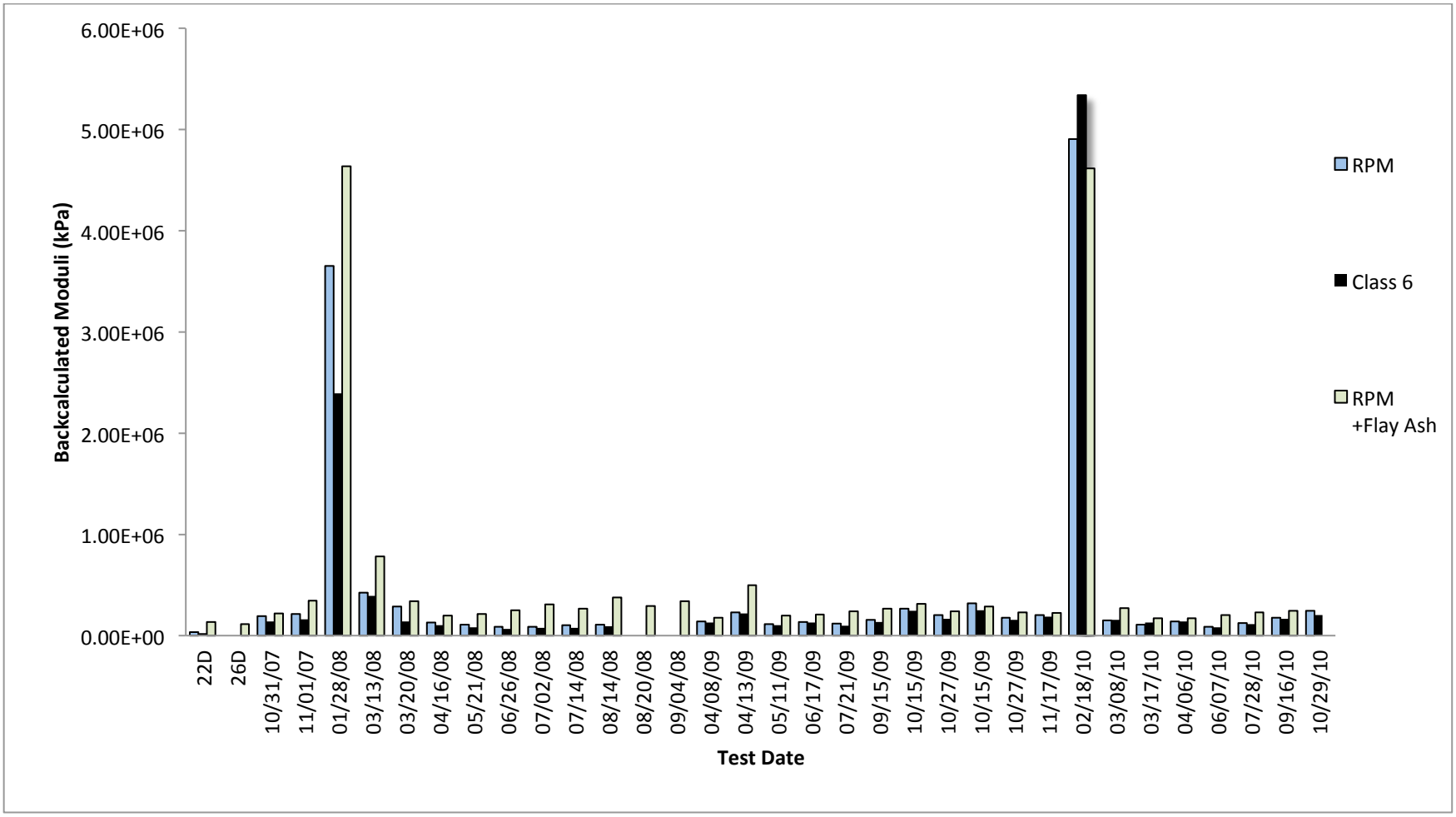

Figure 4.3: The Average Back-calculated Base Moduli by MODULUS.

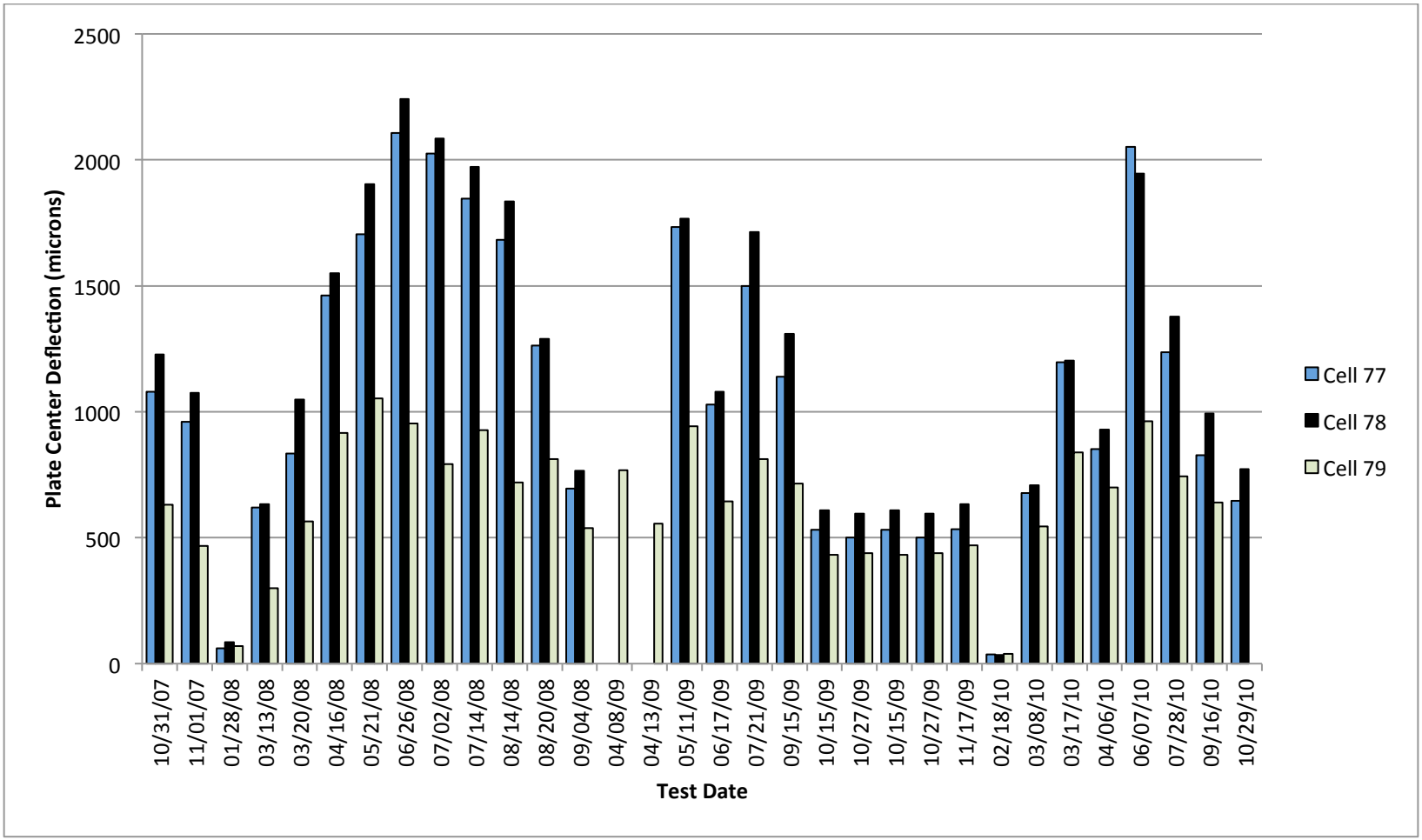

Figure 4.4: The Average Deflection at The Plate Center in FWD Test.

4.2.3 Instrumentation Results

During the construction at MnROAD, various sensors were placed in the pavement by MnDOT to monitor the responses of materials to traffic and weather. Pressure cells were installed at the top of subgrade. The collected data is shown in Figure 4.5. The fly ash stabilized RPM base course resulted in the least pressure on the subgrade, followed by RPM and Class 6. This is in agreement with the moduli of base materials from the field and laboratory tests. Fly ash stabilized RPM had the highest modulus and can distribute the stress more effectively than the other two base materials. This indicates as a result of reduced compressive stress on the subgrade, the subgrade under the fly ash stabilized RPM will have less rutting than the subgrade in other sections.

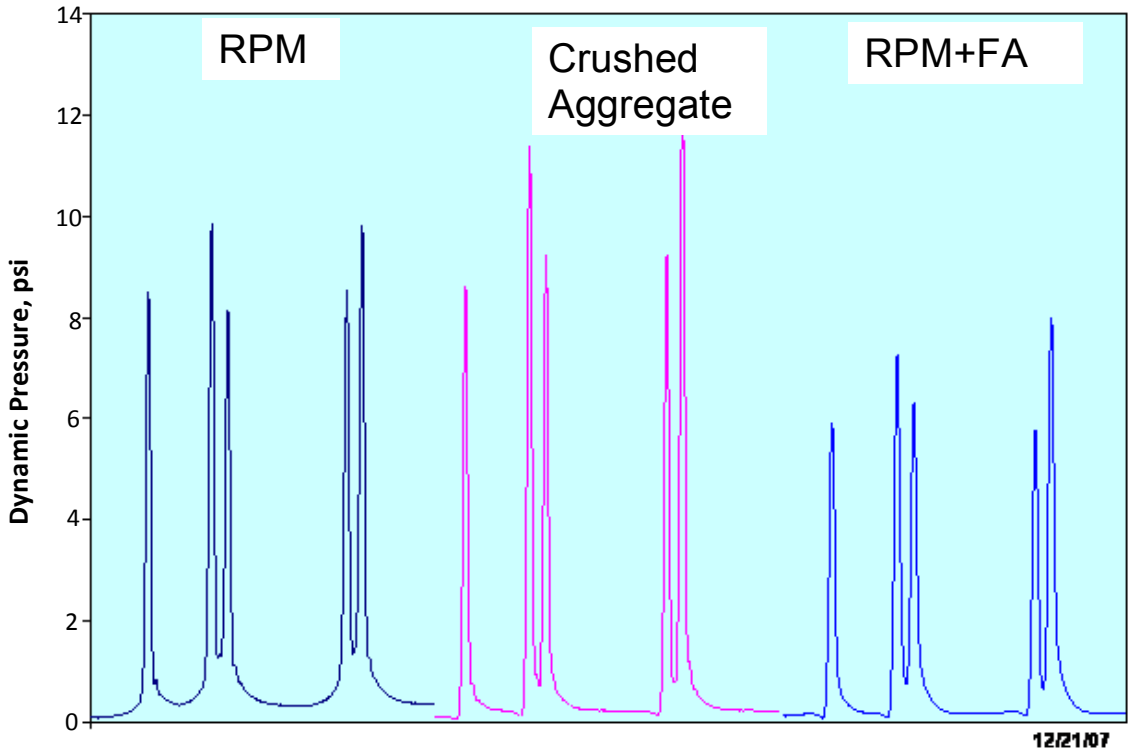

Figure 4.5: Instrumentation Results at MnROAD.

CHAPTER 5: PERFORMANCE PREDICTION AND LIFE CYCLE COST ANALYSIS

Life cycle cost analysis (LCCA) is a method to assess the cost of the construction operation over the service life, including operations, maintenance, repair, replacement, and disposal costs (Mearig et al. 1999). It's an effective way to compare the economic efficiency of alternatives. The service lives of the Cells 77, 78, 79, which are needed in the LCCA, were obtained from the performance prediction. There are various performance prediction softwares based on different theories. Among them, the MEPDG software, version 1.1 (ARA, 2009) is a powerful one because it's partially based on mechanical theory

5.1 Performance Prediction by MEPDG

5.1.1 MEPDG Input

5.1.1.1 Traffic

The traffic on Cells 77, 78, and 79 is an 18-wheel, 5-axle, tractor/trailer with the loading configurations of gross vehicle weight of 80 kips, as shown in Figure 5.1 and Table 5.1 (MnDOT, 2009) The truck runs on these 3 cells during a normal 8 hour working time with the average of 48 laps per day. The real traffic information was input into the MEPDG software, version 1.1 (ARA, 2009) to predict the future performance.

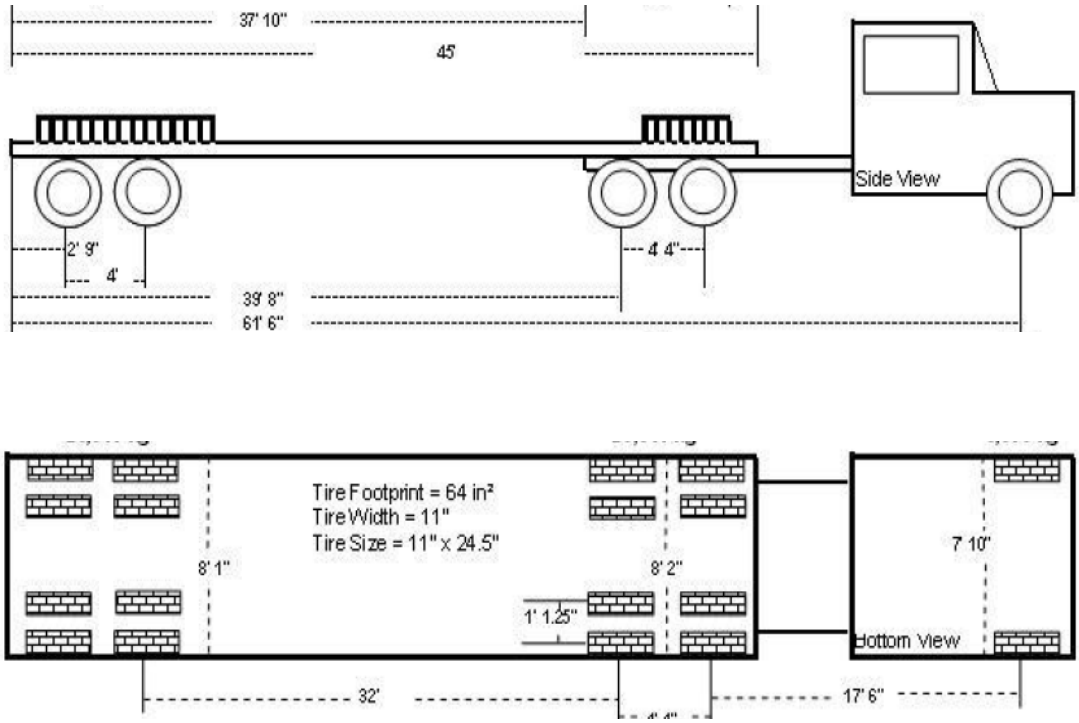

Figure 5.1: Truck Configuration (MnDOT).

Table 5.1: The Traffic Configuration (MnDOT)

The Traffic Configuration	Weight (N)	
Total Weight	353,634	
Steering Axle	53,379	
Front axle Tractor tandem	75,175	
Back axle Tractor tandem	73,840	149,015
Front axle Trailer Tandem	69,392	
Back axle Trailer Tandem	81,847	151,240

5.1.1.2 Climate

The Cells 77, 78, and 79 are located about 40 miles north east of Minneapolis, MN. The hourly climatic data of the nearest station was exported from the climatic database provided in the MEPDG program.

5.1.1.3 Structure

1. HMA Layer:

1) Dynamic Modulus of HMA:

The dynamic modulus was tested at temperatures of -10, 4, and 21 ^{o}C, as shown in Table 3.6 in Chapter 3, which does not cover the high temperature recommended by MEPDG software. Therefore, the extrapolation was conducted to predict the property at 54.4 ^{o}C. First the master curve of the dynamic modulus was obtained based on the test data, which is shown in Figure 5.2. The shift factors at different temperature follow a linear relation as shown in Figure 5.3. The shift factor of 54.4 ^{o}C was predicted by the regression linear equation (5.1). At last, the dynamic moduli at different frequency for 54.4 ^{o}C could be backcalculated using the predicted shift factor, as shown in Table 5.2. In Table 5.2, the dynamic moduli at 54.4 ^{o}C were predicted, the dynamic moduli at other temperatures were measured.

$$\text{Shift Factor} = -0.1115 * \text{Temp } (^{\circ}\text{C}) + 0.1513 \qquad (5.1)$$

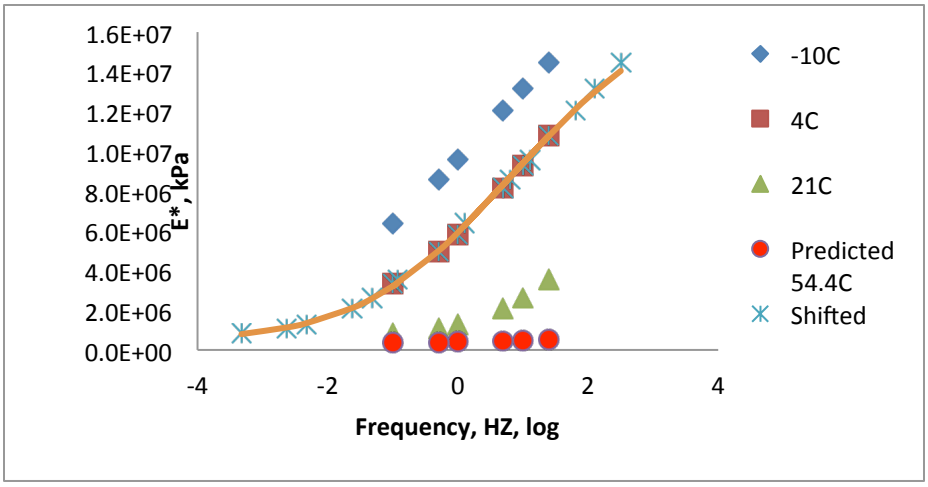

Figure 5.2: Master Curve of E*.

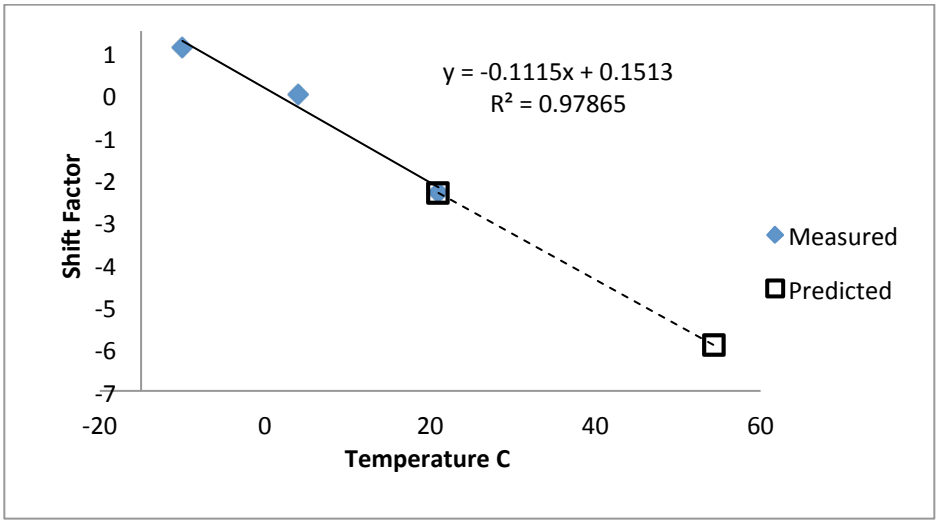

Figure 5.3: Linear Relation of Shift Factor of E*.

Table 5.2: The Measured E* at -10, 4, and 21°C and the Predicted E* at 54.4 °C

Temp. (C)	Frequency (HZ)	E* (kPa)
-10	25	14,453,026
-10	10	13,129,023
-10	5	12,043,021
-10	1	9,556,017
-10	0.5	8,554,015
-10	0.1	6,364,011
4	25	10,803,019
4	10	9,262,016
4	5	8,140,014
4	1	5,804,010
4	0.5	4,953,009
4	0.1	3,338,006
21	25	3,548,006
21	10	2,608,005
21	5	2,079,004
21	1	1,294,002
21	0.5	1,072,002
21	0.1	839,001
54.44	25	527,228
54.44	10	481,761
54.44	5	455,504
54.44	1	413,176
54.44	0.5	400,648
54.44	0.1	380,138

2) Creep Compliance of HMA:

The creep compliance was tested at -36, -24, and -12°C as shown in Table 3.4 in Chapter 3, which is different from the temperature required by MEPDG software. The same prediction procedure as the E* was followed to predict the creep compliance at -20, -10, and 0 °C. The master curve and linear relation of the shift factors at different temperature are shown in Figure 5.4 and Figure 5.5, respectively. The shift factors at -20, -10, and 0 °C was predicted by the Equation (5.2). The predicted creep compliance was calculated by the predicted shift factors of -20, -10, and 0 °C as shown in Table 5.3.

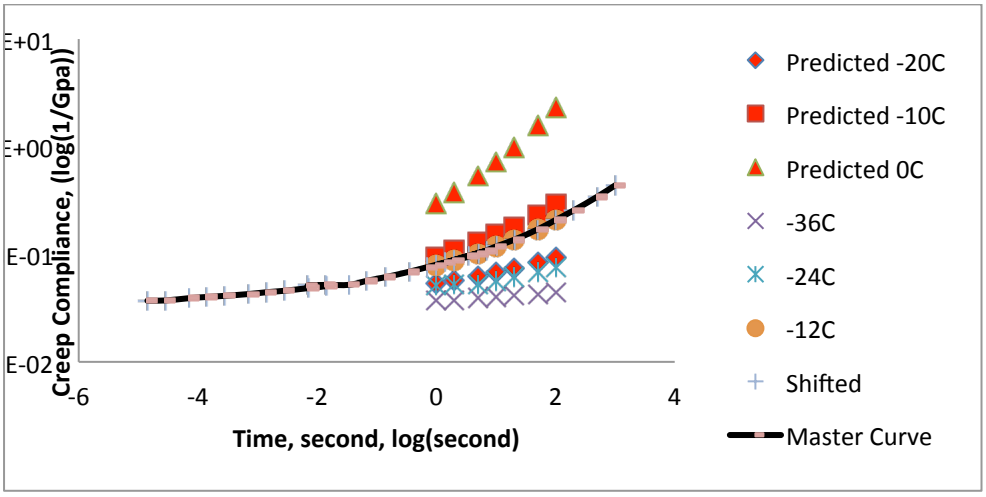

Figure 5.4: Master Curve of Creep Compliance.

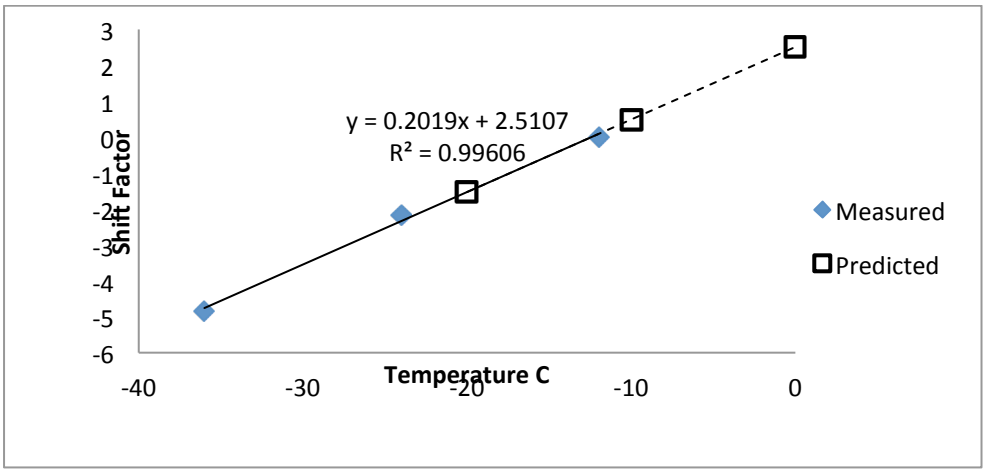

Figure 5.5: Linear Relation of Shift Factor of Creep Compliance.

$$\text{Shift Factor} = 0.2019 * \text{Temp } (°C) + 2.5107 \quad (5.2)$$

Table 5.3: The Predicted Creep Compliance at -20, -10, and 0 ^{0}C

Temp. C	Time, t	Predicted D(t) (1/GPa)
-20	1	5.3688E-02
-20	2	5.7024E-02
-20	5	6.2437E-02
-20	10	6.7496E-02
-20	20	7.3624E-02
-20	50	8.3867E-02
-20	100	9.3760E-02
-20	200	1.0613E-01
-20	500	1.2767E-01
-20	1000	1.4943E-01
-10	1	9.4482E-02
-10	2	1.0704E-01
-10	5	1.2893E-01
-10	10	1.5106E-01
-10	20	1.7996E-01
-10	50	2.3325E-01
-10	100	2.9039E-01
-10	200	3.6931E-01
-10	500	5.2554E-01
-10	1000	7.0584E-01
0	1	2.9477E-01
0	2	3.7543E-01
0	5	5.3532E-01
0	10	7.2015E-01
0	20	9.9383E-01
0	50	1.5846E+00
0	100	2.3278E+00
0	200	3.5153E+00
0	500	6.3239E+00
0	1000	1.0174E+01

3) Binder Properties:

The binder property test was performed by MTE. The complex moduli and phase angle are shown in Table 5.4.

Table 5.4: The Binder DSR Test Results

Temp. (C)	G*/Sin(δ) (Pa)	Phase Angle δ (deg.)	Sin(δ)	G* (Pa)
64	3900	69.0	0.93358	3640.962
58	7700	66.2	0.914959	7045.186
52	15000	63.7	0.896486	13447.29

2. Base and Subgrade:

Because the level 1 input in MEPDG is not calibrated with the field performance, level 2 input was used in this study. The resilient moduli of RPM, Class 6, fly ash stabilized RPM bases were normalized to the peak cyclic stress of 103 kPa and confining stress of 45 kPa. The resilient modulus of subgrade was normalized to the peak cyclic stress of 41 kPa and confining stress of 14 kPa. The results are shown in Table 3.11 in Chapter 3.

5.1.2 Predicted Performance

The performance of Cells 77, 78, and 79 were predicted by MEPDG software with same traffic, climate, HMA surface layer, and subgrade properties. Only the properties of the base layer materials were different as shown in Table 3.11 in Chapter 3. The performance modeling results were summarized in Table 5.5. It can be seen that the time to thermal cracking failure is same for Cell 77, 78, and 79, which is 144 months. This is because the same HMA material was used in the three Cells. However, the purpose of this study is to compare the performance of base materials. Therefore, the modeling results of other distresses such as top-down cracking, bottom-up cracking, rutting, and IRI which are related to the base materials, were used to determine the service life.

The detailed performance modeling results are shown in Table 5.6 and Figures 5.6 through 5.8 for Cell 77, Table 5.7 and Figures 5.9 through 5.11 for Cell 78, and Table 5.8 and Figures 5.12 through 5.14 for Cell 79.

Table 5.5: Summary of Service Life Analysis

Distress	Time to Failure (month)		
	Cell 77 (RPM)	Cell 78 (Class 6)	Cell 79 (RPM+Fly Ash)
AC Surface Down Cracking	132	90	Pass
AC Bottom Up Cracking	Pass	Pass	Pass
AC Thermal Fracture	144	144	144
Total Rutting	Pass	Pass	Pass
IRI	270	270	282
Service Life (Year)	11	7.5	23.5
Rehabilitation Times (within service life of Cell 79)	1.14	2.13	0

Table 5.6: Reliability Summary of Cell 77 (RPM)

Project: CELL77-48-Mr-30.dgp Reliability Summary					
Performance Criteria	Distress Target	Reliability Target	Distress Predicted	Reliability Predicted	Acceptable
Terminal IRI (in/mi)	172	90	152.9	68.77	Fail
AC Surface Down Cracking (Long. Cracking) (ft/mile):	2000	90	391	79.13	Fail
AC Bottom Up Cracking (Alligator Cracking) (%):	25	90	1.4	99.88	Pass
AC Thermal Fracture (Transverse Cracking) (ft/mi):	1000	90	1785.8	0.82	Fail
Chemically Stabilized Layer (Fatigue Fracture)	25	90			N/A
Permanent Deformation (AC Only) (in):	0.25	90	0.11	99.94	Pass
Permanent Deformation (Total Pavement) (in):	0.75	90	0.28	99.999	Pass

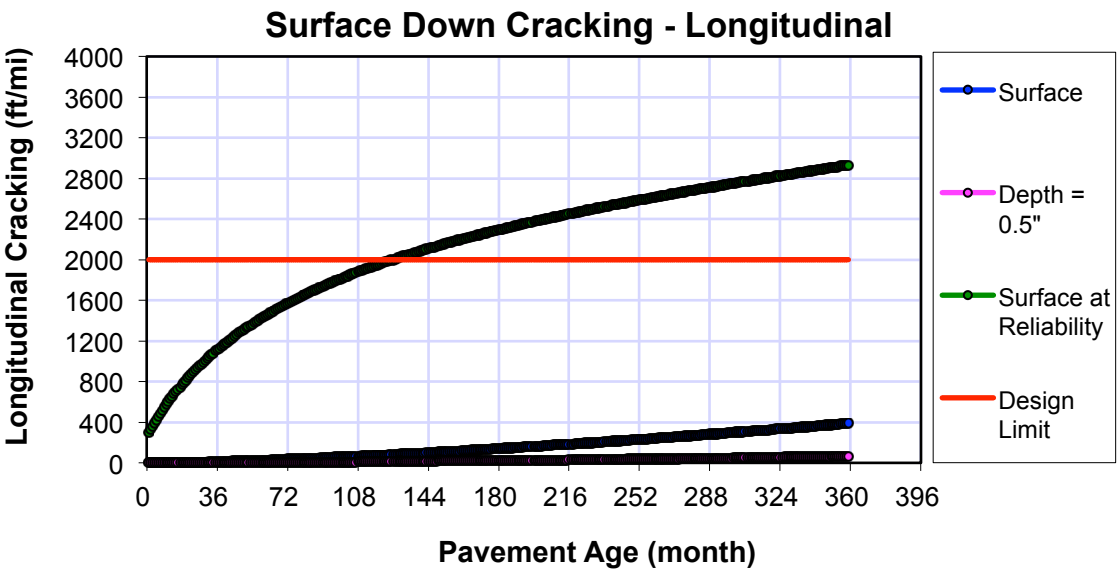

Figure 5.6: Surface Down Cracking of Cell 77 (RPM).

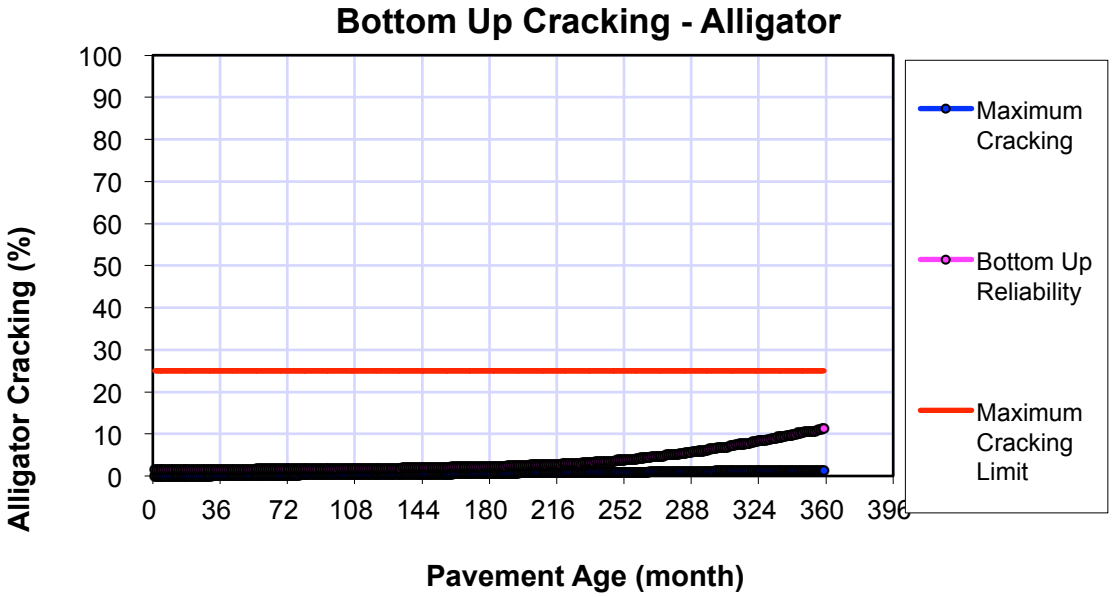

Figure 5.7: Bottom Up Cracking of Cell 77 (RPM).

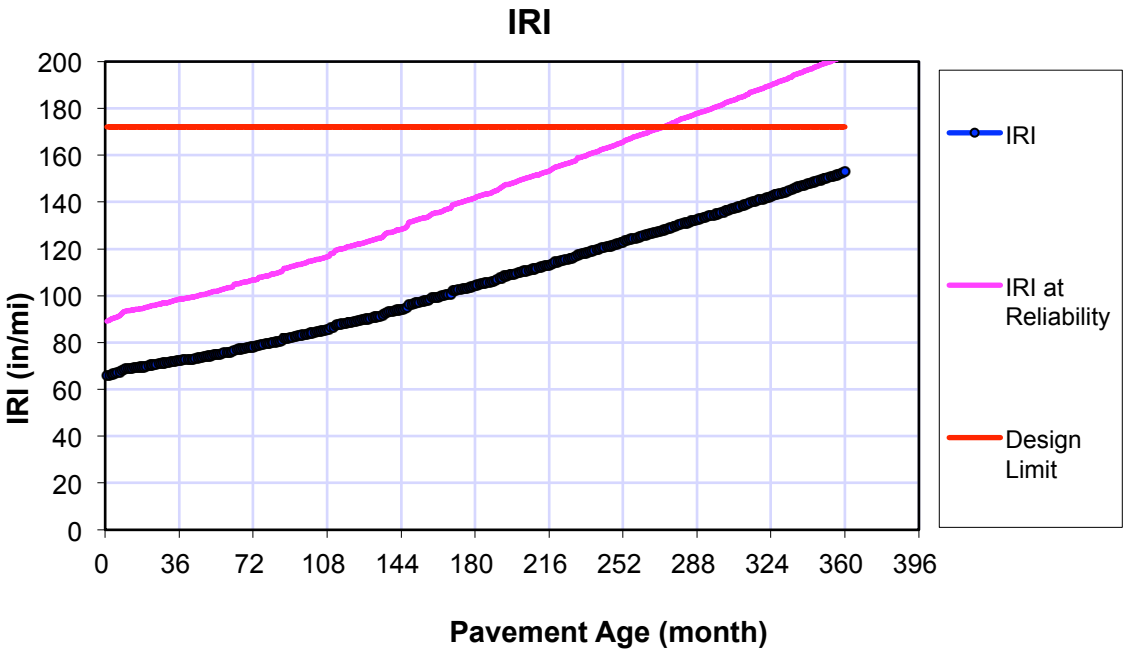

Figure 5.8: IRI of Cell 77 (RPM).

Table 5.7: Reliability Summary of Cell 78 (RPM)

Project: CELL78-48-Mr-30.dgp Reliability Summary					
Performance Criteria	Distress Target	Reliability Target	Distress Predicted	Reliability Predicted	Acceptable
Terminal IRI (in/mi)	172	90	153.8	67.86	Fail
AC Surface Down Cracking (Long. Cracking) (ft/mile):	2000	90	638	74.17	Fail
AC Bottom Up Cracking (Alligator Cracking) (%):	25	90	2	96.77	Pass
AC Thermal Fracture (Transverse Cracking) (ft/mi):	1000	90	1785.8	0.82	Fail
Chemically Stabilized Layer (Fatigue Fracture)	25	90			N/A
Permanent Deformation (AC Only) (in):	0.25	90	0.12	99.9	Pass
Permanent Deformation (Total Pavement) (in):	0.75	90	0.3	99.999	Pass

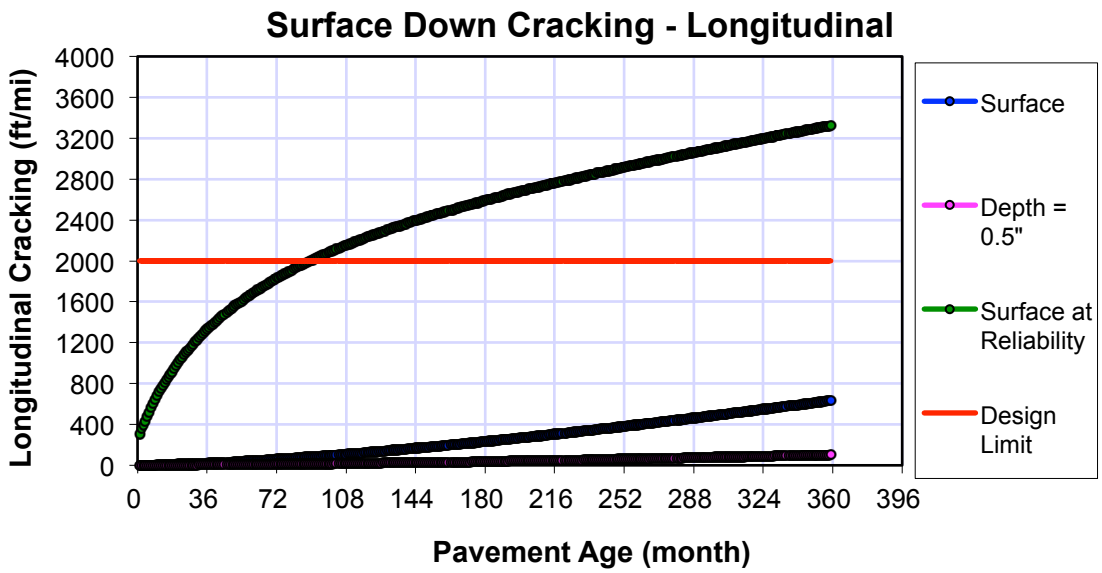

Figure 5.9: Surface Down Cracking of Cell 78 (RPM).

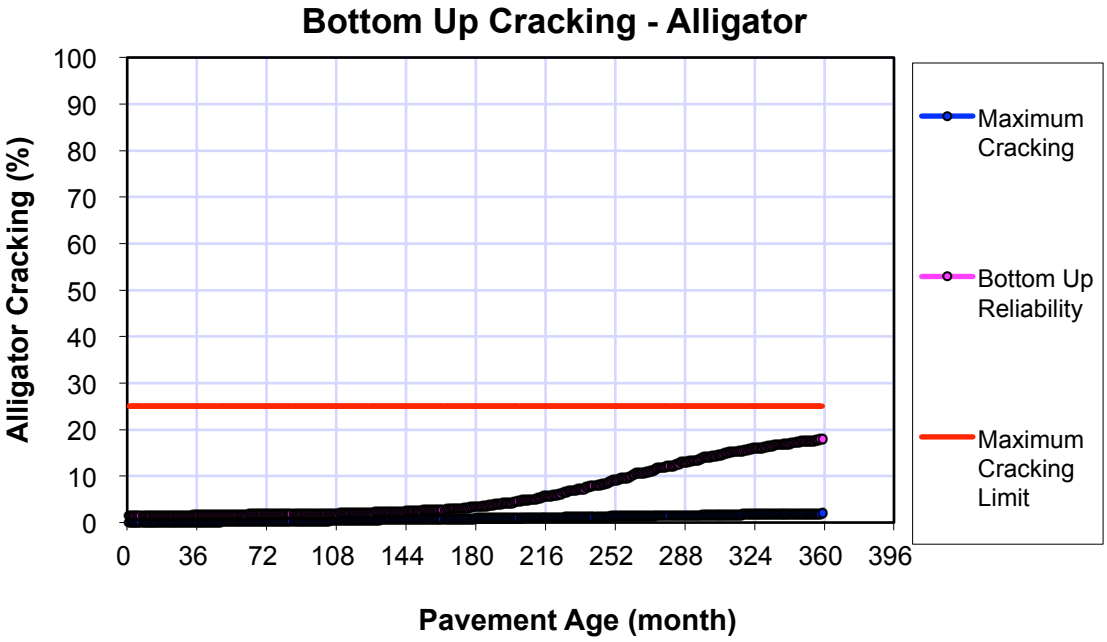

Figure 5.10: Bottom Up Cracking of Cell 78 (RPM).

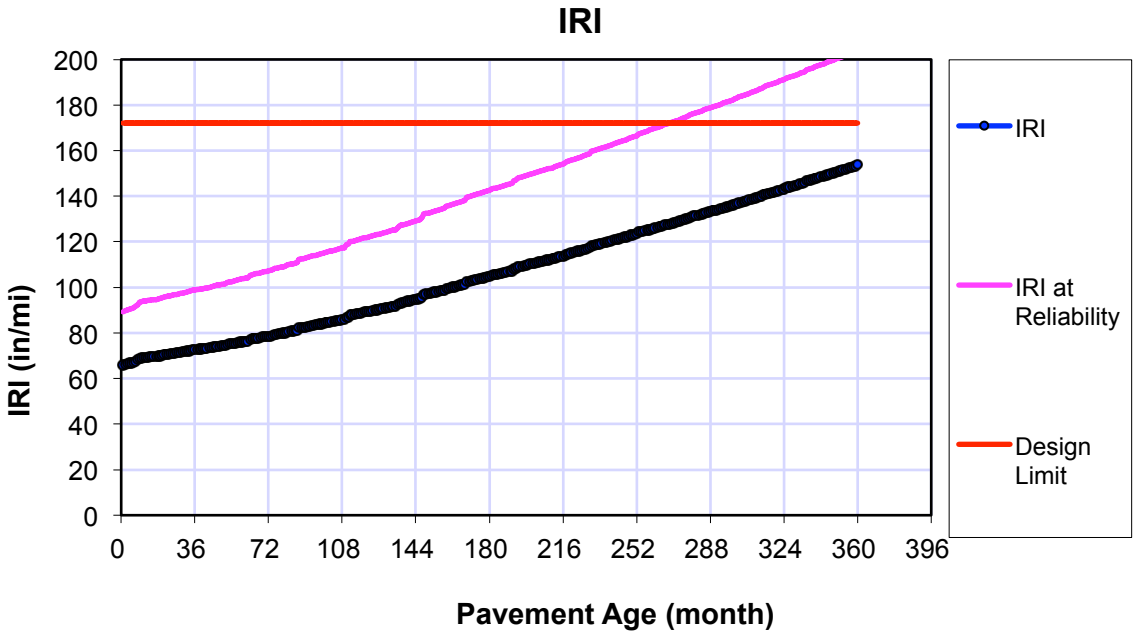

Figure 5.11: IRI of Cell 78 (RPM).

Table 5.8: Reliability Summary of Cell 79 (RPM)

Project: CELL79-48-Mr-30.dgp Reliability Summary					
Performance Criteria	Distress Target	Reliability Target	Distress Predicted	Reliability Predicted	Acceptable
Terminal IRI (in/mi)	172	90	147.9	73.72	Fail
AC Surface Down Cracking (Long. Cracking) (ft/mile):	2000	90	0	99.999	Pass
AC Bottom Up Cracking (Alligator Cracking) (%):	25	90	0	99.999	Pass
AC Thermal Fracture (Transverse Cracking) (ft/mi):	1000	90	1785.8	0.82	Fail
Chemically Stabilized Layer (Fatigue Fracture)	25	90			N/A
Permanent Deformation (AC Only) (in):	0.25	90	0.1	99.99	Pass
Permanent Deformation (Total Pavement) (in):	0.75	90	0.19	99.999	Pass

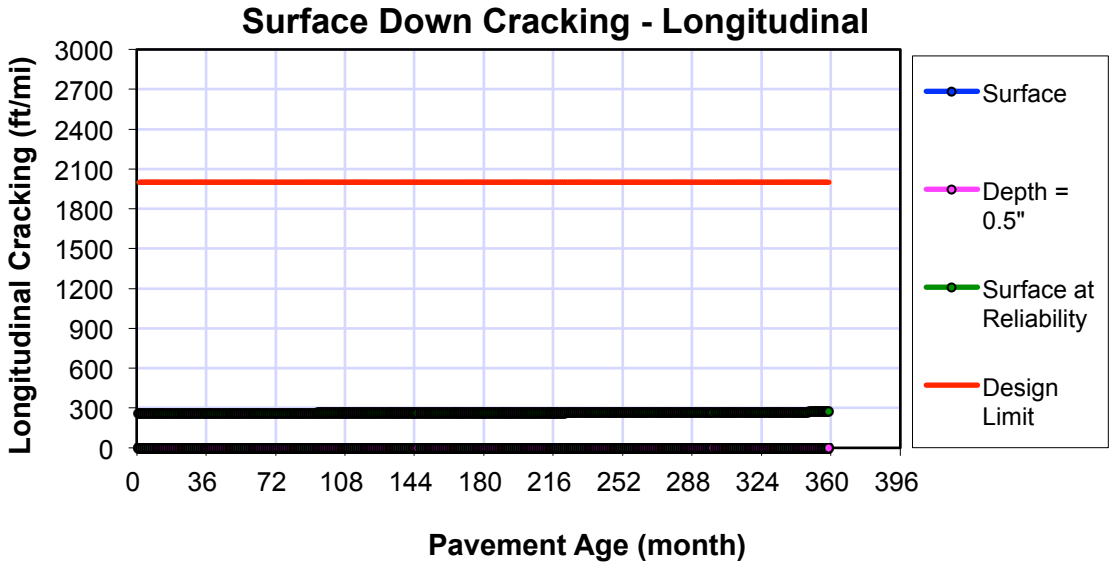

Figure 5.12: Surface Down Cracking of Cell 79 (RPM).

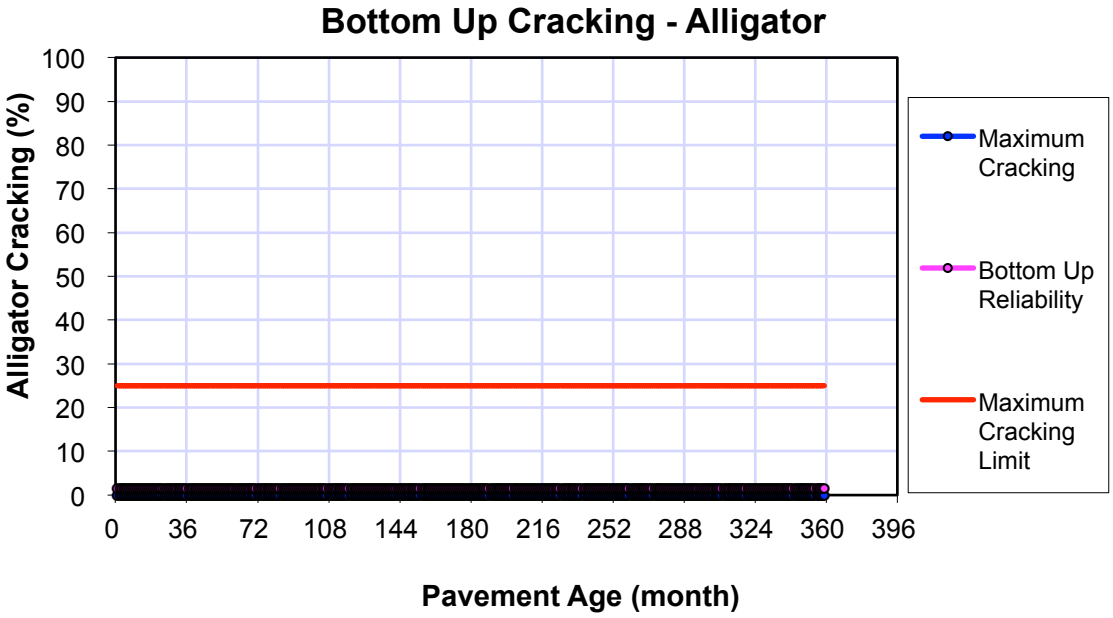

Figure 5.13: Bottom Up Cracking of Cell 79 (RPM).

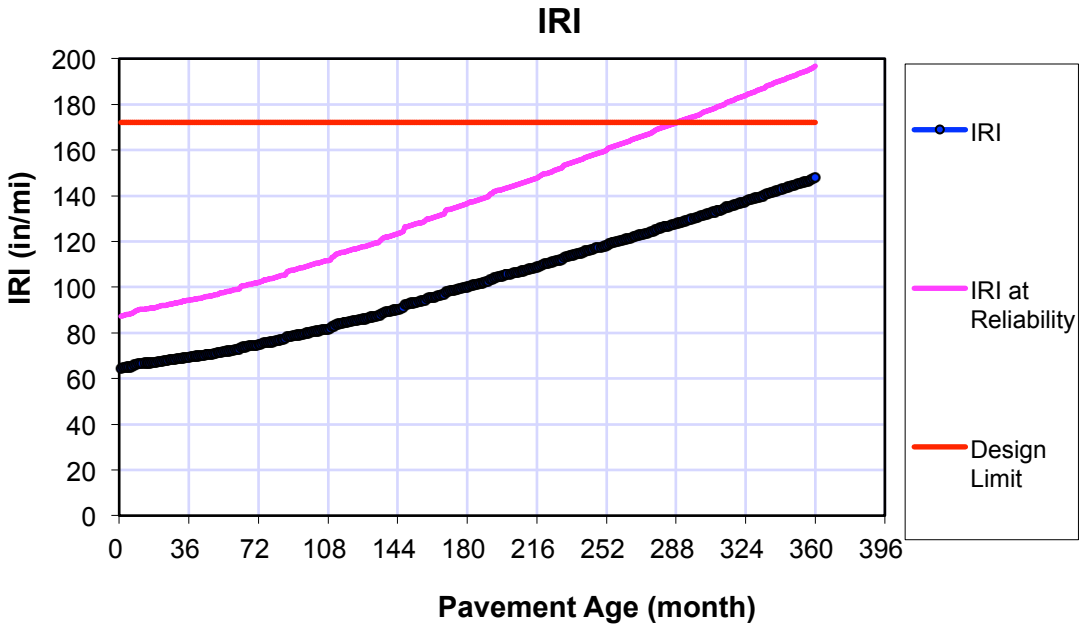

Figure 5.14: IRI of Cell 79 (RPM).

5.2 Life Cycle Cost Analysis

Upon the completion of construction at MnROAD, the initial construction costs are available for comparison between different technologies. The comparison of the initial construction costs are shown in Figure 5.15. As seen from the Figure 5.15, the Cell 79 with fly ash stabilized RPM base has the lowest cost and the Cell 78 with Class 6 aggregate has the highest cost. Some of the costs for Class 6 crushed aggregate and untreated RPM are associated with the second base work, due to the rainfall during the construction. It can be seen that if there were not the re-work of the base course due to weather, the Cell 77 with RPM base would have the lowest cost and the costs of Cell 78 and Cell 79 are comparable.

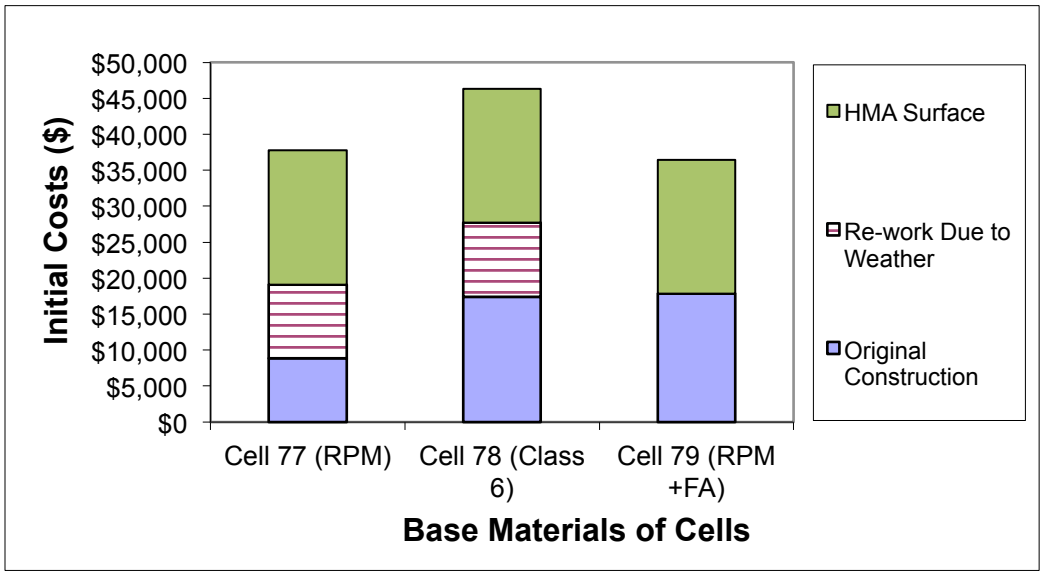

Figure 5.15: Comparison of Initial Construction Costs.

Based on the MEPDG performance prediction, the service life of the Cell 79 with fly ash stabilized RPM, is 23.5 years, which is about twice of the service life of the Cell 77 with RPM base (11 years, Table 5.5), and about three times of the service life of the Cell 78 with Class 6 aggregate base (7.5 years, Table 5.5). The typical rehabilitation of surface milling and HMA overlay was assumed at the end of each service life. It is assumed that the overlay life is essentially same as that of original asphalt pavement life (WisDOT 2011). Therefore, for Cell 77, the rehabilitation would be carried out at 11 and 22 years. At the end of 23.5 years, the pavement would be still there and had a remaining service life of 9.5 years. For Cell 78, the rehabilitation would be carried out at 7.5, 15, and 22.5 years. At the end of 23.5 years, the pavement would be still there and had a remaining service life 6.5 years. The salvage value was considered in the LCCA. A 3% of inflation rate was assumed in the analysis.

For the convenience of comparison, the procedure of the rehabilitation was assumed to consist of milling of the entire roadway surface, the application of tack coat to

the milled surface, placement of HMA overlay, and the compaction of the HMA overlay. The depth of the milling and the thickness of the HMA overlay was assumed to be 3 in. (WSDOT, 2005) for both Cell 77 with untreated RPM base and Cell 78 with Class 6 aggregate base. There will be no rehabilitation within the 23.5 years life cycle analysis period for Cell 79 with the fly ash stabilized RPM base. The cost analysis results were reported as net present value (NPV).

The comparison of the life cycle costs are shown in Figure 5.16 which indicates that, from the life cycle point of view, the Cell 79 with fly ash stabilized RPM base has the lowest cost and the Cell 78 with the Class 6 aggregate base has the highest cost. The ratio of the life cycle cost of Cells 77, 78, and 79 is 1.57: 2.34: 1.

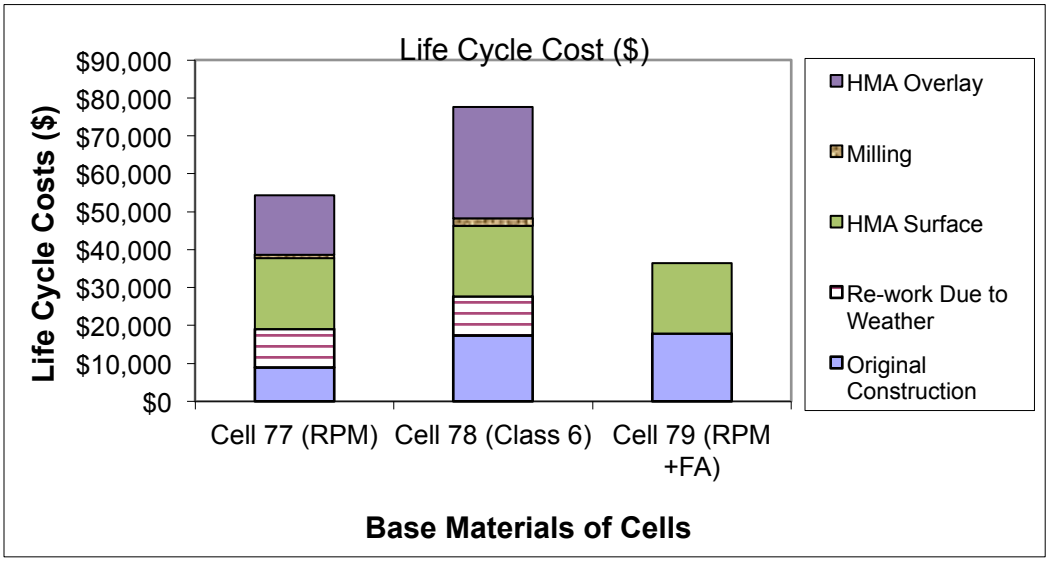

Figure 5.16: Comparison of Life Cycle Costs.

CHAPTER 6: ENVIRONMENTAL ANALYSIS

6.1 Energy and Greenhouse Gases Analysis

As the pavement performance affects maintenance and rehabilitation activities, both the initial and life cycle energy consumption and greenhouse gas emission of Cells 77, 78, and 79 were compared, using the PaLATE program. It should also be noted that, due to the wet weather during construction, the untreated RPM and Class 6 crushed aggregate bases had to be removed and replaced, while the fly ash stabilized RPM base was not affected by the weather.

The method of determining the energy consumption and greenhouse gases emission is relatively straightforward. First, the construction material quantities were determined for original construction or projected rehabilitation. Second, the energy consumption and the greenhouse gases emission per unit construction material were determined as reported by others (Halstead 1981, Meil 2006). Finally, the energy consumption and the greenhouse gases emission were obtained by multiplying the unit value by the quantities of construction materials.

The assumption of the rehabilitation procedure was the same as that in the LCCA. Similarly, at the end of the 23.5 years analysis period, Cell 77 and Cell 78 would have remaining service lives of 9.5 and 6.5 years, respectively., The same procedure as calculating the salvage value in the LCCA was also used in the energy and greenhouse gases analysis.

6.1.1 Energy Analysis

The energy involved in the highway development consists of construction energy, transport energy, processing energy, and calorific energy (Halstead 1981). The

calculation results of the initial and life cycle energy consumption are shown in Table 6.1. The ratio of the life cycle energy consumption between the Cells 77, 78, and 79 is 2.06: 3.12: 1. Figure 6.1 shows the comparison of the initial energy consumption upon the completion of the construction. It can be seen that Cell 79 with the fly ash stabilized RPM base had the lowest energy consumption and Cell 78 with the Class 6 aggregate base had the highest energy consumption. Some of the energy consumption of the crushed aggregate and untreated RPM was associated with the second base work, due to the rainfall during the construction. If there were no the re-work of the base course due to weather, the energy consumption of Cell 77 and Cell 79 which are lower than that of the Cell 78 would be comparable.

Table 6.1: Energy Consumption and Greenhouse Gases Emission of Cell 77, 78, and 79

Items				Energy [MJ]	Total Energy [MJ]	CO2 [Mg] = GWP	Total CO2 [kg]
RPM	Initial Construction	Base	Materials Production	24,425	1,273,149	2.84	27,144
			Materials Transportation	0			
			Processes (Equipment)	3,313		0.25	
			Force Account	77,612		5.00	
		HMA Sruface		623,547		14,149.87	
	Rehabilitation	Milling (twice-salvage)		12,821		1,059.10	
		HMA Overlay (twice-salvage)		531,432		11,926.71	
Class 6 Aggregate	Initial Construction	Base	Materials Production	81,803	1,823,287	7.14	38,542
			Materials Transportation	13,147		0.98	
			Processes (Equipment)	5,435		0.41	
			Force Account	77,612		5.00	
		HMA Sruface		623,547		14,149.87	
	Rehabilitation	Milling (thrice-salvage)		24,069		1,988.28	
		HMA overlay (thrice-salvage)		997,674		22,390.41	
RPM+FA	Initial Construction	Base	Materials Production	24,425	661,728	2.84	14,154
			Materials Transportation	9,141		0.68	
			Processes (Equipment)	4,615		0.35	
			Force Account	0		0.00	
		HMA Sruface		623,547		14,149.87	
	Rehabilitation	no		0		0.00	

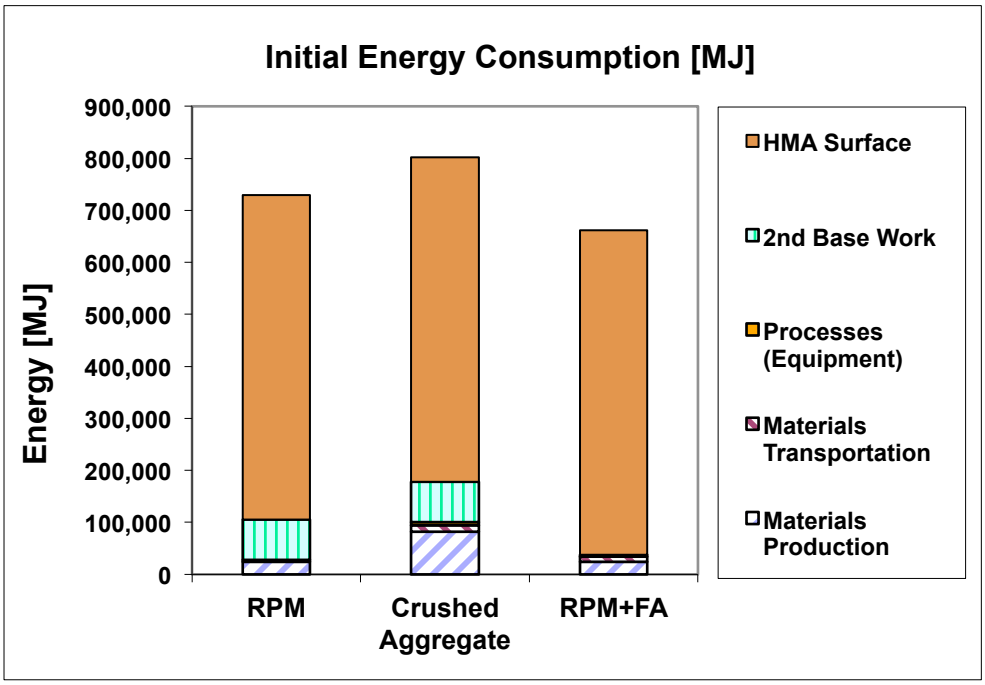

Figure 6.1: Comparison of Initial Energy Consumption.

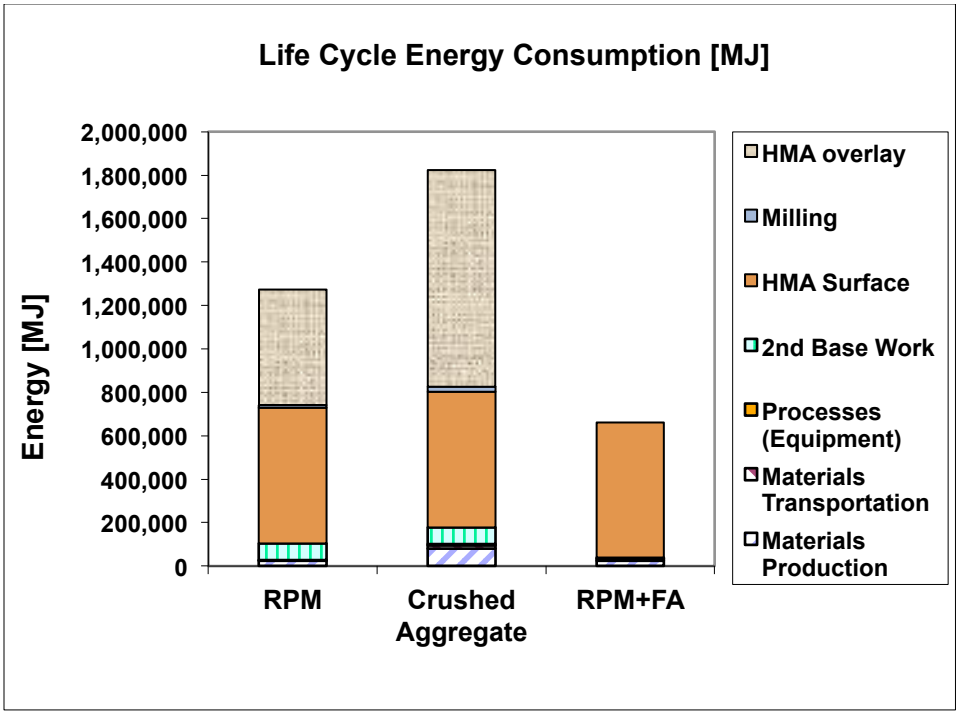

Figure 6.2: Comparison of Life Cycle Energy Consumption.

Similar to the life cycle cost analysis, within the 23.5 years life cycle cost analysis period, Cell 77 was assumed to have one time of rehabilitation with HMA overlay and

Cell 78 was assumed to have two times of rehabilitation with HMA overlay. As indicated by Figure 6.2, the Cell 79 with the fly ash stabilized RPM base has lower life cycle energy consumption than Cell 77 with RPM base, followed by Cell 78 with Class 6 base.

6.1.2 Greenhouse Gases Emissions Analysis

The greenhouse gasses CO_2, CH_4, and N_2O, etc., were converted to a measure of direct global warming potential (GWP) using the well-accepted CO_2 equivalence method as developed by the International Panel on Climate Change. The calculation results are shown in Table 6.1. The ratio of the life cycle CO_2 emission between Cells 77, 78, and 79 is 2.04: 3.09: 1. The comparison of the initial CO_2 emissions and global warming potential (GWP) for the base construction only are shown in Figure 6.3. It can be seen from Figure 6.3 that the Cell 79 with fly ash stabilized RPM base had the lowest CO_2 emissions and the Cell 78 with Class 6 aggregate base had the largest one. As discussed in cost and energy analysis, some of the CO_2 emission of the crushed aggregate and untreated RPM was associated with the second base work.

If the HMA surface is included in the initial construction CO_2 emission analysis, similar results were found. Note that Figure 6.4 is plotted on a log scale of the CO_2 emission, the difference in the CO_2 emission in the initial construction of the base course was actually negligible, when compared to the relatively large CO_2 emission during the initial HMA surface construction. Similarly, the life cycle CO_2 emission was plotted on a log scale as well, as shown in Figure 6.5. It can be seen that the Cell 79 has the lowest CO_2 emission, followed by the Cells 77 and 78.

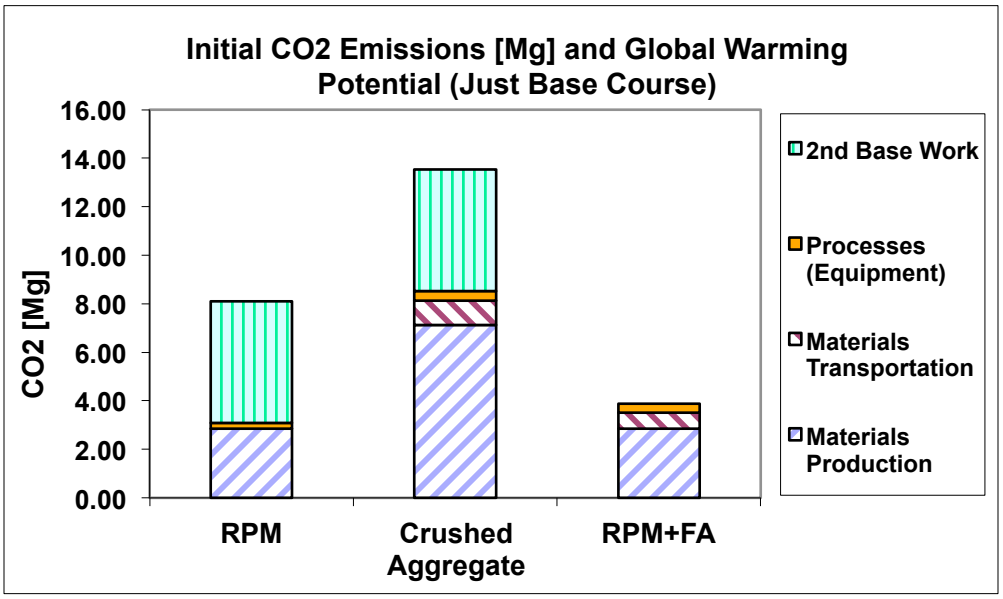

Figure 6.3: Comparison of Initial Greenhouse Gas Emission of Base Construction.

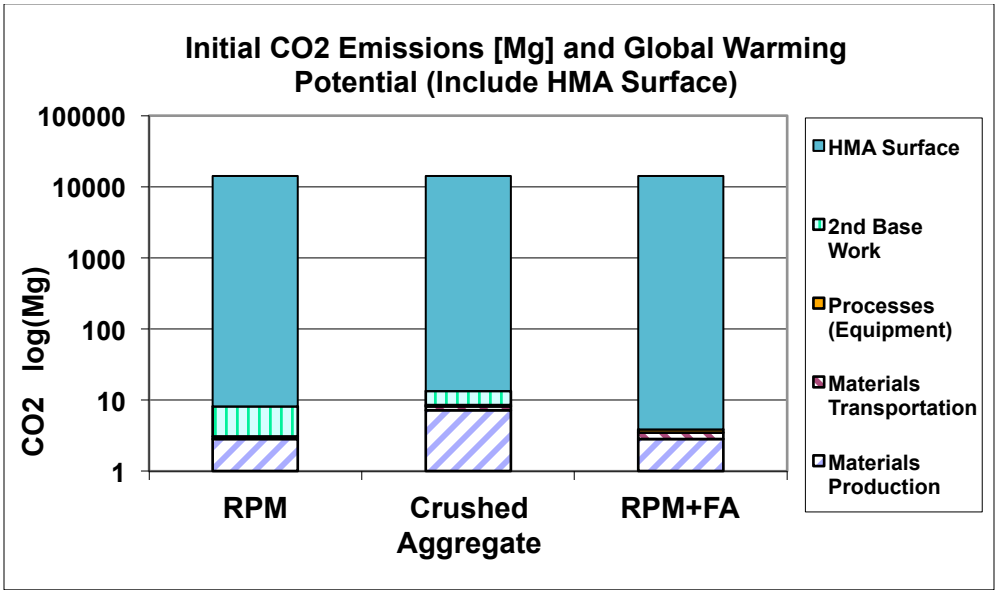

Figure 6.4: Comparison of Initial Greenhouse Gas Emission.

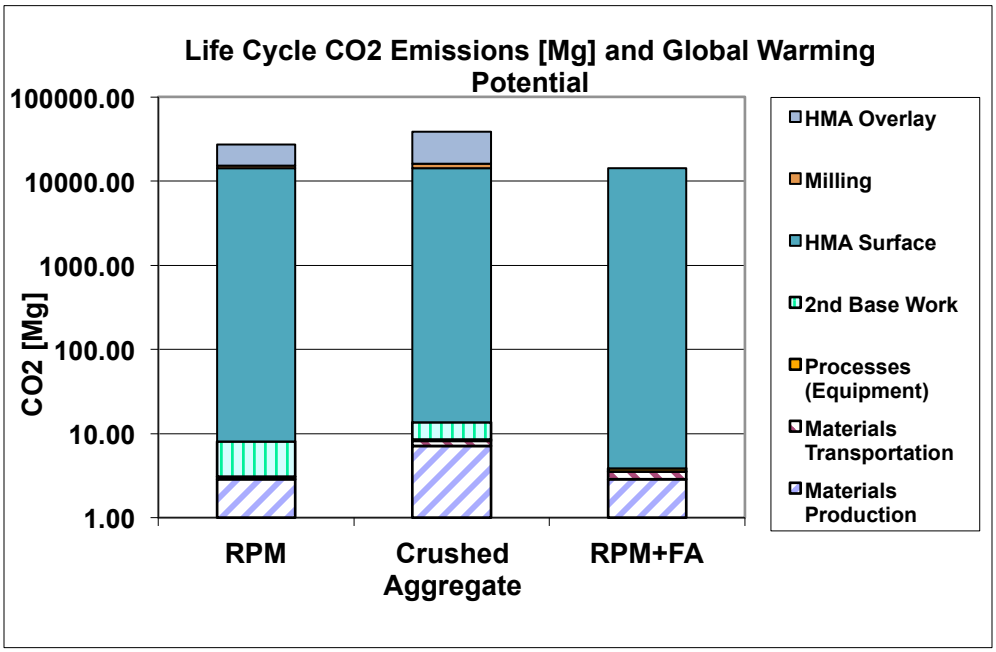

Figure 6.5: Comparison of Life Cycle Greenhouse Gas Emission.

6.2 Leaching Analysis

6.2.1 Methods and Materials

6.2.1.1 Fly Ash

Fly ash is classified based on chemical composition by ASTM C 618 as either Class C or Class F. Fly ash that does not meet the requirements of Class C or F is often referred to as "off-specification". The composition within a class can vary significantly (US EPA 2008). The majority of the fly ash that is recycled in the United States is Class C or F (US EPA, 2008).

Fly ash is in a highly oxidized state and chemically reacts and cements in the presence of water and lime (CaO and CaOH) at standard conditions. Lime may already be present in the ash, constituting a self-cementitious fly ash, or lime may be added too produce cementitious ash. This study employed Riverside 8 cementitious fly ashes for stabilization of base course or subgrade. Riverside 8 fly ashes are from Xcel Energy's

Riverside Power Plant. Chemical and physical properties of one sample of Riverside 8 fly ash are presented as Table 6.2.

Table 6.2: Use Classification of Riverside 8 Fly Ash

Parameter	Percent of Composition	Specifications	
		ASTM C 618	AASHTO M 295
		Class C	Class C
SiO_2 (silicon dioxide) (%)	19		
Al_2O_3 (aluminum oxide) (%)	14		
Fe_2O_3 (iron oxide) (%)	6		
$SiO_2 + Al_2O_3 + Fe_2O_3$ (%)	39	50 Min	50 Min
CaO (calcium oxide) (%)	22		
MgO (magnesium oxide) (%)	5.5		
SO_3 (sulfur trioxide) (%)	5.4	5 Max	5 Max
CaO/SiO_2	1.18		
$CaO/(SiO_2+Al_2O_3)$	0.68		
Loss on Ignition (%)	16.4	6 Max	5 Max
Moisture Content (%)	0.32	3 Max	3 Max
Specific Gravity	2.65		
Fineness, amount retained on #325 sieve (%)	15.5	34 Max	34 Max
Classification	Off-Spec.		

Riverside 8 fly ash was captured using electrostatic precipitators. Fly ashes are classified for use as either Class C or Class F by ASTM C 618 and AASHTO M 295. Riverside 8 does not meet the requirement for Class C or F, and is considered an off-specification ash due to its high carbon content (>5%) (Table 6.2). Elemental composition of the Riverside 8 ash is presented in Table 6.3. The major components of

the fly ash (in descending order) are Ca, Al, S, Fe, Mg, Na, Si, P, K, Ba, and V. All other elements comprised less than 0.1% of the fly ash mass (Table 6.3).

Table 6.3: Total Elemental Analysis of Riverside 8 Ash

Element	Riverside 8 Ash	
	(mg/kg)	% of Total Mass
Ag	0.40	0.000040
Al	66000	6.600000
As	24	0.002400
B	780	0.078000
Ba	2600	0.260000
Be	5.3	0.000530
Ca	120000	12.000000
Cd	5.4	0.000540
Co	28	0.002800
Cr	71	0.007100
Cu	230	0.023000
Fe	36000	3.600000
Hg	0.80	0.000080
K	2600	0.260000
Mg	29000	2.900000
Mn	120	0.012000
Mo	140	0.014000
Na	15000	1.500000
Ni	620	0.062000
P	4800	0.480000
Pb	63	0.006300
S	41100	4.11
Sb	3.3	0.000330
Se	16	0.001600
Si	6700	0.67
Sn	ND	-
Sr	ND	-
Ti	130	0.013000
Tl	1.1	0.00011
V	1400	0.140000
Zn	130	0.01300

6.2.1.2 Bases Course Materials

Particle size distribution of the RPM used at the MnROAD site is presented in Figure 6.6. The RPM classifies as well graded silty gravel (GW-GM) in the USCS system and A-1-a in AASHTO.

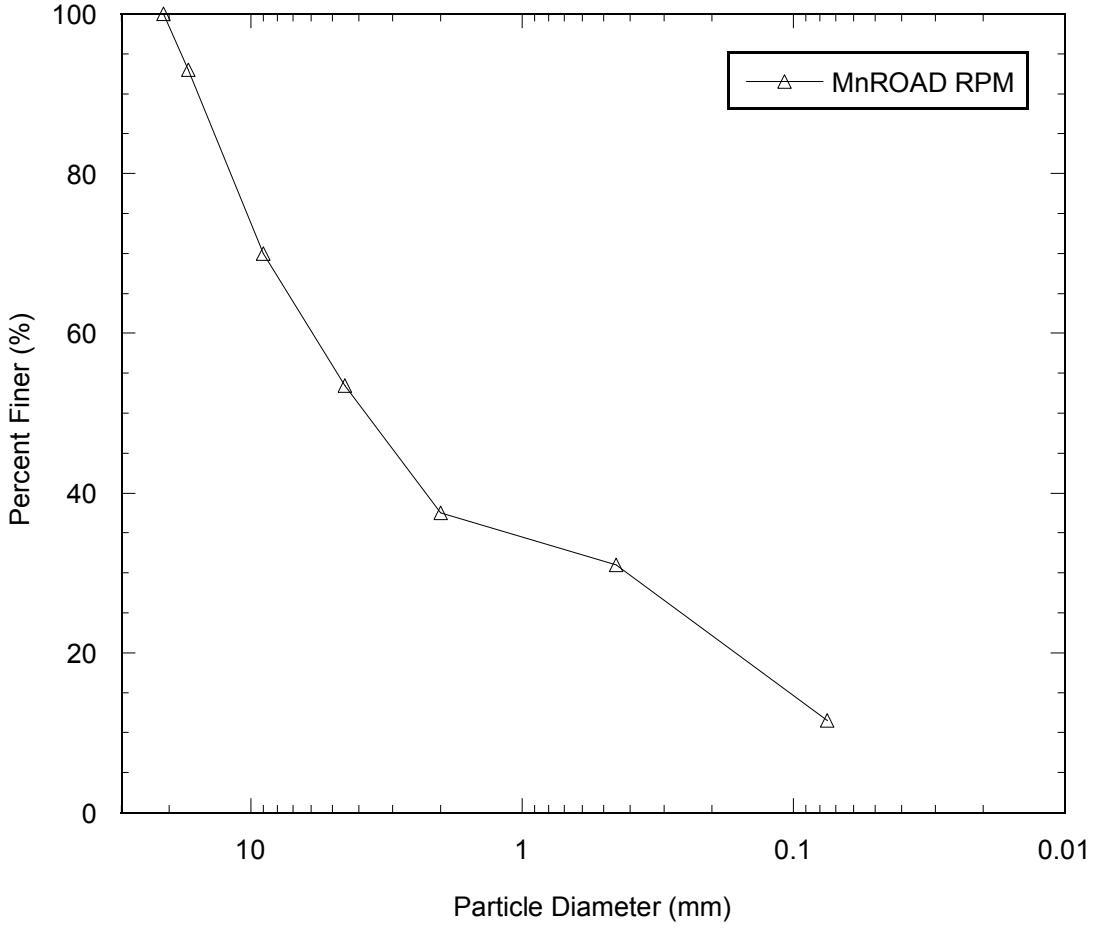

Figure 6.6: Particle Size Distribution of RPM

6.2.1.3 Field Leachate Monitoring

The pan lysimeters were employed in this study to monitor leachate transmitted from the overlying pavement layers. A profile of a pan lysimeter is shown in Figure 6.7. A depression was excavated to the size of the desired lysimeter and the depression

bottom was graded for drainage to a single point. A 120-L HDPE leachate collection tank was installed along the road shoulder, buried approx. 2 m deep. The tanks were connected to the lysimeter through a trench using PVC pipe with adequate drainage gradient from the pan to the tank, and were connected vertically to the surface for leachate collection. The depression was lined with 1.5 mm thick LDPE geomembrane which was connected and heat-sealed to the PVC drainage pipe. A drainage layer consisting of geonet between two layers of geotextile was installed in the lysimeter. The stabilized layers were then compacted above the lysimeter. Photographs of lysimeter construction are located in Appendix A.

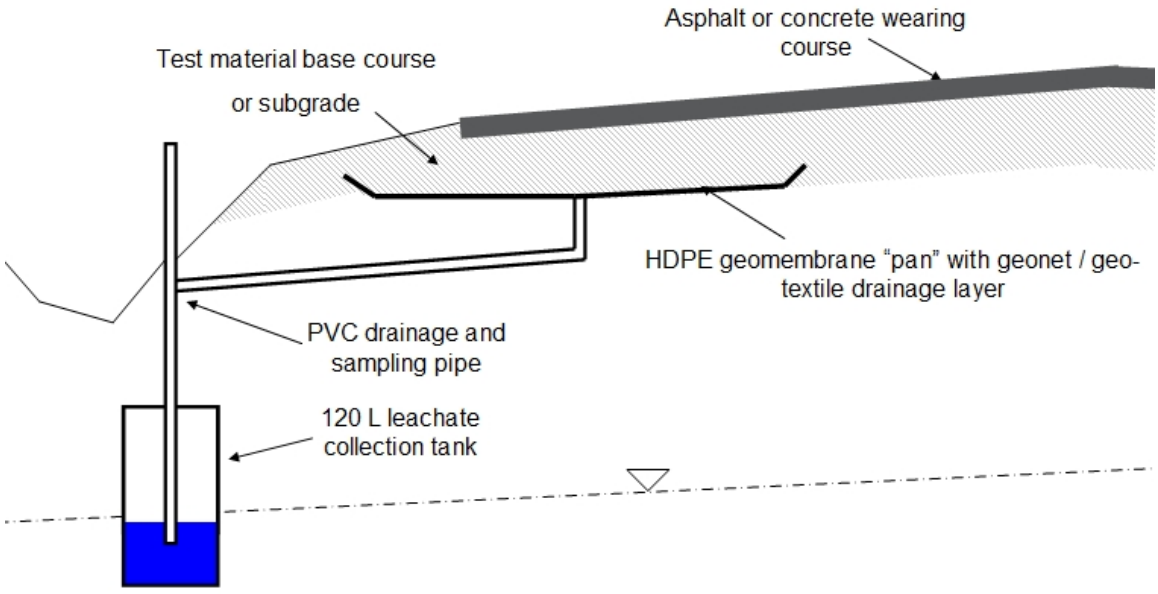

Figure 6.7: Profile of pan lysimeter construction

Leachate in the 120-L tanks was pumped and sampled periodically. Volume of leachate discharged from the layer was recorded and total pore volumes of flow (PVF) were calculated from the porosity of the stabilized layer. Volumetric fluxes from the

layers were compared to local precipitation data. A daily precipitation rate was averaged for each month of the study (mm/day), and flux from the layer (mm/day) was calculated from the volume of leachate collected, the time between tank pumping events, and the area of the lysimeter. Long term average fluxes were calculated from the total volume collected, lysimeter area, and total days of lysimeter operation.

Aqueous samples were collected for chemical analysis during pumping events. All samples were collected in HDPE sample bottles with zero head space. Within 24 hr of sampling pH and oxidation-reduction potential (Eh) were measured in the laboratory. The equipment used to test pH and Eh varied over the course of the study. The leachate was then filtered with a 0.2 μm micropore filter and preserved to pH<2 using trace-metal-grade HNO_3.

6.2.1.4 Laboratory Leach Tests

(1) Column Leach Tests (CLTs)

Column leach tests (CLT) were conducted on materials from MnROAD. The column testing conditions are summarized in Table 6.4. The CLTs were used to evaluate leaching under saturated steady-flow conditions.

Specimens were prepared from each material by compaction to field dry unit weight and water content (Table 6.4). Material was mixed to field water content using deionized water in a spray bottle, and compacted in rigid wall permeameters by mallet and tamp in several lifts. After compaction the stabilized specimens were cured for one week at constant temperature and 100% humidity.

Table 6.4: Properties of Column Leach Testing

Site	Material		
Material	**RPM**	**Class 5 crushed stone**	**Stabilized RPM**
Rigid or Flexible Wall Permeameter	Rigid		
Specimen Diameter (mm)	202		
Specimen Length (mm)	102		
Specimen Volume (mL)	3269		
Effective Confining Pressure (kPa)	0		
Porosity	0.25	0.21	0.25
Dry Unit Weight (kN/m3)	19.4	20.5	19.6
Approx. Darcy Flux (mm/day)	16		

All specimens were permeated from bottom to top with 0.1 M LiBr solution using peristaltic pumps. This solution was chosen to simulate percolate in regions where salt is used to manage ice and snow (Bin-Shafique *et al.* 2006). Neither lithium nor bromide have drinking water maximum contaminant levels (MCLs), and therefore would not be chemicals of interest in the leachate analysis. Effluent was collected in sealed Teflon bags to minimize chemical interaction with the atmosphere. Volume of leachate was measured by weighing the bag afterwards, and total pore volumes of flow (PVF) were calculated using weight-volume computations based on layer compaction and material properties. A

sample was collected for chemical analysis and filtered with 0.2 μm mircopore filters and preserved with trace-metals-grade nitric acid to pH < 2. The Teflon bags were rinsed with deionized water between sampling events.

(2) Water Leach Tests (WLTs)

Water leach tests (WLTs) were conducted on the three materials from MnROAD according to ASTM D3987-85. The stabilized materials were compacted to average field dry unit weight and water content, and then were cured for 7-d at constant temperature and 100% humidity. After curing, the stabilized materials were crushed by hand until the grain size gradation appeared similar to the unstabilized RPM.

WLTs were conducted on all the materials using a 20:1 liquid:solid (L:S) ratio (by mass) with deionized water as the eluent as described in the ASTM D3987-85. The materials were also tested with deionized water at 3:1, 5:1, and 10:1 L:S ratios. Only the 20:1 ratio is described in the standard.

Leaching was conducted in 2-L HDPE bottles rotated for eighteen hours. Afterwards the solids were allowed to settle 5 min., and then a sample was collected from the supernatant using a wide mouth syringe. The sample was filtered with 0.2-μm micropore filters, and preserved to < pH of 2 using trace-metal-grade HNO_3. Pictures of the WLTs are in Appendix A.

6.2.1.5 Leachate Analysis

(1) Chemical Indicator Parameters

The pH and oxidation-reduction potential (Eh) of all field and laboratory leachate samples were measured in the laboratory within 24 hours of sampling. The water quality instruments used for leachate testing varied between sites and over the years of testing.

(2) Major and Minor Elements

The methods used for chemical analysis were inductively coupled plasma (ICP) and cold vapor atomic fluorescence spectrometry (CVAFS). These methods with the dates of use, chemicals analyzed for, and minimum detection limits are summarized in Table 6.5.

Table 6.5: Minimum detection limits of chemical analytical methods used throughout the monitoring program. All MDLs are in µg/L. Hyphens indicate elements that were not tested with the method indicated

Site	**MnROAD**	
Element	ICP-OES	CVAFS
Ag		-
Al	2.5	-
As	2.0	-
B	4.0	-
Ba	0.04	-
Be	1.0	-
Cd	0.2	-
Co	0.6	-
Cr	0.5	-
Cu	0.7	-
Hg		0.001
Fe	3.2	-
Mn	0.05	-
Mo	0.5	-
Ni	0.7	-
Pb	4.0	-
Sb	3.0	-
Se	17	-
Sn	5.0	-
Sr	0.3	-
Ti	0.4	-
Tl	4.7	-
V	0.1	-
Zn	0.1	-

Field and laboratory leachates for were analyzed by inductively coupled plasma - optical emission spectrometry (ICP-OES) using a Varian Vista-MPX CCD Simultaneous ICP-OES instrument for 23 elements. The analytes tested for using ICO-OES are presented with MDLs in Table 6.5.

Beginning in 2008 leachate from field lysimeters was sampled and analyzed for mercury (Hg) using USEPA Method 1631, Revision E: Mercury in Water by Oxidation, Purge and Trap, and Cold Vapor Atomic Fluorescence Spectrometry (CVASF). All sampling equipment that contacted the leachate samples was acid cleaned, dried, and double bagged in cleaned and sealed bags. Samples were collected using two people following the procedure in USEPA Method 1669. In this method, one person only touched the sample bottle and the inner of the two bags containing the bottle. Handling of the outer of the two bags containing the sample bottle and all other equipment and was conducted by the other person. A field blank and duplicate sample were collected for every 10 to 15 lysimeters sampled. Samples were collected in LDPE bottles with zero head space All Samples were maintained at 4° C, and were preserved and analyzed according to USEPA Method 1631.

Minimum detection limits (MDL) for ICP-OES and CVAFS are determined for each instrument and set of calibration solutions according to US Code of Federal Regulations Title 40, Appendix B to Part 136. The method and analytes tested for are presented with MDLs in Table 6.5.

6.2.2 Results and Discussion

6.2.2.1 Field Leaching Behavior

(1) Precipitation Patterns and Lysimeter Drainage

The flux of leachate from the bottom of the stabilized RPM and control layers was compared to the local precipitation rate for the site location. Short-term leachate fluxes and precipitation rates from stabilized RPM are shown in Figure 6.8. Peak fluxes from the layers tend to occur in the spring months when heavy rains and snowmelt occur, and again in late summer and early fall (Figure 6.8). The minimum flux tends to occur in the winter when precipitation and pore water are often frozen, and in July or August when evaporation tends to exceed precipitation in the upper Midwest. Occasionally the flux from the stabilized layers approaches 15% of precipitation (Figure 6.8). However, as shown subsequently, the long-term average is never more than 7.8% for stabilized RPM (Figure 6.9). Short-term fluxes were calculated from the volume of leachate collected during each pumping event, the surface area of the lysimeter pan, and the time between pumping events (Flux = Volume/Area/Time). The daily precipitation corresponds to an average of the precipitation per day during each month (Figures 6.8 and 6.9) (NOAA 2009).

Long-term fluxes from the pavement layers and precipitation rates averaged over the entire time of the study are shown in Figure 6.4. Long-term flux of leachate discharged from the fly-ash-stabilized layers was 7.8% of the local precipitation. Flux from the RPM control base course was 6.1% of precipitation and flux from the stone aggregate base course was 14% of precipitation (Figure 6.9).

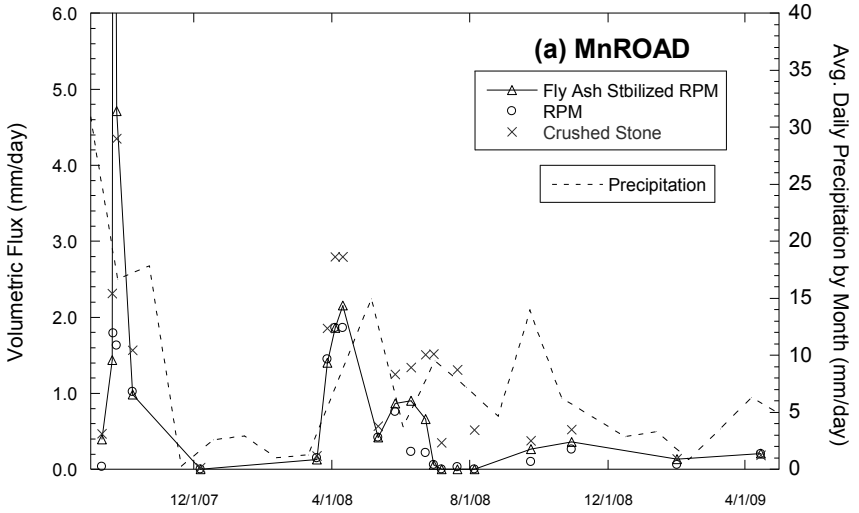

Figure 6.8: Volumetric flux from the stabilized RPM base courses and control layers with local average daily precipitation rates

The regional average percentage of precipitation recharging the groundwater is estimated to range from 19% to 24% for the MnROAD site (USGS 2007). The asphalt wearing course on the roadway likely has lower permeability than adjacent road shoulder and native soils. Therefore recharge rates in the areas adjacent to a stabilized roadway may be significantly higher than the percentage of precipitation that leaches from the stabilized layers, which may affect the transport of leachate in the subsurface.

According to the US National Weather Service (May 2009), the annual precipitation in the region that includes MnROAD ranges from approximately 500 mm to 900 mm, with an average of 750 mm. Based on the leachate volumes collected, total annual flux from a stabilized base course in eastern-central Minnesota should range from 11 to 70 mm/year.

Long-term fluxes from the layers were calculated from the total volume of leachate collected, the surface area of the lysimeter pan, and the total time of leachate

collection, and are shown in Figure 6.9 with long-term average precipitation rates for each site during the testing periods (NOAA 2009). The long-term average precipitation was calculated as the total precipitation during the study divided by the total time of the study.

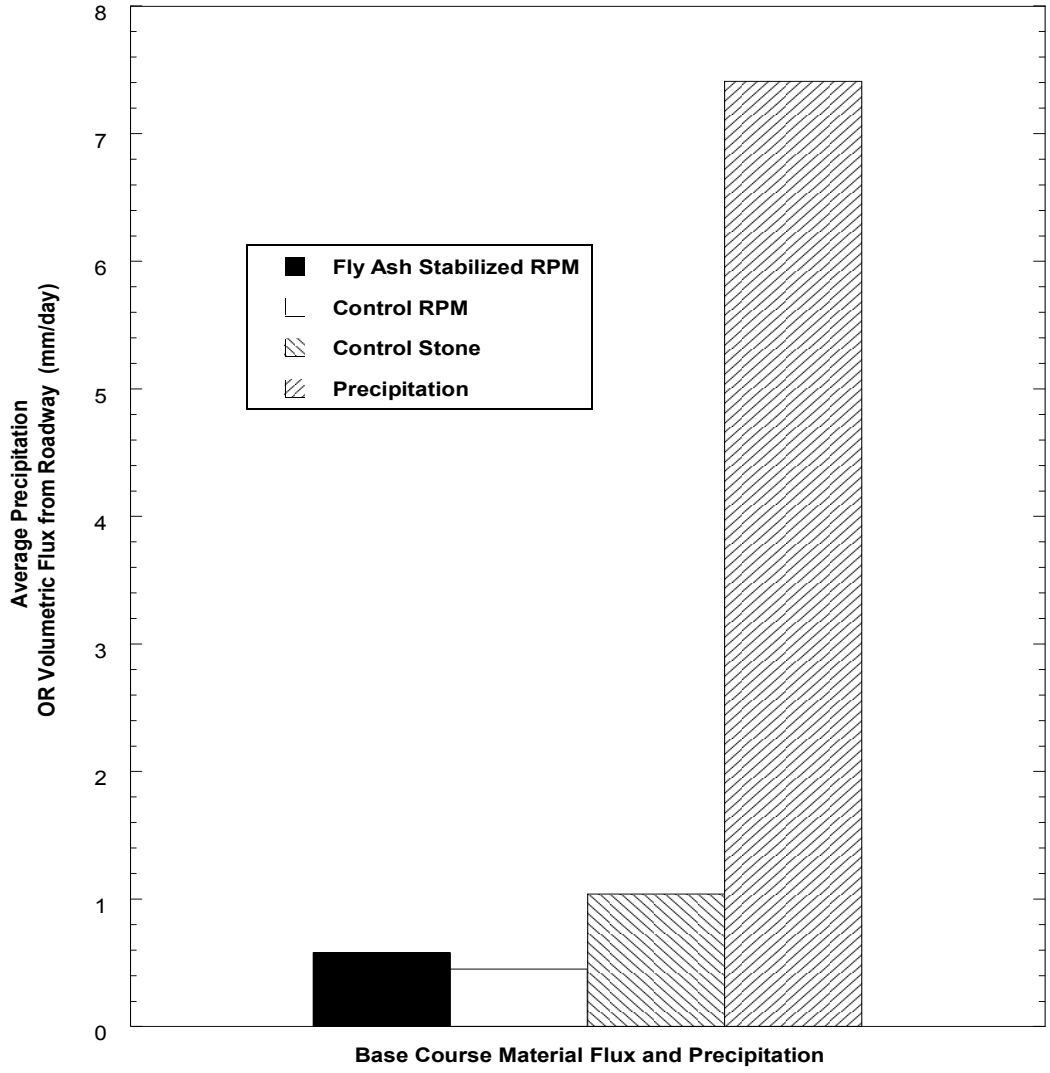

Figure 6.9: Comparison of Long-term Volumetric Flux from the Road Layers Relative to Average Daily Precipitation

(2) Chemical Indicator Parameters

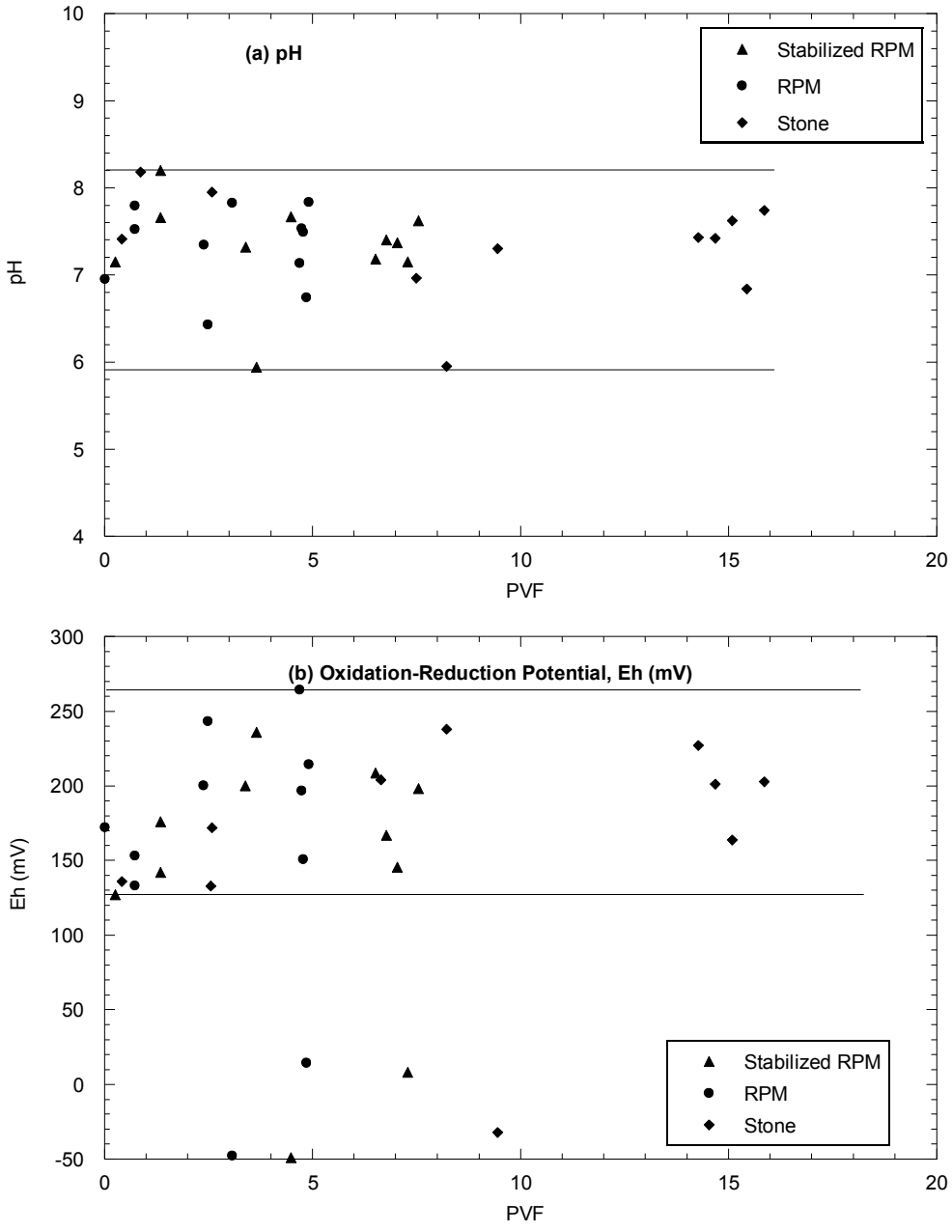

Figure 6.10: (a) pH and (b) Eh of Leachate from Field Lysimeters for Fly-ash-stabilized and Control Materials.

The pH and Eh of the leachates collected in the lysimeters are presented in Fig. 4.3. The pH in field leachate ranged from 5.9 to 8.2, with most of the data between 7 and 8 (Figure 6.10.a) for both stabilized and control materials. Ganglof *et al.* (1997) found near neutral pH in leachate collected from fly ash amended sandy soil using ceramic-cup pore-water lysimeters in an agricultural field. The leachate from all materials was oxidizing (Eh > 0), with Eh data ranging from -50 to 264 mV but most of the data in the range of +121 to +250 mV. The Eh of leachate from the stabilized RPM appears becoming more oxidizing as the total PVF increases (Figure 6.10.b). All field leachates were clear to yellow and had no noticeable odor.

(3) Elements Released and Magnitude of Concentrations

Of the twenty-three trace elements considered in the analysis (Ag, Al, As, B, Be, Cd, Co, Cr, Cu, Fe, Hg, Mn, Mo, Ni, Pb, Sb, Se, Sn, Sr, Ti, Tl, V, and Zn), all except Al, Be, Pb, and Ti were present in detectable quantities in leachate from the fly-ash-stabilized RPM. The elements detected in the leachate are presented in Table 6.6 with the peak concentration and average peak concentration (average of the three highest concentrations). The following elements are presented in order of descending peak concentration observed in leachate from the fly-ash-stabilized materials (Table 6.6): Mo (peak concentration of 18,176 μg/L), Sr, B, Mn, and V (peak concentration between 10,000 and 1,000 μg/L), Fe, Se, Zn, Tl, Cr, and As (peak concentration between 1,000 and 100 μg/L), and Sb, Sn, Cu, Cd, Ni, Co, and Ag (peak concentration between 100 and 1 μg/L). Peak concentration of Hg was less than 0.1 μg/L.

Table 6.6: Magnitude of Peak Concentrations and the Average of the Three Highest Concentrations in Field Leachate

Element	Peak Conc. (µg/L)	Average Peak Conc. (µg/L)
Mo #	18176	11710.00
Sr #	7770	5161
B #	4151.85	3739
Mn ^	1094.57	439.5
V #	510	316.7
Fe ^	442.81	157.75
Se *	392.84	229.7
Zn ^	301.58	135.4
Tl ^	228.8	170.8
Al ^	172.15	155.0
Cr *	119.18	81.25
As ^	107.46	69.15
Sb ^	95.2	45.73
Sn #	65.5	27.12
Cu ^	12.83	10.93
Ag *	8.9	4.23
Cd *	7.69	5.23
Ni ^	4.84	4.384
Co ^	3.44	3.22
Ti #	1.49809	1.16603
Hg $	0.01	0.01
Be ^	All BDL	All BDL
Pb ^	All BDL	All BDL

BDL - below detection limit
NT - element not tested for at site

@ - concentration is out of method calibration range, and is estimated from linear extrapolation

(4) Elution Patterns

Concentrations of each element recorded in each lysimeter are reported as a function of PVF in Appendix B. Among elements that were detected at the site, 72% of

elements had the peak concentration occur during the first two PVF (Table 6.7). As an example of early peak concentration, the leaching pattern of Cd and Cr is shown in Figure 6.11.

Table 6.7 Elements with peak concentrations occurring during or after the first 2 PVF

Element	Timing of Peak Concentration
Ag	▼
Al	X
As	▼
B	X
Be	ND
Cd	▼
Co	▼
Cr	▼
Cu	X
Fe	X
Mn	X
Mo	▼
Ni	▼
Pb	X
Sb	▼
Se	▼
Sn	X
Sr	X
Ti	X
Tl	X
V	X
Zn	X

▼ - Peak Concentration occurred during the first 2 PVF
X - Peak Concentration occurred after the first 2 PVF
ND - All concentrations were below detection limit

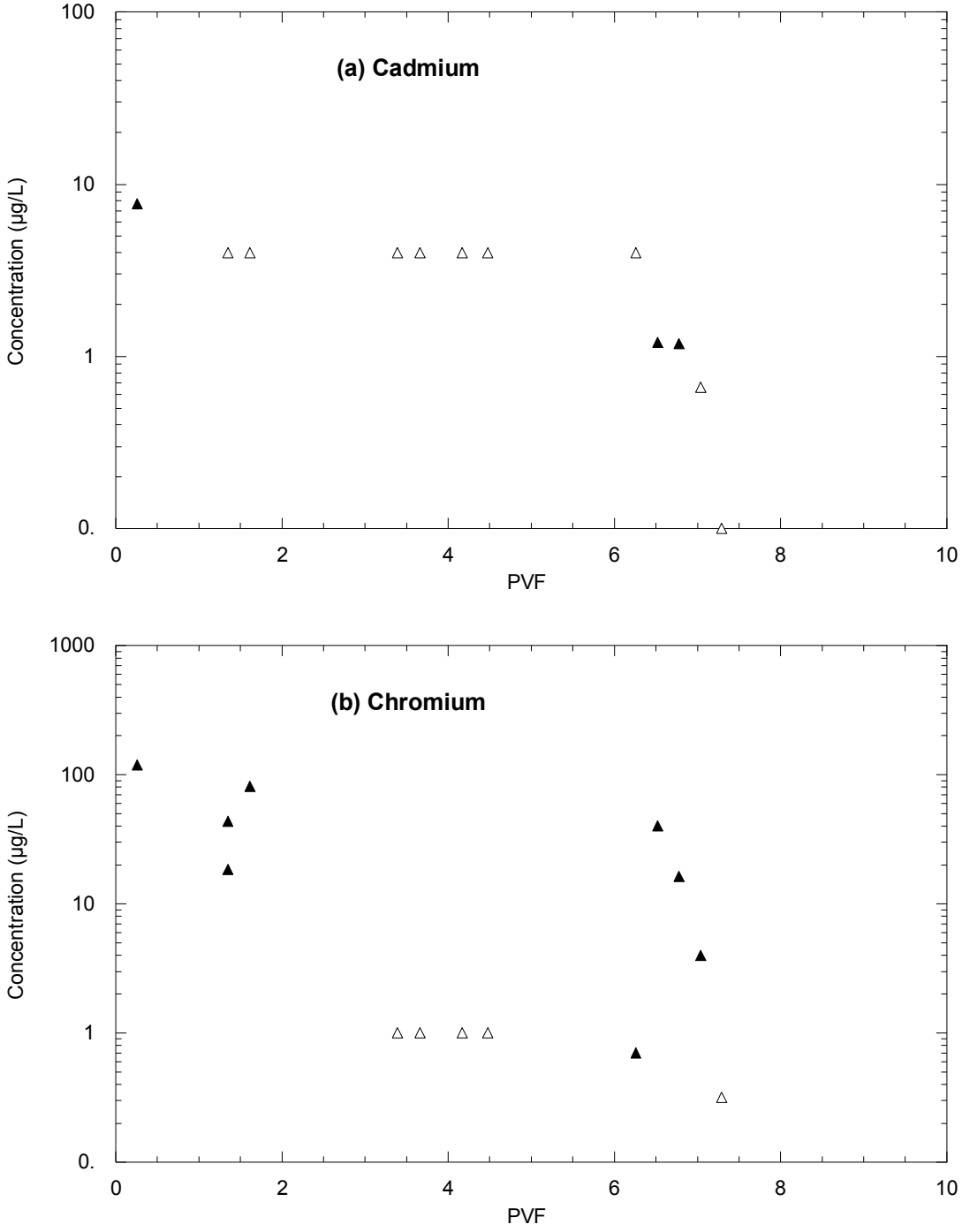

Figure 6.11: Peak Concentrations occurring during first 0.2 PVF for (a) cadmium and (b) chromium.

6.2.2.2 Potential Environmental Impacts

(1) Field Concentrations Compared to Control Sections

An analysis was conducted to determine if element concentrations in leachate from stabilized materials were elevated relative to concentrations in leachate from adjacent control sections. The average peak concentration and the geometric mean of all observed concentrations for each site and element were compared. The determination of concentration elevation was conducted using Equation (6.1).

If: $(C^*_c + 2\sigma) \geq (C^*_s - 2\sigma)$ (6.1)

Then, the concentration from stabilized material *was not* significantly elevated relative to concentration from control material.

If : $(C^*_c + 2\sigma) \leq (C^*_s - 2\sigma)$ (6.1)

Then, the concentration from stabilized material *was* significantly elevated relative to concentration from control material.

where: C^*_s = Average peak or geometric mean concentration from stabilized materials,

C^*_c = Average peak or geometric mean concentration from control materials,

σ = Standard deviation.

σ was obtained as a product of the average peak or geometric mean concentration and the coefficient of variation (COV), and COV for each element was calculated from 7 replicates tested on the ICP-OES at 20 μg/L.

10 of the 23 elements had average peak concentrations (average of the three highest concentrations) or geometric mean (of all samples) concentrations that were elevated in leachate from stabilized materials relative to the concentration from the

control materials. These (in order of descending magnitude of concentration elevation): Mo, B, V, Sr, Cr, Se, As, Mn, Cu, and Cd (Table 6.8).

Table 6.8: Comparison of field concentrations from fly ash stabilized sections and control sections to determine if element is statistically elevated in the stabilized material leachate. Elevated concentrations in stabilized material leachate are highlighted.

Element	Ratio of Stabilized Concentration / Control Concentration	
	Average Peak Concentration	Geometric Mean of Concentrations
Mo	**52.2**	**48.5**
B	**19.2**	**16.1**
V	**28.6**	**15.2**
Sr	**10.1**	**4.7**
Cr	**14.2**	**4.2**
Se	**5**	**1.4**
As	**1.4**	**1.3**
Mn	**0.6**	**1.3**
Cu	**1.8**	**1.2**
Cd	**1.3**	**1.1**
Al	**1**	**1**
Be	**1**	**1**
Co	**0.9**	**1**
Ni	**1**	**1**
Pb	**1**	**1**
Ti	**1**	**1**
Ag	**0.4**	**0.9**
Fe	**1**	**0.9**
Sb	**0.1**	**0.7**
Tl	**1.1**	**0.7**
Zn	**0.7**	**0.6**
Hg	**0.5**	**0.2**
Sn	**0.03**	**0.1**

(2) Elements Exceeding Regulatory Maximum Contaminant Levels

Concentrations of all elements observed in lysimeter leachates were compared to the maximum contaminant levels (MCLs) for groundwater or drinking water promulgated by the States of Minnesota (Minnesota - MN MDH IC 141-0791). The US government also has enforceable MCLs for groundwater (US CFR Title 40 Chapter 141.62), but the State MCLs are equal to or lower than those promulgated by the US government (Table 6.9). Please note that although Minnesota does not have a MCL for Mo, the Wisconsin MCL was used to compare Mo concentrations.

Table 6.9: USEPA and Minnesota, maximum contaminant limits (MCLs) for groundwater and drinking water

Element	MN MCL (µg/L)	USEPA MCL (µg/L)
Ag	-	30
As	10	-
B	600	-
Ba	2000	2000
Be	4	0.08
Cd	4	5
Co	-	-
Cr	100	100
Cu	-	-
Hg	2	-
Mo*	-	-
Ni	100	-
Pb	15	-
Sb	6	6
Se	30	50
Sn	4000	-
Tl	0.6	2
V	50	-
Zn	-	2000

*WI

Concentrations of the following ten elements in lysimeter leachate from fly-ash stabilized materials exceeded MCLs at least once: As, B, Cd, Cr, Mo, Pb, Sb, Se, Tl, and V (Table 6.10). The other thirteen elements never exceeded an applicable MCL in leachate from stabilized materials. Concentrations observed in the lysimeters are only representative of leachate as it exits the bottom of the stabilized or control layer, and do not represent concentrations as leachate drains downward from the pavement through the unsaturated zone and then merges with local groundwater flow. Adriano *et al.* (2002) found elevated As, B, Be, Ba, Mo, and Se in pore water in fly ash amended soil, but found all these elements were below detection limits in groundwater collected from a depth of 3.6-m below the amended soil.

Table 6.10: Ratio of average peak concentration or geometric mean of all concentrations to MCLs in field leachate

Ratio for Average Peak Concentrations										
Element	**As**	**B**	**Cd**	**Cr**	**Mo**	**Pb**	**Sb**	**Se**	**Tl**	**V**
Stabilized RPM	11	2.5	1.5	1.2	450*	1.3	24	13	380	10
RPM	9.1	-	-	-	11*	1.3	260	-	380	-
Stone	5.3	-	-	-	-	1.3	6.8	-	460	-
Ratio for Geometric Mean of Concentrations										
Element	**As**	**B**	**Cd**	**Cr**	**Mo**	**Pb**	**Sb**	**Se**	**Tl**	**V**
Stabilized RPM	3.8	-	1.1	-	8.7	1.3	2.7	-	52.0	1.3
RPM	2.9	-	-	-	-	1.3	3.6	-	73.9	-
Stone	3.2	-	-	-	-	1.3	2.5	-	87.2	-

(3) Concentrations Exceeding MCL and Elevated Compared to Control

Concentrations of B, Mo, V, Cr, As, and Cd in leachate from fly-ash-stabilized materials exceeded MCLs and were elevated relative to the adjacent control sections (Figures 6.12 to 6.17) (Table 6.8).

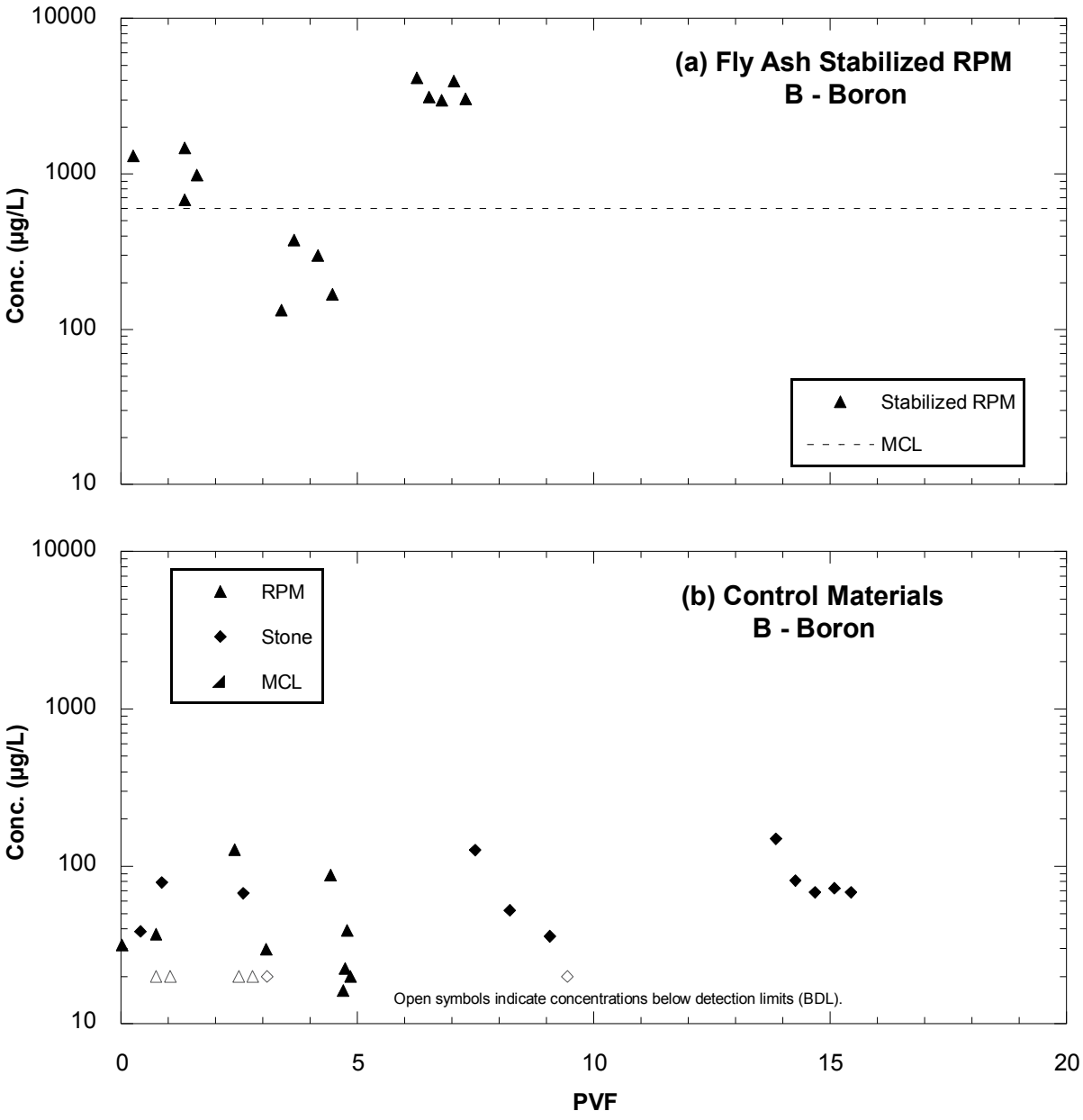

Figure 6.12: Boron (B) concentrations in leachate from field base course composed of (a) fly-ash-stabilized RPM, and (b) control materials.

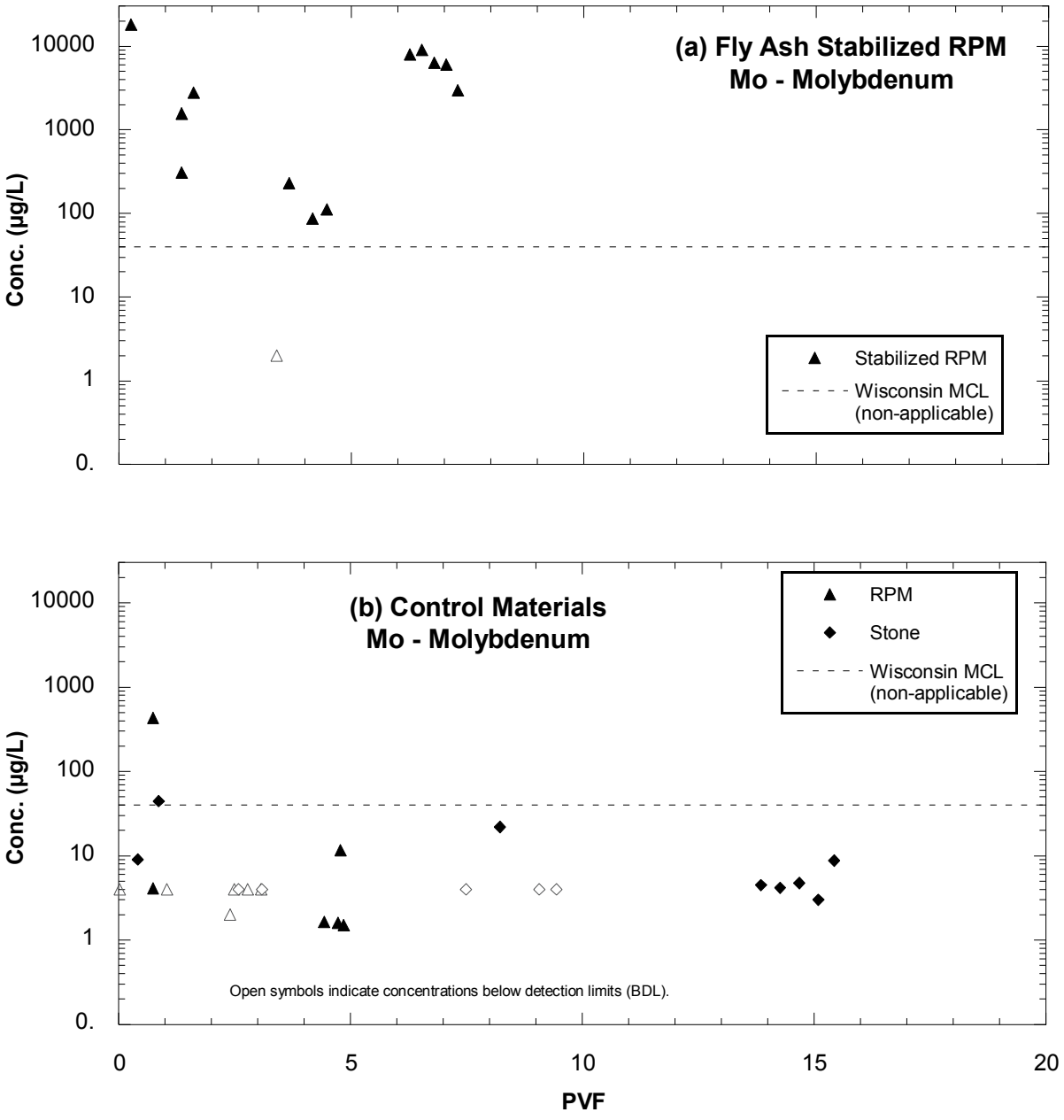

Figure 6.13: Molybdenum (Mo) concentrations in leachate from field base course composed of (a) fly-ash-stabilized RPM, and (b) control materials. Concentrations are compared to the MCL from Wisconsin.

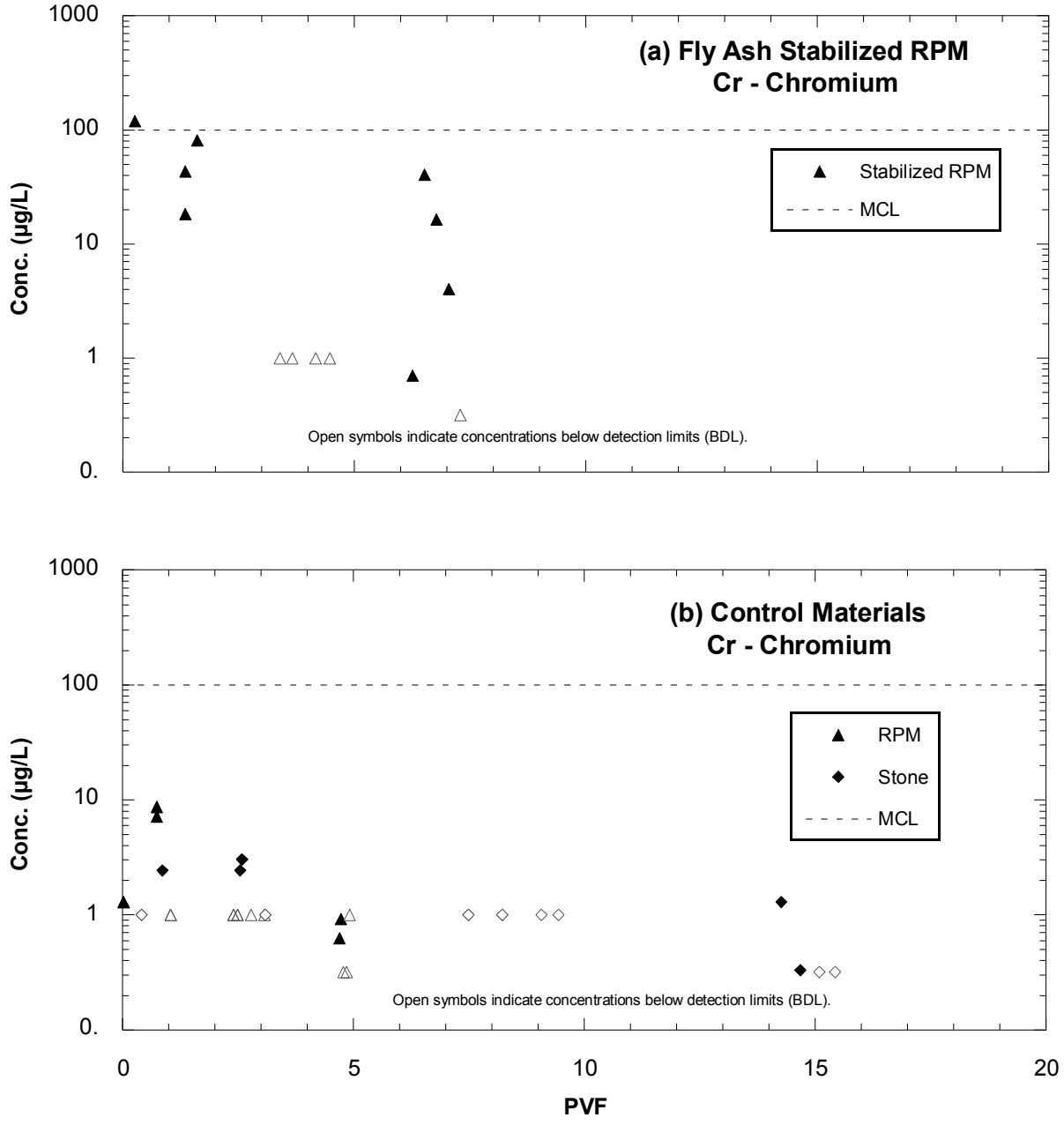

Figure 6.14: Chromium (Cr) concentrations in leachate from field base course composed of (a) fly-ash-stabilized RPM, and (b) control materials.

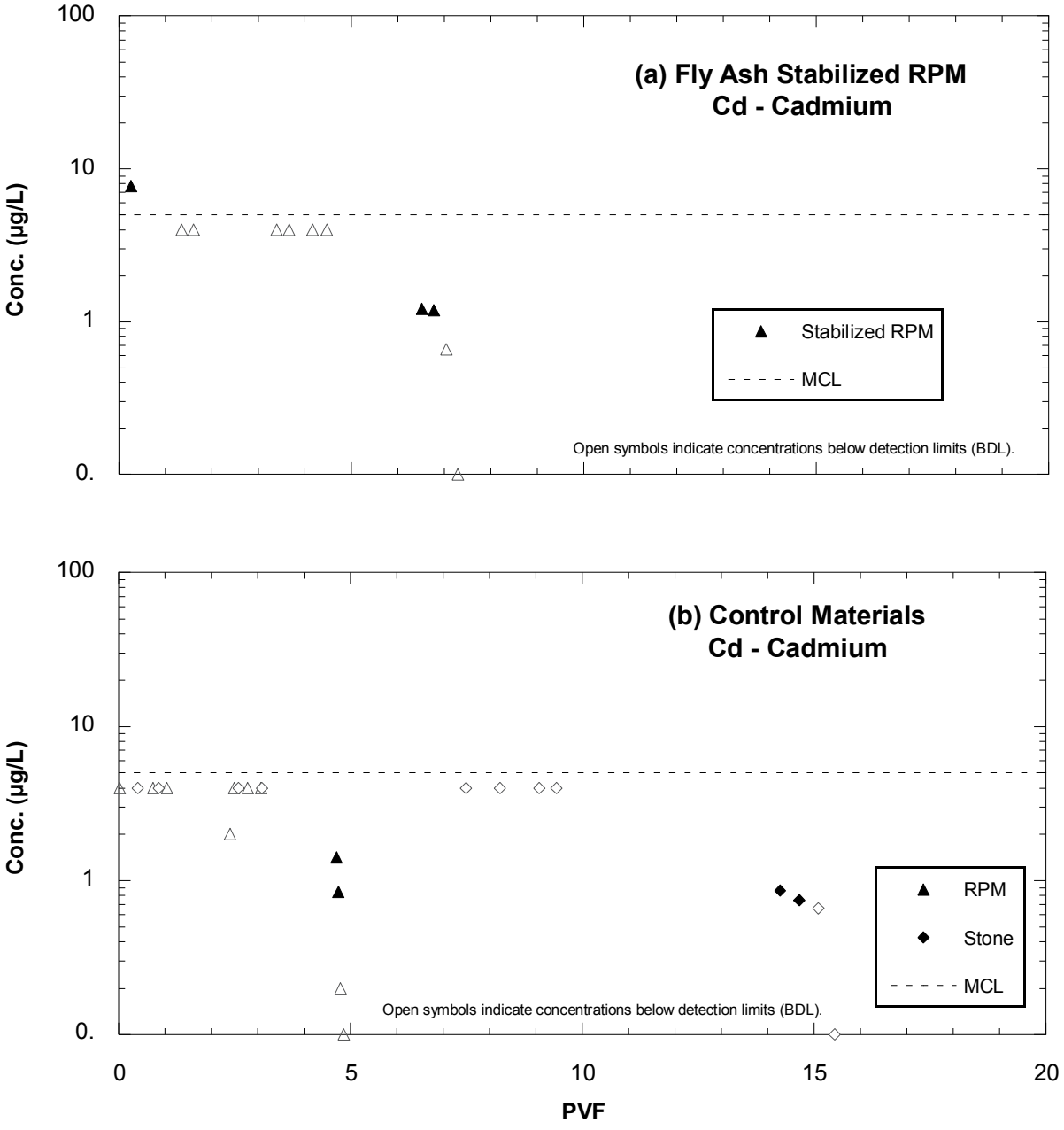

Figure 6.15: Cadmium (Cd) concentrations in leachate from field base course composed of (a) fly-ash-stabilized RPM, and (b) control materials.

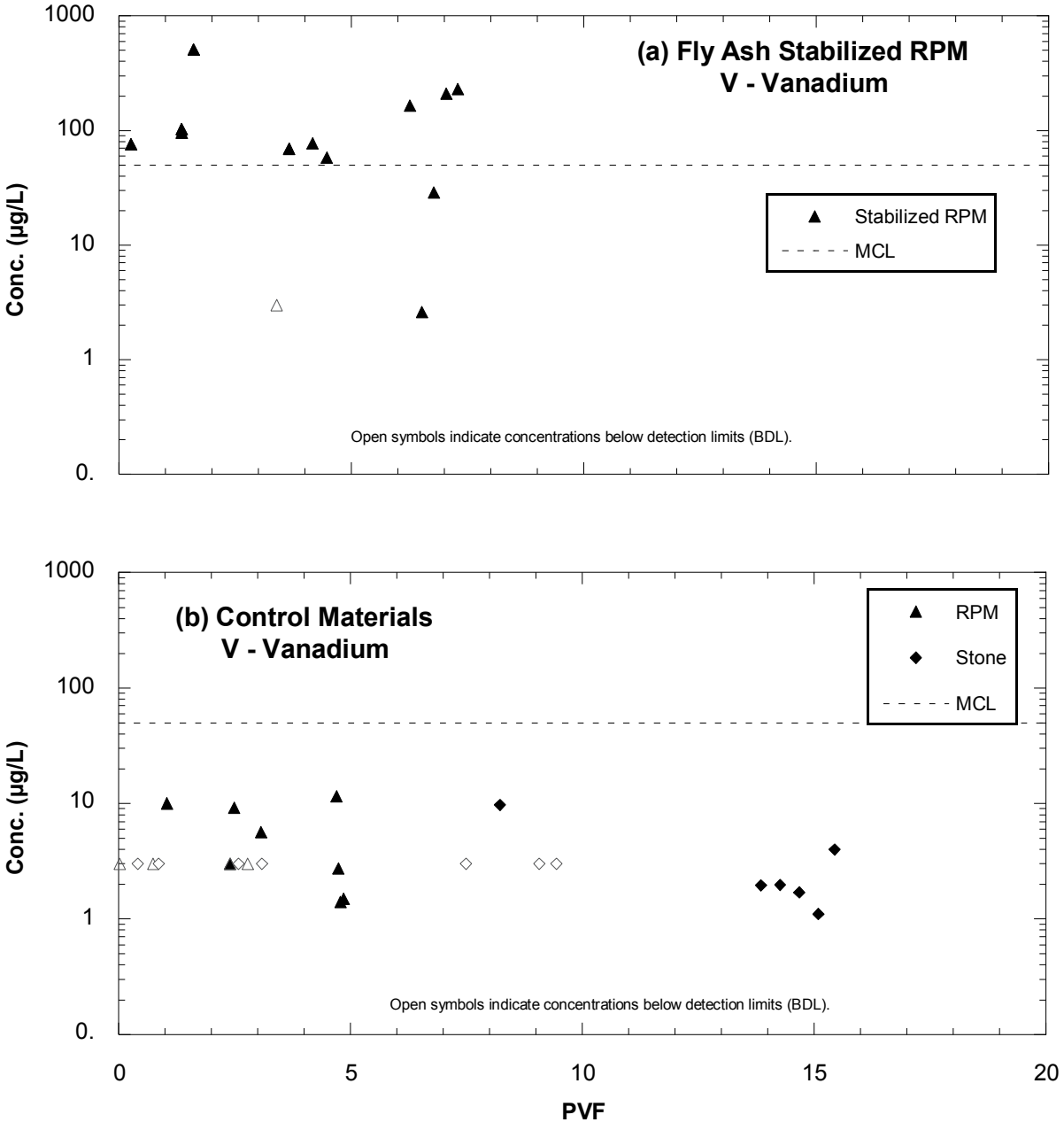

Figure 6.16: Vanadium (V) concentrations in leachate from field base course composed of (a) fly-ash-stabilized RPM, and (b) control materials.

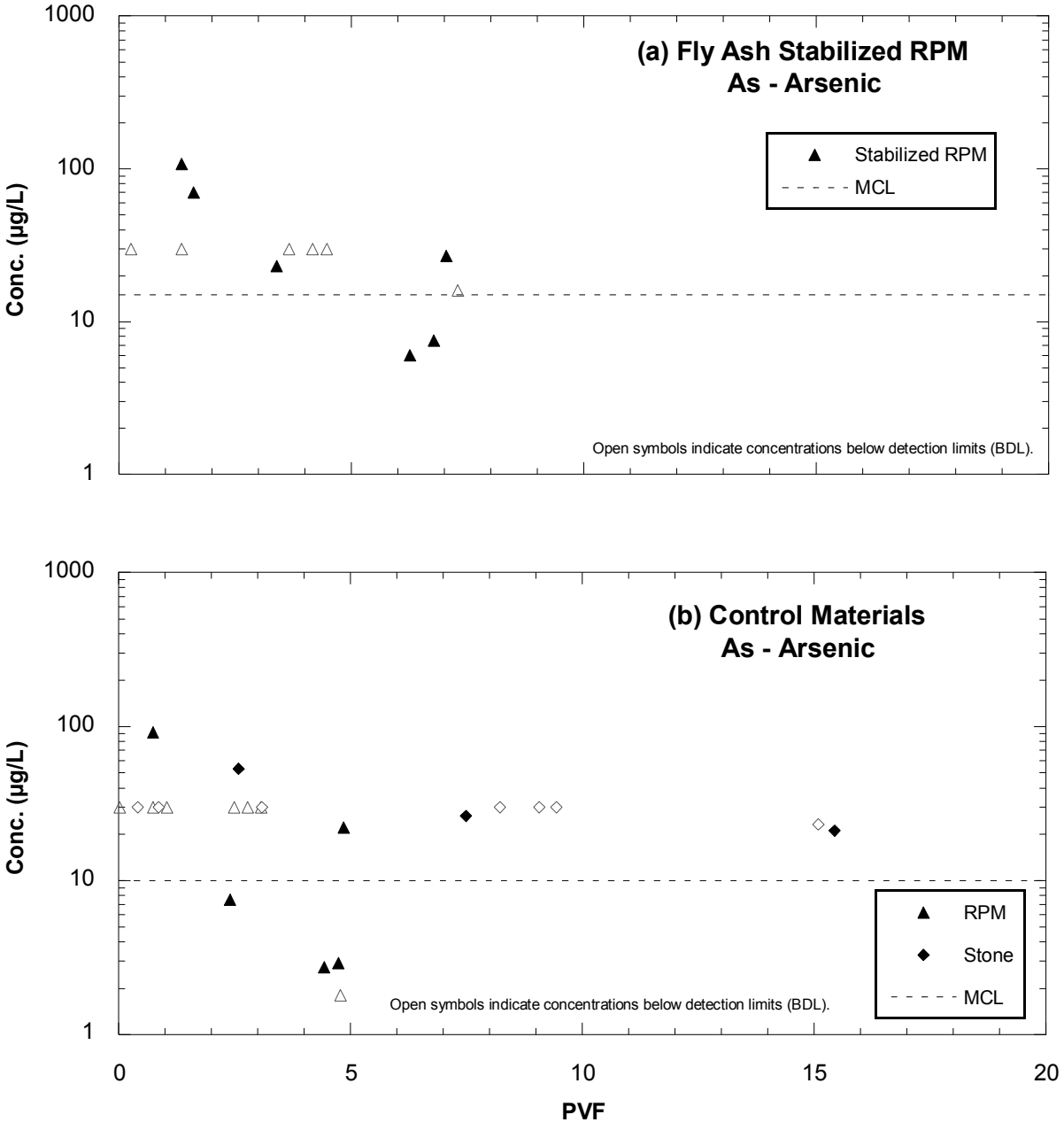

Figure 6.17: Arsenic (As) concentrations in leachate from field base course composed of (a) fly-ash-stabilized RPM, and (b) control materials.

(4) Concentrations Exceeding MCL but Not Elevated Compared to Control

Concentrations of Pb, Sb, Se, and Tl in leachate from fly-ash-stabilized materials exceeded MCLs but were not elevated relative to the adjacent control sections (Figures 6.18 to 6.21) (Table 6.8).

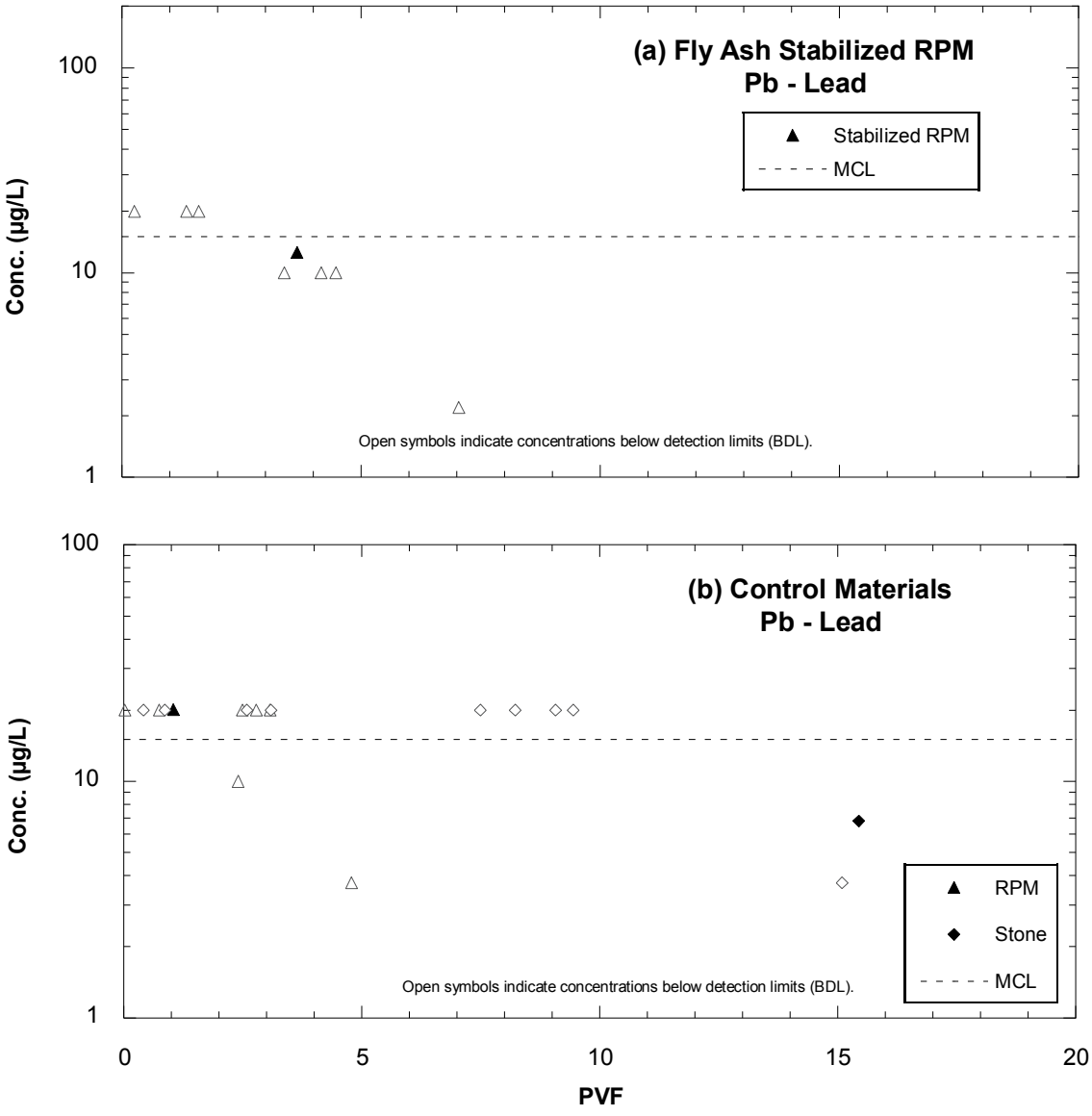

Figure 6.18: Lead (Pb) concentrations in leachate from field base course composed of (a) fly-ash-stabilized RPM, and (b) control materials.

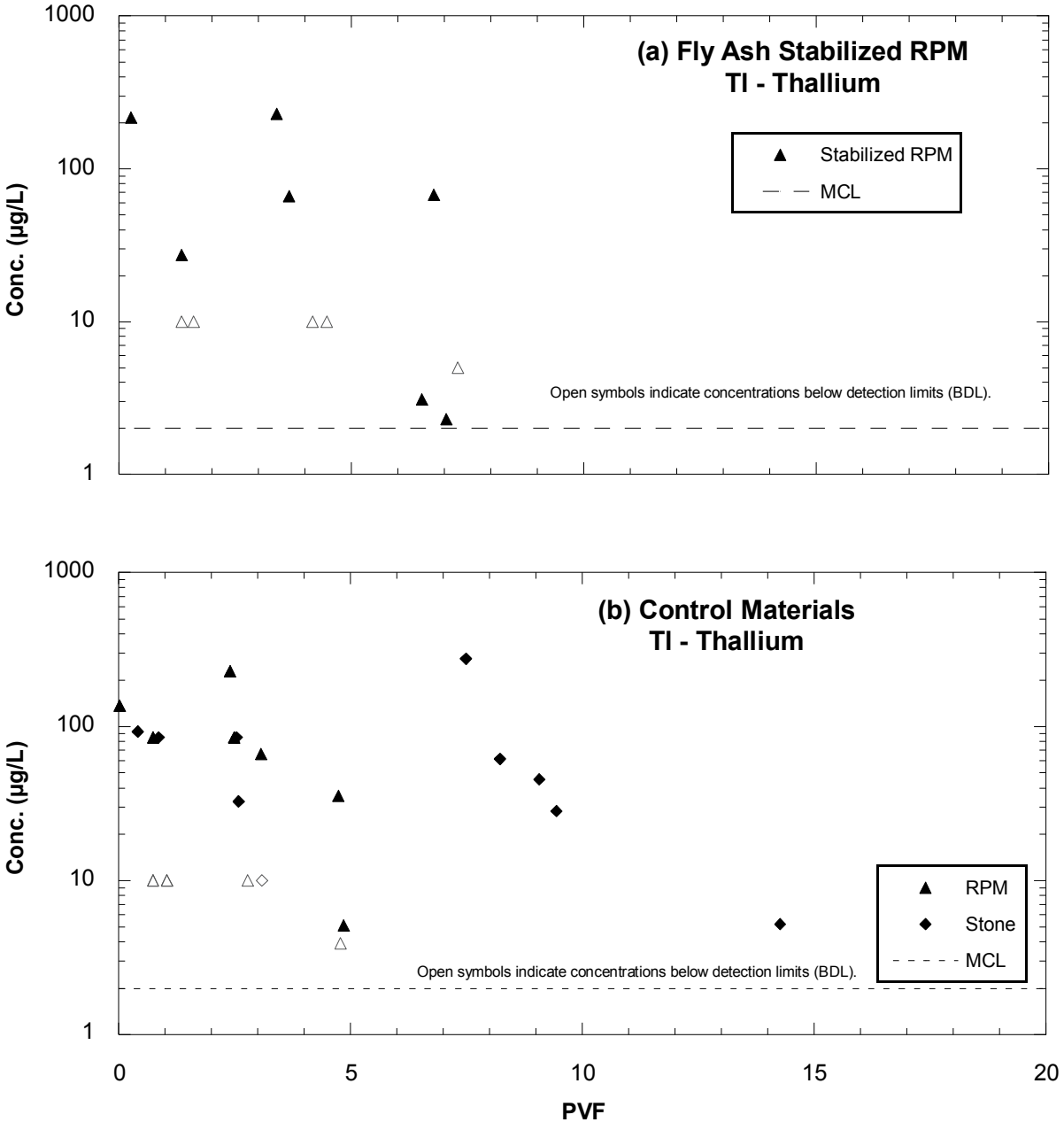

Figure 6.19: Thallium (Tl) concentrations in leachate from field base course composed of (a) fly-ash-stabilized RPM, and (b) control materials.

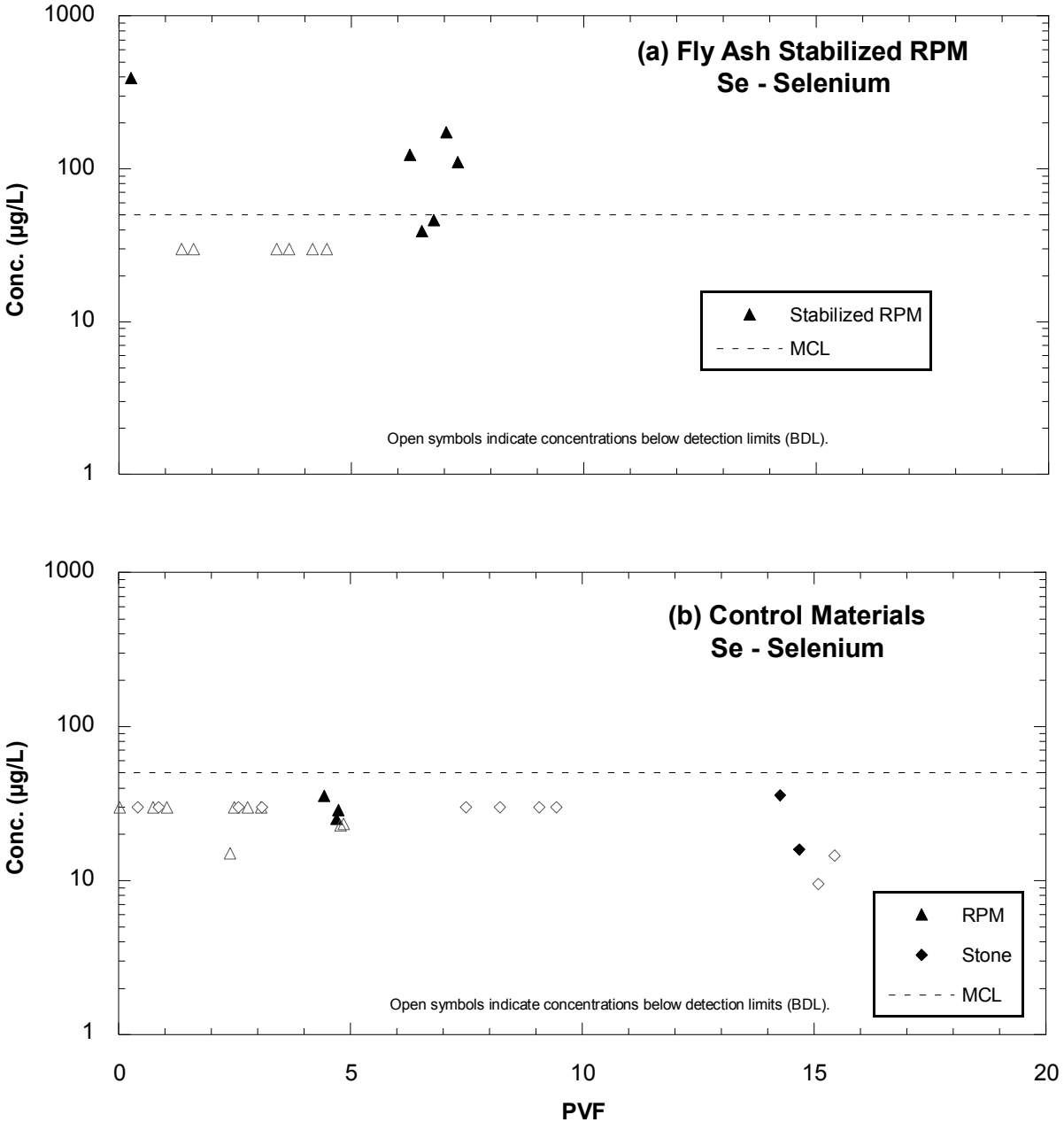

Figure 6.20: Selenium (Se) concentrations in leachate from field base course composed of (a) fly-ash-stabilized RPM, and (b) control materials.

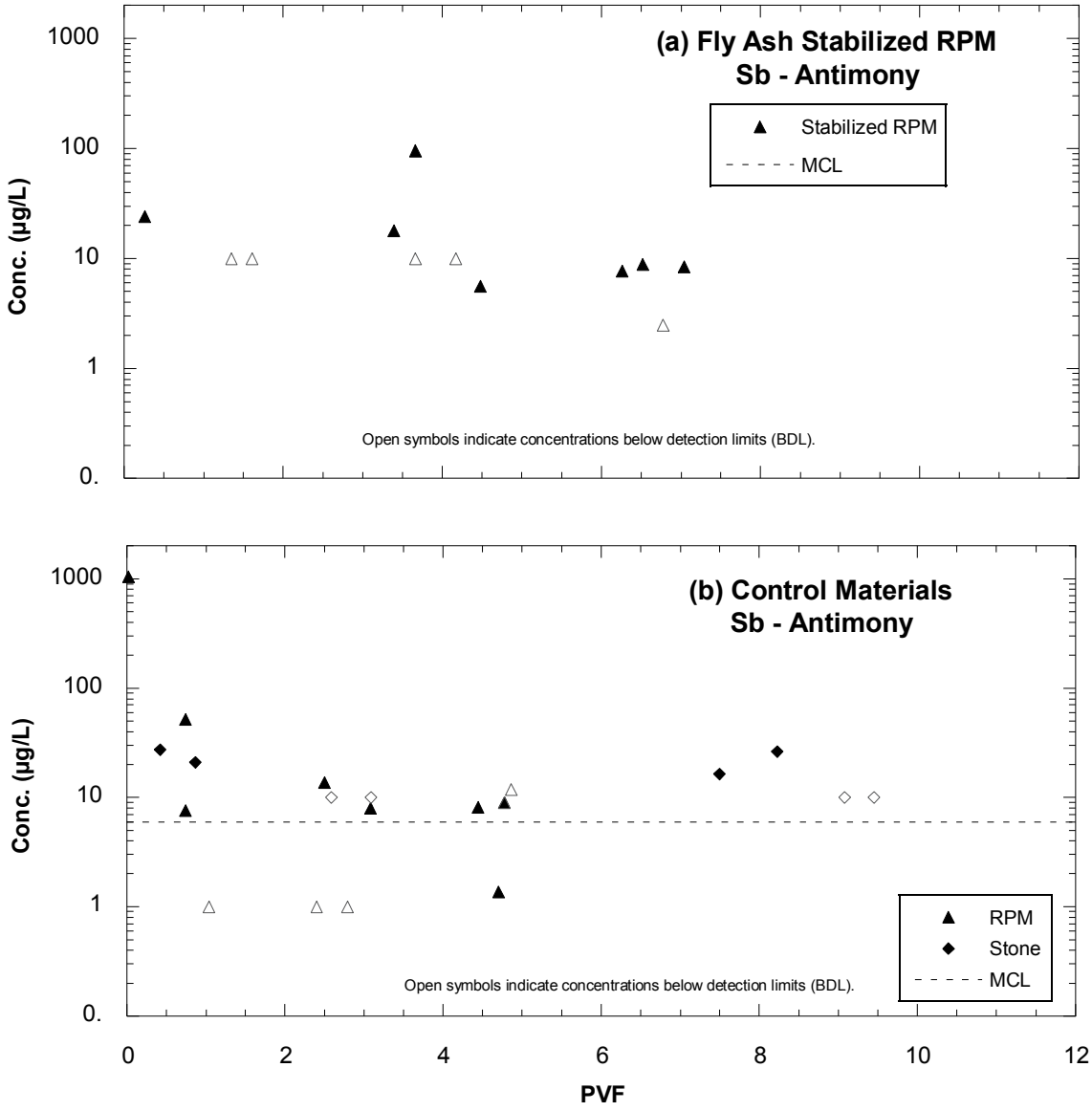

Figure 6.21: Antimony (Sb concentrations in leachate from field base course composed of (a) fly-ash-stabilized RPM, and (b) control materials.

(5) Effects of pH and Eh on Element Mobility

Chemical speciation of elements in the roadway pore water will affect element mobility and concentrations. Elements that exist as anions, oxy-anions, or non-ionic soluble molecules at the range of pH and Eh in the field leachate are less likely to be

sorbed to solids, and therefore will have greater mobility than elements that form cations (which are likely to sorb on mineral surfaces) or elements that precipitate out as a solid (Jury and Horton 2004). For the elements that exceeded MCLs the most probable speciation was estimated by pH-Eh speciation diagrams produced by the Geologic Survey of Japan (2005). All probable species over the range of pH and Eh observed in the field leachates were included (Table6.11). Speciation was not determined in the laboratory.

Six of the ten elements that exceeded MCLs are likely to form anions, oxy-anions, or non-ionic soluble molecules at the observed pH-Eh conditions (As, B, Mo, Sb, Se, and V). Four of the elements primarily form cations (Cd, Cr, Pb, and Tl) (Geologic Survey of Japan 2005) (Table 6.11).

Three elements had concentrations exceeding MCLs in early PVF and then fall below the MCL (Cd, Cr, and Se). Two of these elements (Cd and Cr) primarily form cations at field pH-Eh conditions. Se is likely to be present as an anion or oxy-anion.

Seven elements had concentrations that persistently exceed MCLs for at least two to three PVF (As, B, Mo, Pb, Sb, Tl, and V). Five of these elements (As, B, Mo, Sb, and V) form anions, oxy-anions, or non-ionic soluble molecules at field pH-Eh conditions (Table6.11). The other two elements with concentrations that persistently exceed the MCL (Pb and Tl) primarily form cations at the observed field pH-Eh conditions.

Table 6.11: Speciation of Select Trace Elements under Eh-pH Conditions

Element	pH	Species			
		Eh (mV)			
		-150	0	150	+300
As	6	$HAsO_2^{(aq)}$		$H_2AsO_4^{[-]}$	
	7				
	8		$HAsO_4^{[2-]}$		
	9				
B	6	$H_3BO_3^{(aq)}$			
	7				
	8				
	9				
Cd	6	$Cd^{[2+]}$			
	7				
	8				
	9				
Cr	6	$CrOH^{[2+]}$			
	7				
	8	$Cr_2O_3^{(s)}$			
	9				$CrO_4^{[2-]}$
Mo	6	$MoO_4^{[2-]}$			
	7				
	8				
	9				
Ni	6	$Ni^{[2+]}$			
	7				
	8				
	9				
Pb	6	$Pb^{[2+]}$			
	7	$PbOH^{[+]}$			
	8				
	9				
Sb	6	$HSbO_2^{(aq)}$			$SbO4^{(s)}$
	7				
	8				
	9				
Se	6	$HSe^{[-]}$		$HSeO_3^{[-]}$	
	7				
	8		$SeO_3^{[2-]}$		
	9				
Tl	6	$Tl^{[+]}$			
	7				
	8				
	9				
V	6	$VO^{[2+]}$			
	7	$VO_3^{[-]}$			
	8				
	9	$HVO_4^{[2-]}$			

6.2.2.3 Laboratory Tests

Two laboratory leaching methods were employed on samples of fly-ash-stabilized and control materials prepared in the laboratory using materials obtained from the field sites, and using field conditions whenever possible. Chemical properties of the laboratory leachates were compared to those of the field lysimeter leachates to determine the effectiveness of the tests in predicting field leachate qualities. The tests performed were Column Leach Tests (CLTs) and Water Leach Tests (WLTs). CLTs and WLTs were conducted on stabilized RPM and two control materials; RPM and crushed stone.

(1) Chemical Indicator Parameters

The pH of the CLT and field leachates are presented in Figure 6.22. The pH of leachate from the fly-ash-stabilized CLTs is 3 to 4 pH units higher than from the same materials in the field (Figure 6.22). All field leachate had pH near neutral (Figure 6.11.a). The CLT leachate from the control materials also tended to be near neutral. In contrast, the pH of leachate from stabilized CLTs remained elevated relative to the field pH for over 45 pore volumes of flow, which is longer than the life-cycle flow for most of the field lysimeters. The lower pH in the field compared to WLTs and CLTs on stabilized material may be due to unsaturated conditions in the field. Microbial respiration in the field can enhance soil pore gas CO_2 (Zwick *et al.*, 1984). Diffusion of CO_2 from the atmosphere or microbial respiration into pore water may form weak carbonic acid and may reduce the pH. In contrast, the CLTs are saturated and therefore have no opportunity for CO_2 to reduce the pH. The pH of WLT leachate from MnROAD materials was also 3 to 4 pH units higher than field leachate. Bin-Shafique *et al.* (2006) also found similar pH

levels in leachate from CLT and WLT on stabilized soils and sand. The WLT data is given in Appendix C.

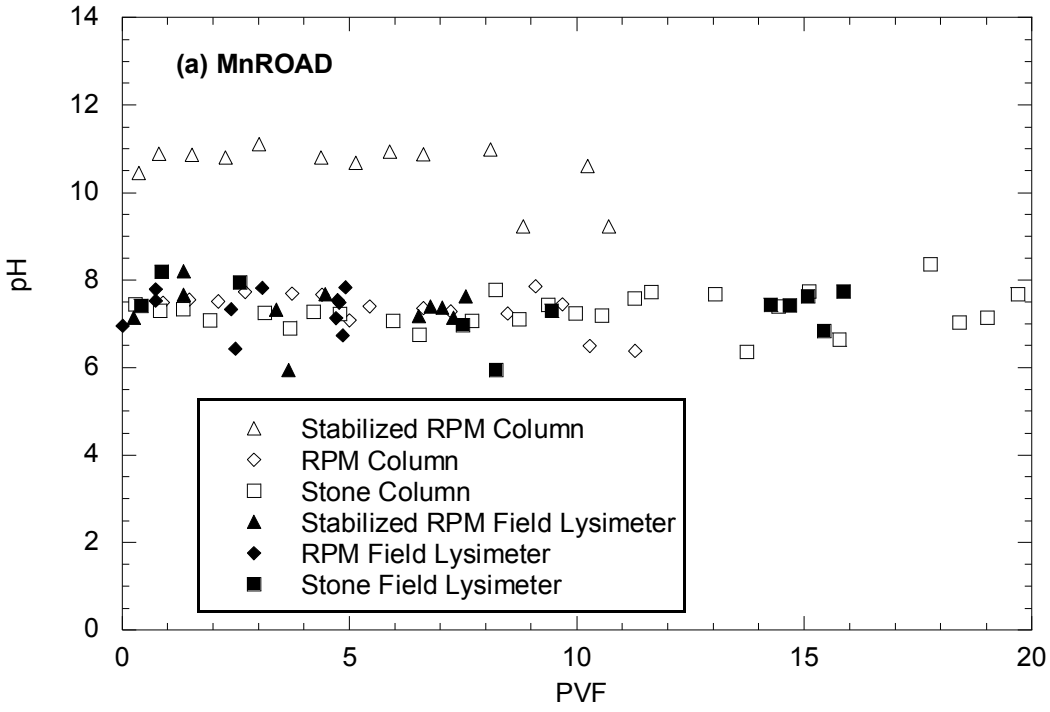

Figure 6.17: Comparison of leachate pH from Field Lysimeters and CLTs

The Eh of the CLT and field leachates are presented in Figure 6.23. Leachate from stabilized RPM in the field consistently had positive oxidation-reduction potential (Eh), of approximately +150 mV, indicating oxidized conditions (Figure 6.23). The stabilized RPM CLT leachate had lower Eh than the field, ranging generally from -5 mV to +40 mV. Leachate from control CLTs had similar Eh to the field leachates.

The differences in Eh between field and CLT concentrations are likely associated with the differences in pH between field and CLT concentrations. For field and CLT

leachates (the only site with CLT, pH, and EH results), leachate Eh is linearly correlated moderately well (and statistically significant) with leachate pH ($R^2 = 0.80$, F-Test P = $5.7 * 10^{-20}$) (Figure 6.24). Altering the CLT method used in this study to obtain pH near neutral in CLT leachate may cause the Eh of CLT leachate to more closely match the observed field Eh.

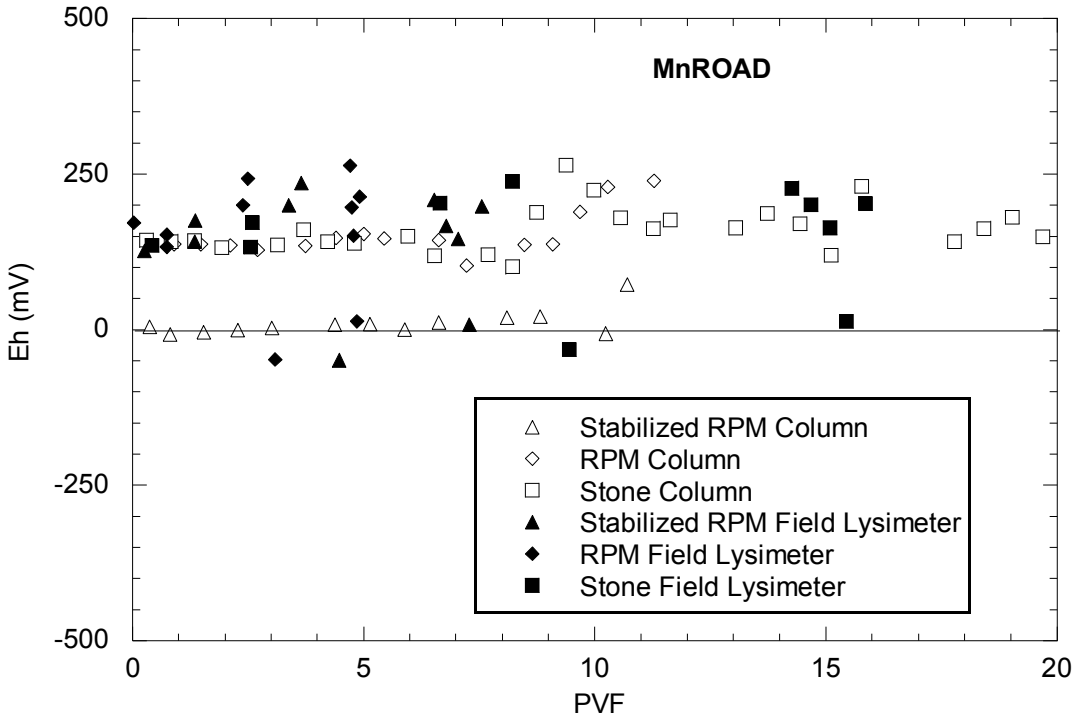

Figure 6.23: Comparison of leachate Eh from Field Lysimeters and CLTs

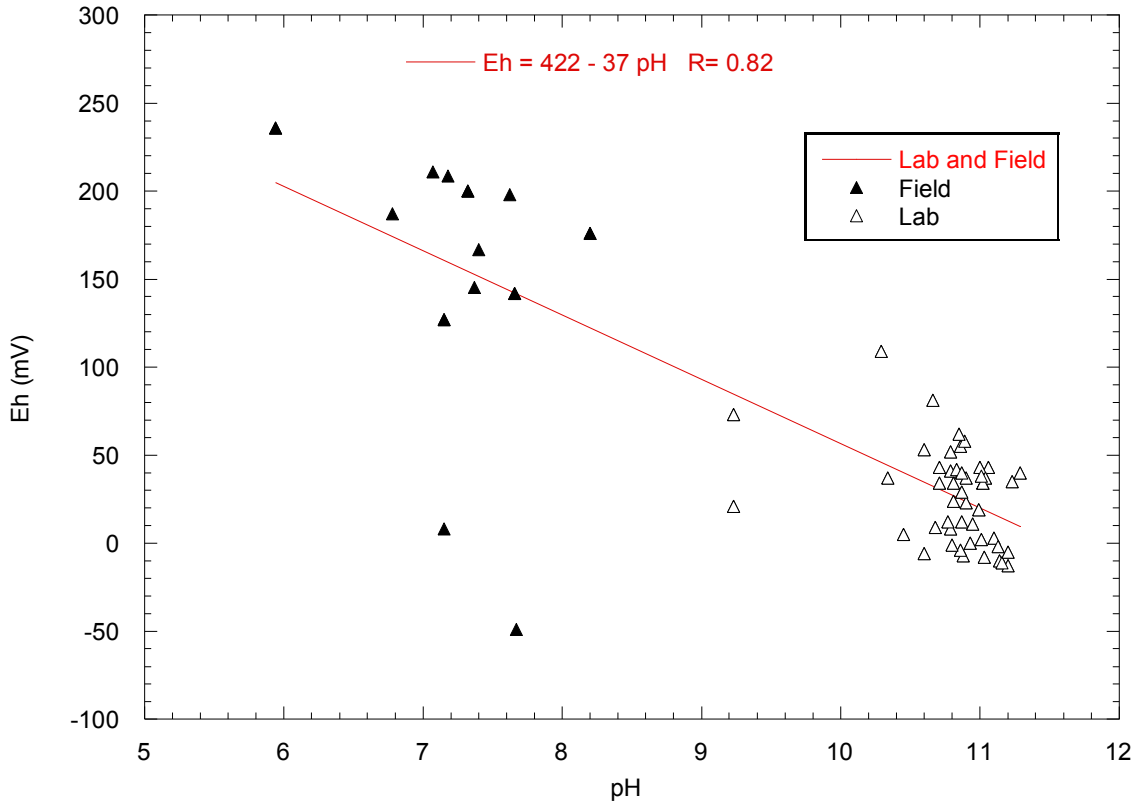

Figure 6.24: Analysis of Eh and pH relationship in field and CLT leachate

(2) Column Leach Tests

Prediction of Field Leaching Concentrations

Average peak concentrations of 23 elements (calculated from the mean of the three highest concentrations) in leachate from the field lysimeters and CLTs on the same materials are compared in Figure 6. 25. The comparison of field and CLT concentrations was conducted to determine the usefulness of the CLTs in estimating field average peak concentrations. The average peak concentrations from the CLTs are within one order of magnitude of the average peak field concentration for 77% of elements (Figure 6.25).

Graphs of all field concentrations as a function of PVF are included in Appendix B and all CLT concentrations as a function of PVF are included in Appendix C.

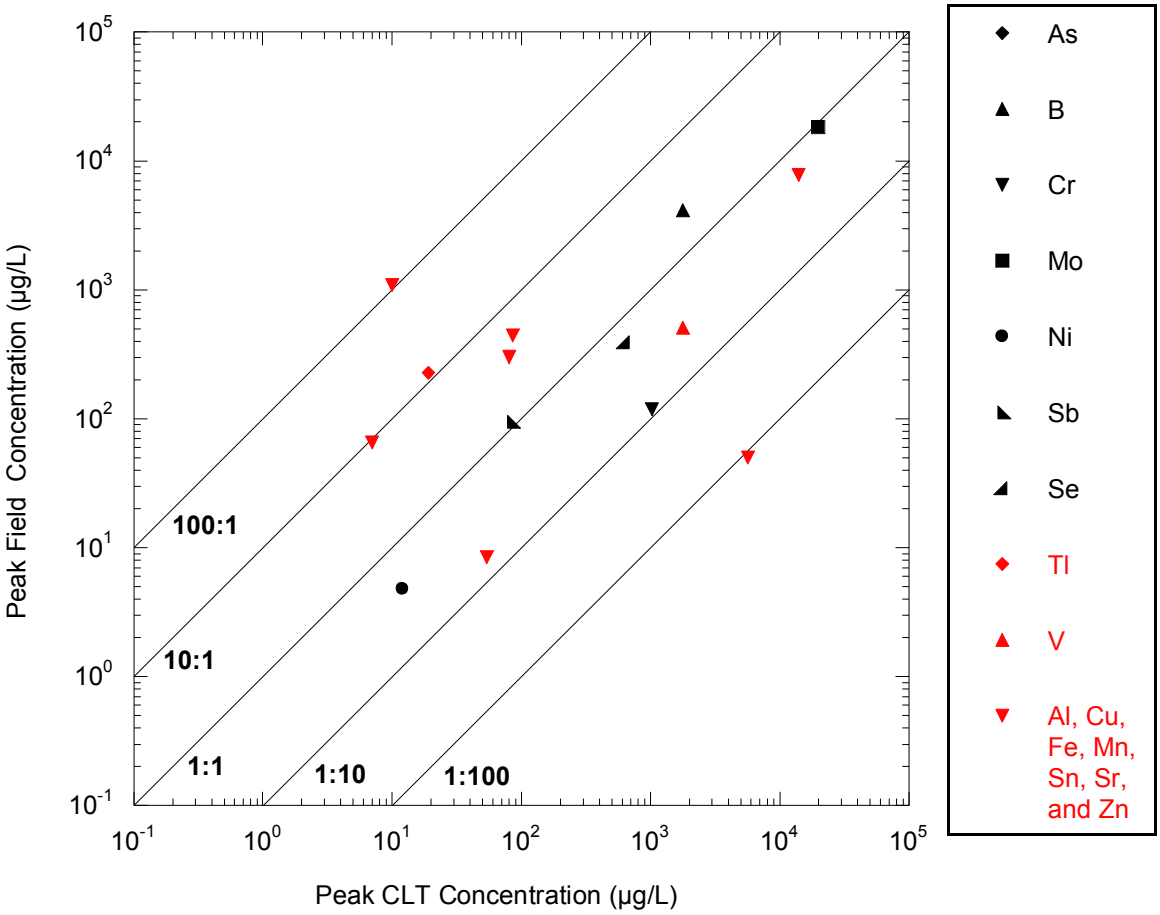

Figure 6.25: Comparison of peak concentrations in field lysimeters and column leach tests

Of the six elements in field leachate with concentrations elevated relative to the control section and exceeding MCLs (As, B, Cd, Cr, Mo, and V), four also exceeded the MCL and were elevated in the CLT leachate (B, Cr, Mo, and V) (Figure 6.26) (Tables 6.12 and 6.13). Concentrations of these four elements were among the most elevated

relative to the control concentrations. In addition, concentrations of B, Mo, and V may remain higher than MCL for many pore volumes of flow in both the field and CLTs.

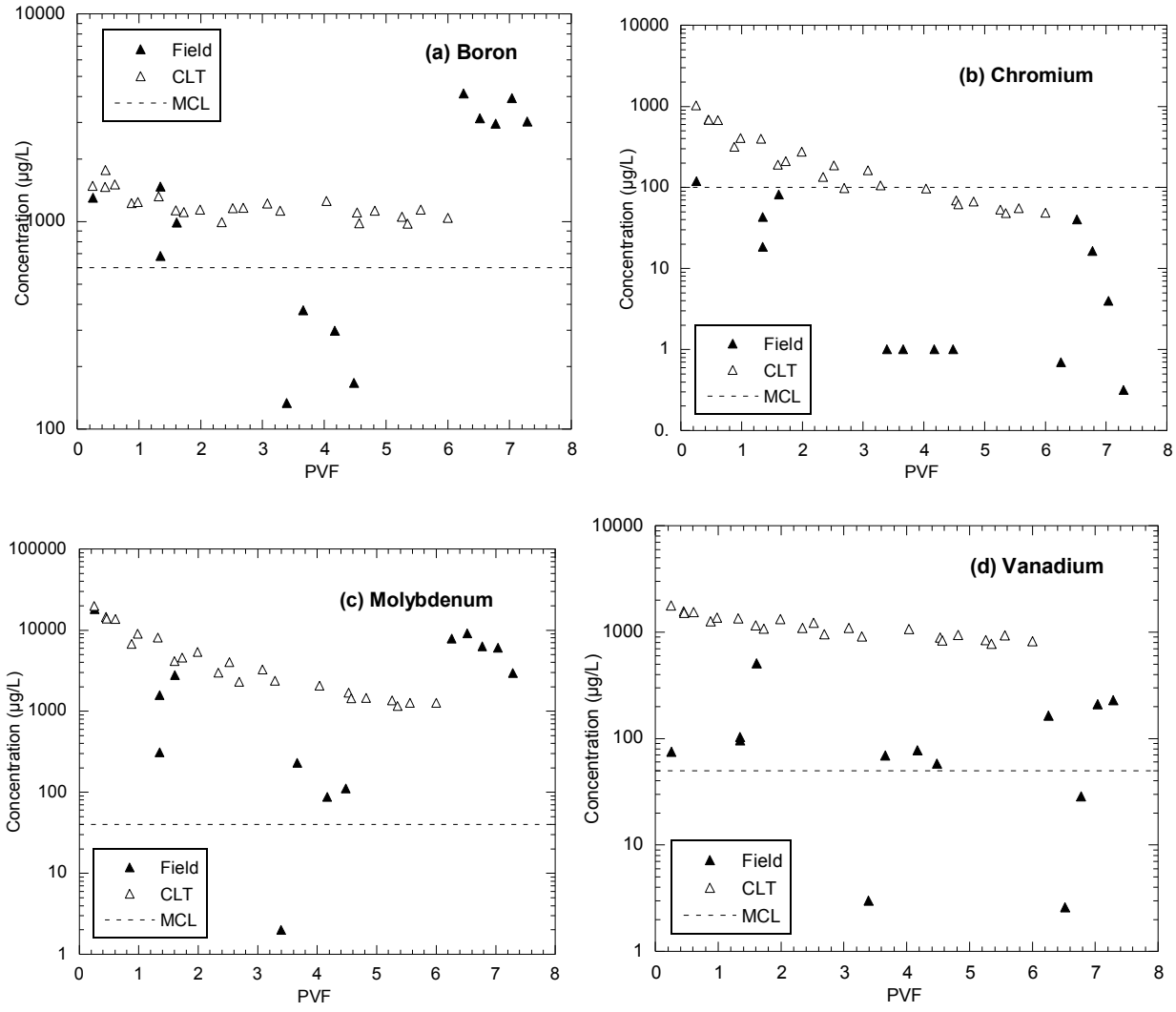

Figure 6.26: Elements in both field and CLT Leachate that were elevated relative to the control and exceeded the MCL. Downward facing triangles indicate concentrations that are BDL.

Table 6.12: Concentrations of Elements Elevated in the CLT Stabilized Leachate relative to the Control Leachate

Average Peak Concentration	
Element	**Avg. Magnitude of elevated concentration (µg/L)** (more negative indicates a greater difference between stabilized and control concentrations
Mo	-15021.91
Sr	-12187.36
Al	-4828.99
V	-1473.99
B	-1168.34
Cr	-790.71
Ba	-325.89
Cu	-37.78
Sb	-31.39
Se	-4.66
Ni	-3.36
Be	-3.24
Ti	-0.1
Co	0.03
Cd	0.67
As	2.13
Pb	2.88
Sn	2.89
Zn	23.46
Tl	25.02
Fe	64.04
Mn	980.51
Ag	Not Tested in CLT
Hg	Not Tested in CLT

Geo. Mean of Concentrations	
Element	**Avg. Magnitude of elevated concentration (µg/L)** (more negative indicates a greater difference between stabilized and control concentrations
Sr	-4512.66
Al	-2721.92
V	-764.32
B	-667.87
Mo	-629.6
Ba	-168.48
Cr	-16.48
Cu	-0.41
Ti	0.01
Cd	0.02
Co	0.03
Be	0.05
Ni	0.07
As	0.51
Zn	0.81
Sn	1.9
Pb	2.07
Fe	3.12
Sb	3.57
Tl	10.77
Mn	14.42
Se	29.71
Ag	Not Tested in CLT
Hg	Not Tested in CLT

Table 6.13: Comparison of Field and CLT Leachate MCL Exceedances and Concentration Relative to Control Materials

All Elements	Elevated in the field	Exceeded MCL in Field	**Exceeded MCL and Elevated**	Exceeded MCL but the same or less than Controls (Field)	Elevated in Columns	Exceeded MCL in Columns	**Exceeded MCL and Elevated in Columns**	Exceeded MCL but the same or less than Controls (Columns)
Ag	Ag				Ag			
Al	Al				Al			
As	As	As	**As**					
B	B	B	**B**		B	B	**B**	
Ba	Ba				Ba			
Be								
Cd	Cd	Cd	**Cd**					
Co	Co							
Cr	Cr	Cr	**Cr**		Cr	Cr	**Cr**	
Cu	Cu				Cu			
Fe	Fe							
Hg								
Mn	Mn							
Mo	Mo	Mo	**Mo**		Mo	Mo	**Mo**	
Ni	Ni	Ni	**Ni**		Ni			
Pb	Pb	Pb	**Pb**					
Sb		Sb		Sb	Sb	Sb	**Sb**	
Se		Se		Se	Se	Se	**Se**	
Sn	Sn							
Sr	Sr				Sr			
Ti	Ti				Ti			
Tl		Tl		Tl		Tl		Tl
V	V	V	**V**		V	V	**V**	
Zn	Zn							

Note: Bold indicates elements that were both elevated and in exceedance of the MC

The CLT provided measurable concentrations of all 23 elements analyzed, and was most successful at estimating the average peak field concentrations for the three elements most likely to leach at concentrations above MCL for long periods of time (B, Mo, and V).

Concentrations of As, Cd, and Pb exceeded the MCL and were elevated relative to control concentrations in the field but not in CLTs. Concentrations of these elements were only slightly elevated in the field but not in the CLT. Of these elements, only As had a peak field concentration greater than 20 μg/L.

Average peak field concentrations of As and Cd may be significantly underestimated by the CLT procedure used in this study. The CLT concentrations of As and Cd tend to be below or near the detection limit and well below the MCL. In contrast, the peak field concentrations for these elements may exceed the MCL. For example, the average peak field concentration of As was 26 time the average peak from the CLT, and Cd was 15 times the peak from the CLT. Detection limits for Pb differed significantly for the field and CLT leachates. All field Pb concentrations were below the detection limit (above the MCL) and most CLT concentrations were below a lower detection limit (below the MCL). Because of these differences the ability of CLTs to predict field leaching of Pb cannot be adequately assessed from this study.

Of the three elements that exceeded MCLs in the field but were not elevated relative to control materials (Sb, Se, and Tl) all three also exceeded the MCL in CLTs. However, Sb and Se concentrations were elevated relative to controls concentrations

from the CLTs. These differences are possibly due to differences in pH and Eh between the field and CLT leachates.

Comparison of Leaching Patterns

Under saturated constant-flow conditions in the CLTs, concentrations of thirteen of the 24 elements displayed a first-flush elution pattern, with the peak concentration occurring during the first or second PVF (Ag, B, Be, Cd, Cr, Cu, Mo, Mn, Sb, Se, Sr, V, and Zn). All of these elements also had first-flush elution pattern for at least one field site. Concentrations of these thirteen elements peaked at an average of 1.5 PVF, with the latest peak at 6 PVF for Zn. The remaining 11 elements either had very low initial CLT concentrations (As, Co, Hg, Ni, Pb, Sn, Ti, and Tl) and long-term concentrations just above or below the MDL, or had distinctly different leaching patterns (Al, Ba, and Fe). Elements that exceeded the MCL and did not have a first-flush pattern in the CLTs were As, Ni, Pb, and Tl.

Flow through the CLT columns was halted after approximately 40 pore volumes of flow. The columns were then left saturated with no flow for 54 days, and then restarted. Concentrations of 11 elements then increased when flow was restarted (As, B, Be, Cd, Cu, Mo, Sb, Se, Sr, V, and Zn). This spike in concentrations suggests that under the constant flow conditions in the CLT the flow rate prevented the aqueous concentrations from coming to an equilibrium state with the solids. Following the spike, concentrations decreased to those observed just before the flow was stopped (Figure 6.27).

Three elements had the concentration rise back to original peak (Sb), or higher (1.5 to 2.9 times) after the columns were restarted (As and Cd), although As and Cd had

very low initial CLT concentrations. For the other seven elements the initial peak concentration was significantly higher then the secondary peak concentration caused by the stoppage and restarting (1.5 to 14 times higher than the secondary peak).

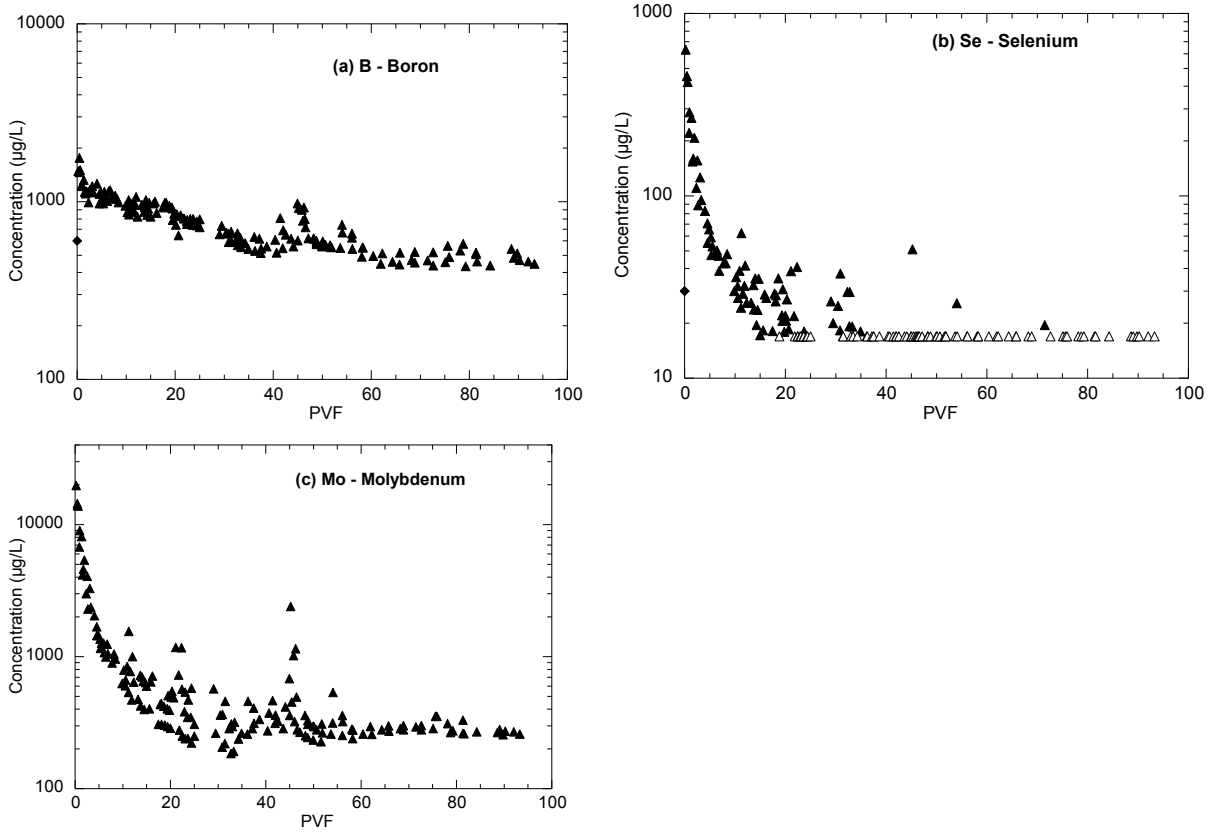

Figure 6.27: Typical first-flush leaching patterns from CLTs for (b) B, (b) Se, and (c) Mo, and increase in concentrations after MnROAD columns were left saturated with no flow

(3) Water Leach Tests

Prediction Of Field Leaching Concentrations

Peak concentrations from the field are compared with concentrations from WLTs on the same materials in Figure 4.22.a. Four liquid to solid mass ratios were tested (3:1, 5:1, 10:1, and 20:1) to determine if decreasing the ratio from the standard 20:1 (ASTM D3987-85) improved the ability of the WLT to predict peak field concentrations. Figure 6.28.a shows that the 3:1 WLT most closely estimated the peak field concentrations. For elements that were detectable in the 3:1 WLT the concentrations were within one order of magnitude of the peak field concentration for 91% of tests (Figure 6.28.b). All further discussion of the WLTs will refer to the 3:1 WLT.

Of twenty elements that were detected in field leachate, eight elements (Ag, Cd, Co, Fe, Mn, Se, Sn, and Tl) were not detected in 3:1 WLTs on the materials. Of these elements, three (Cd, Se, and Tl) had concentrations that exceeded the MCL in field leachate from stabilized materials, but only Cd was found to be elevated relative to the control sections.

The WLT was most useful in predicting field concentrations of elements when peak field concentration was greater than 200 μg/L. Seven of the eight elements that were not detected in WLT leachate had peak field concentrations of 170 μg/L or less. All elements with peak field concentrations of 500 μg/L or greater were detected in the WLT .

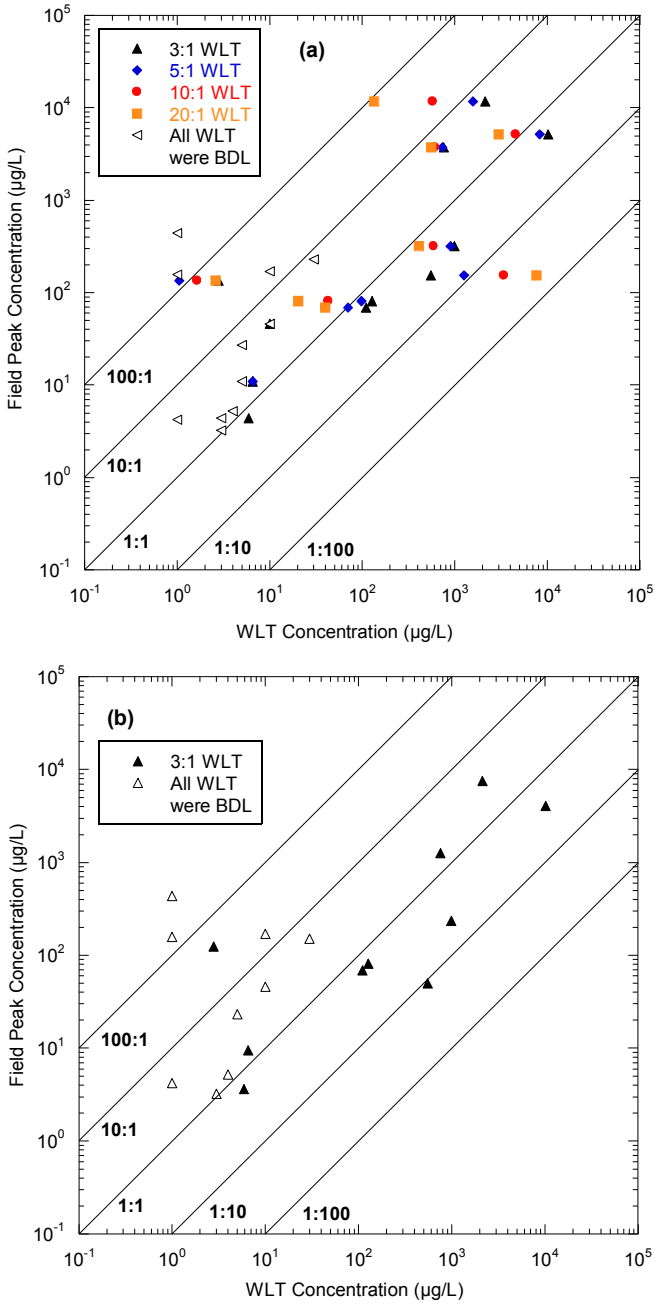

Figure 6.28: Comparison of average peak field concentrations and WLT concentration for (a) all WLT liquid:solid ratios, and (b) only the 3:1 WLT. Only elements detected in the field are shown. Open Symbols indicate WLT below detection limit

(4) Comparison of CLT and WLT Prediction Of Field Leaching

The detection limits for the WLT samples was generally higher than those for the CLT samples, and are shown in Table6.5. Figure 6.29.a shows the predictive ability of the CLT and WLT with two differing sets of detection limits. When the CLT has lower detection limits than the WLT, the CLT detects all elements, and is better at predicting the field concentrations of elements that have lower (< 500 μg/L) peak field concentrations. If the higher WLT detection limits are applied to the CLT data, the WLT and CLT become very similar in their ability to predict peak field concentrations of elements that exceeded MCLs in the field (Figure 6.29.b). The WLT may have been more successful at predicting elements with lower peak field values if the WLT samples were analyzed with lower detection limits similar to those for the CLT leachates (Table 6.5)

Using the same higher (WLT) detection limits for both tests, the WLT fails to detect 45% of elements detected in the field, 36% of elements that exceeded MCLs in the field (Cd, Sb, Se, and Tl), and 13% of elements that exceeded MCL and were elevated relative to the control in the field (Cd). The CLT fails to detect 25% of elements detected in the field, 27% of elements that exceeded MCLs in the field (Cd, Ni, and Pb), and 38% of elements that exceeded MCL and were elevated relative to the control in the field (Cd, Ni, and Pb).

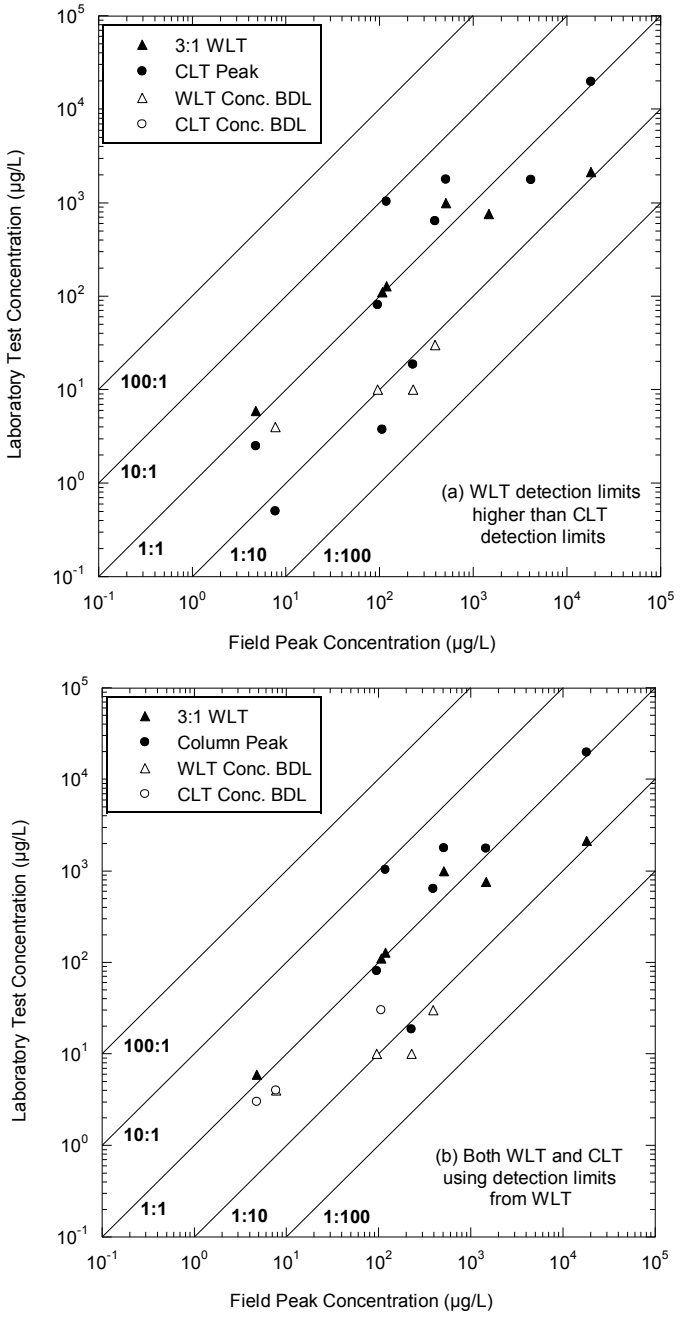

Figure 6.29: Comparison of ability of CLT and WLT to predict peak field concentration of elements that exceeded MCLs in field leachate when (a) detection limits were lower for the CLT, and (b) when both tests use the WLT detection limits

6.2.3 Conclusions on Chemical Analysis

6.2.3.1 Conclusions from Field Results

- Flux discharged from the stabilized roadway layers is expected to be 2% to 8% of precipitation for stabilized RPM base course. Flux discharged from the stabilized roadway layers is also less than the average regional recharge rates likely to occur in areas immediately adjacent to the road (average recharge is approximately 20% of precipitation).
- Peak volumetric fluxes from the layers tend to occur in the spring months when heavy rains and snow melt occur, and again in the late summer and early fall. Minimum fluxes tend to occur in the winter when precipitation and pore water are often frozen, and in July or August. Occasionally the flux from the stabilized materials approaches 15% of precipitation for a period of several months, but the long-term average is never more than 7.8% of precipitation.
- All field cells had pH near 7 and predominantly oxidizing Eh of approximately +150 to +300 mV.
- Among elements that were tested for during the entire operation of the site and that were detected at the site, 61% of elements had the peak concentration occur during the first two PVF.
- B, Mo, and V concentrations in leachate from the fly-ash-stabilized materials were elevated relative to concentrations from the control sections, have peak concentrations above the MCL, and exceed the MCL for many PVF.
- Both As and Pb have concentrations that remain near the MCL and were observed to periodically exceed the MCL over many PVF. The concentrations of As and Pb are only slightly statistically elevated relative to the control concentrations.

- At sites where Cd and Cr exceeded the MCL, they only exceeded the MCL during the first sampling event (PVF at Peak ≤ 0.26) and were below in all subsequent PVF.
- Concentrations of many trace elements, particularly those with relatively low water quality standards, diminish over time as water flows through the pavement profile. For many elements, concentrations below US water drinking water quality standards are attained at the bottom of the pavement profile within 2-4 pore volumes of flow.

6.2.3.2 Conclusions from Laboratory Results

- When using lab tests to predict field leaching concentrations, an analytical method with minimum detection limits equal to or less than the lowest MCL should be used. Peak concentrations of many elements in leachate from the CLTs and WLTs are likely to be less than peak concentrations from the field leachate. Elements that are not detected in the lab tests may be present in field leachate, and may exceed the MCL in the field. The method detection limits should be determined before testing of samples begins.
- The pH of leachate from CLT and WLT on stabilized materials (generally 10 to 11) is higher than from the same materials in the field (6 to 8). Eh of leachate from CLT and WLT on stabilized materials is lower (-5 to +40 mV) than from the same materials in the field (mostly between +150 to +300 mV), where leachate was generally oxidizing. The differences in pH and Eh between stabilized materials in the field and in a CLT may be caused by the difference in conditions (saturated flow in CLTs and unsaturated flow in the field. This may affect element speciation, solubility, and mobility, and therefore affect the prediction of field concentrations using the CLT and WLT methods employed in this study.

- CLT average peak concentration was within one order of magnitude of the average peak field concentration 77% of the time. CLT provides similar results (concentrations above the MCL, elevated relative to the control, and 1.1 to 3.5 times higher than the field average peak) for the elements consistently elevated relative to the control concentrations and MCLs (B, Mo, and V), as well as for Cr (CLT average peak 8.6 times higher than the field average peak).
- Three elements exceed the MCL in the field, but not in the CLTs (As, Cd, and Pb). These were either only slightly elevated in the field but not in the CLT (As, Cd, and Pb), or elevated in both the field and CLT (Ni).
- Three elements exceeded MCLs in the field but were not elevated relative to control materials (Sb, Se, and Tl), and also exceeded the MCL in CLTs. However, Sb and Se were elevated relative to controls in the CLT.
- B, Cd, Cr, Mo, Sb, Se, and V exceeded MCLs in field leachate and had first-flush leaching patterns in CLTs. As, Pb, and Tl exceeded the MCL in the field and did not have a first-flush CLT patterns.
- Stopping and restarting the CLTs caused concentrations of 11 of the elements to experienced a spike (As, B, Be, Cd, Cu, Mo, Sb, Se, Sr, V, and Zn). This spike in concentrations suggests that under the constant flow conditions in the CLT the flow rate prevented the aqueous concentrations from coming to an equilibrium state with the solids. Following the spike, concentrations decreased to those observed just before the flow was stopped.
- Of the four liquid to solid ratios tested, the 3:1 WLT provides the best prediction of field peak concentrations. Of twenty elements that were detected in field leachate at the MnROAD site, eight of these were not detected in 3:1 WLTs on the materials. Seven of the eight

elements that were not detected in WLT leachate had peak field concentrations of 170 μg/L or less. All elements with peak field concentrations of 500 μg/L or greater were detected in the WLT. If the WLT leachates were analyzed with lower detection limits, the 3:1 WLT may have detected more or all of the elements detected in the field.

- When CLT and WLT results are compared using the same detection limits the ability of both tests to predict peak field concentrations is similar. Both have peak or average peak within one order of magnitude of the field for B, Mo, and V, which have peak concentrations above the MCL for many PVF.

CHAPTER 7: CONCLUSIONS AND RECOMMENDATIONS

This study indicated the economic and environmental benefits of CHCFA stabilized RPM base course material when compared to the unstabilized RPM and crushed aggregate as base materials. The conclusions and recommendations are listed as follows.

7.1 Conclusions

1) For any laboratory or field test methods in this study, such as M_r, DCP, LWD, DCP, FWD, SSG, and FWD, fly ash stabilized RPM had higher modulus than untreated RPM, followed by crushed aggregate.
2) The backcalculated moduli of the base courses from FWD tests were extremely higher for the winter season when the base course materials were frozen. The moduli of base courses were lower in Spring than the moduli in other seasons, indicating the weakening of materials by spring thaw.
3) The backcalculated moduli of base materials from the FWD tests on HMA surface is higher than that directly tested on base course during construction.
4) The backcalculated moduli of fly ash stabilized RPM in the field does not show significant increase with the increase of curing age.
5) Although the backcalculated moduli of fly ash stabilized RPM were higher than the other two base materials, the difference was not as significant as the difference between the laboratory resilient moduli.
6) The fly ash stabilized RPM base course resulted in the least pressure on the subgrade, followed by untreated RPM and Class 6, based on the instrumentation results. This is in agreement with the moduli of base materials from the field and laboratory tests.

7) Based on the MEPDG performance prediction, the service life of the Cell 79 with fly ash stabilized RPM, is 23.5 years, which is about twice of the service life of the Cell 77 with RPM base (11 years), and about three times of the service life of the Cell 78 with Class 6 aggregate base (7.5 years).
8) The life cycle analysis indicates that the usage of the fly ash stabilized RPM as the base of the flexible pavement can significantly reduce the life cycle cost, the energy consumption, the greenhouse gases emission, and the chemical effect compared with the untreated RPM and Class 6 aggregate base.
9) Concentrations of many trace elements, particularly those with relatively low water quality standards, diminish over time as water flows through the pavement profile. For many elements, concentrations below US water drinking water quality standards are attained at the bottom of the pavement profile within 2-4 pore volumes of flow.

7.2 Recommendations

1) Follow-on performance monitoring of Cells 77, 78, and 79 is needed to validate the MEPDG performance prediction. Especially, the stabilized base course is not calibrated with the field performance in MEPDG.
2) Further research is needed to correlate the FWD backcalculated base moduli with the field performance.

CHAPTER 8: REFERENCES

Adriano, D C., Weber, J., Bolan, N.S., Paramasivam, S., Koo, B.J., and Sajwan, K.S. (2002) "Effects of High Rates of Fly Ash on Soil, Turfgrass, and Groundwater Quality." Water, Air, and Soil Pollution. 139, 365-385.

American Coal Ash Association (ACAA), (2003), "2002 Coal Combustion Product (CCP) Production and Use Survey", November 2003.

American Coal Ash Association (ACAA) website (2009). http://www.acaa-usa.org. Website viewed September 29, 2009.

Applied Research Associates, Inc. (ARA), (2009), "M-EPDG Mechanistic-Empirical Pavement Desigh Guide (version 1.1)", http://onlinepubs.trb.org/onlinepubs/archive/mepdg/software.htm.

Bin-Shafique, S, Edil, T B., Benson, C H., and Senol, A. (2004) "Incorporating a Fly-ash Stabilized Layer into Pavement Design," Geotechnical Engineering, 157, 239-259.

Bin-Shafique, S, Edil, T B., Benson, C H., and Hwang, K. (2006) "Concentrations from Water Leach and Column Leach Tests on Fly Ash Stabilized Soils," Environmental Engineering Science. 23 (1). 53-67.

Buhler, R L. and Cerato, A B. (2007) "Stabilization of Oklahoma Expansive Soils using Lime and Class C Fly Ash," ASCE – GeoDenver 2007: New Peaks in Geotechnics. GSP 162. 1-10.

Clyne, T.R. and L.E. Palek. (2008) "2007 Low Volume Road & Farm Loop Cells 33, 34, 35, 77, 78, 79, 83, 84 Construction Report" Minnesota Department of Transportation, Maplewood, MN.

Cokca, E. (2001) "Use of Class C Fly Ash for the Stabilization of an Expansive Soil," Journal of Geotechnical and Geoenvironmental Engineering. July, 568-573.

DeBeer, M. (1991), "Use of the Dynamic Cone Penetrometer (DCP) in the Design of Road Structures," Proceedings of the tenth regional conference for Africa on Soil Mechanics & Foundation Engineering and the third International Conference on Tropical & Residual Soils. Maseru. 23-27 September 1991. Ham, M.E, 1966, Foundations ojTheoretical Soil Mechanics, McGraw-Hill, p. 8 1

Edil, T B., Benson, C H., Bin-Shafique, S, Tanyu, B F., Kim, W, and Senol, A. (2002) "Field Evaluation of Construction Alternatives for Roadways over Soft Subgrade," Transportation Research Record 1786, Paper No. 02-3808, 36-48.

Federal Highway Administration (FHWA), (1995), "Pavement Recycling Executive Summary and Report", Federal Highway Administration, Report No. FHWA-SA-95-060, Washington, D.C.

Ganglof, W J, Ghodrati, M, Sims, J T, and Vasilas, B L. (1997) "Field Study: Influence of Fly Ash on Leachate Composition in an Excessively Drained Soil." Journal of Environmental Quality. 26. 714-23.

Geologic Survey of Japan (2005). "Atlas of Eh-pH Diagrams-Intercomparison of Thermodynamic Databases." National Institute of Advanced Industrial Science and Technology, Research Center for Deep Geologic Environments. Open File report No. 419.

George K.P., Bajracharya M., and Stubstad R. (2004), "Subgrade Characterization Employing the Falling Weight Deflectometer," Transportation Research Record: Journal of the Transportation Research Board, No. 1869, TRB, National Research Council, Washington, D.C., pp. 73–79.

Hatipoglu, B, Edil, T B., and Benson, C H. (2008) "Evaluation of Base Prepared from Road Surface Gravel Stabilized with Fly Ash," ASCE - GeoCongress 2008: Geotechnics of Waste Management and Remediation. 288-295.

Halstead, Woodrow J. (1981), "Energy involved in construction materials and procedures", National Research Council, Transportation Research Board, Washington, D.C.

Jury, W A. and Horton, R. (2004). Soil Physics. Jon Wiley & Sons. Hoboken, NJ.

*Kumar, S, and Patil, C B. (2006) "*Estimation of Resource Savings Due to Fly Ash Utilization in Road Construction," Resources, Conservation and Recycling. 48. 125-140.

Lee, J. C., Bradshaw, S. L., Edil, T B., and Benson, C. H. (2010) "Green Benefits of Using Coal Ashes," Proc. 2nd International Conference on Sustainable Construction Materials and Technologies, 2010, Università Politecnica delle Marche, Ancona, Italy.

Li, L, Edil, T B., and Benson, C H., Hatipoglu, B, and Tastan, O. (2007) "Evaluation of Recycled Asphalt Paving Layer Stabilized with Fly Ash," ASCE – GeoDenver 2007: New Peaks in Geotechnics. GSP 169. 1-10.

Li, L, Tastan, O, Benson, C H, and Edil, T B. (2009) "Field Evaluation of Fly Ash Stabilized Subgrade in US 12 Highway," ASCE - 2009 International Foundation Congress and Equipment Expo, Ground Modification, Problem Soils, and Geo Support. 385-392.

Li, Lin, C.H. Benson, T.B. Edil, B. Hatipoglu, and O. Tastan, (2008) "Evaluation of Recycled Asphalt Pavement Material Stabilized with Fly Ash." Geotechnical and Geological Engineering, 177-187, Netherlands.

Mearig, Tim, Nathan Coffee, and Michael Morgan, (1999), "Life Cycle Cost Analysis Handbook." State of Alaska - Department of Education & Early Development, Juneau, Alaska.

Meil, Jamie, (2006), "A Life Cycle Perspective on Concrete and Asphalt Roadways: Embodied Primary Energy and Global Warming Potential", Research Report to Cement Association of Canada.

Minnesota Department of Transportation, (2009) "MnROAD - Minnesota's Cold Weather Road Research Facility." http://www.dot.state.mn.us/mnroad, Viewed on May 15, 2009

Minnesota Department of Transportation (MnDOT), (2009) "MNROAD Semi Tractor Trailer"

MODULUS 5.0 For DOS, Texas Transportation Institute (TTI), College Station, TX, 2001

National Oceanic and Atmospheric Administration, (2009) "NNDC Climate Data Online". http://cdo.ncdc.noaa.gov/cgi-bin/cdo/cdostnsearch.pl. Viewed on June 23, 2009

National Research Council, Committee on Mine Placement of Coal Combustion Wastes (2006), Managing Coal Combustion Residues in Mines. National Academies Press. Washington, DC.

Petersen D.L., Siekmeier J., Nelson C.R., and Peterson R.L. (2006), "Intelligent Soil Compaction Technology Results and a Roadmap Toward Widespread Use", Transportation Research Record: Journal of the Transportation Research Board, No. 1975, Transportation Research Board of the National Academies, Washington, D.C., pp. 81–88.

Ramme B. and Tharaniyil M. (2000), "Coal Combustion Byproduct Utilization Handbook", We Energies, 2000.

United States Department of Energy - National Energy Technology Laboratory, (2009), "Current Regulations Governing Coal Combustion By-Products". http://www.netl.doe.gov/technologies/coalpower/ewr/coal_utilization_byproducts/states/select_state.html. Website viewed July 15, 2009.

United States Environmental Protection Agency. (2008) "Waste and Materials-Flow Benchmark Sector Report: Beneficial Use of Secondary Materials - Coal Combustion Products". 530-R-08-003.

United States Geological Survey. (2007) "Ground-Water Recharge in Humid Areas of the United States - A Summary of Ground-Water Resources Program Studies, 2003-2006". USGS FS-2007-3007.

United States National Weather Service, Forecast Office. http://www5.ncdc.noaa.gov/climatenormals/clim60/states/Clim_MN_01.pdf. Data retrieved on 2009-05-03.

Witczak, M.W. (1997) “Harmonized Test Methods for Laboratory Determination of Resilient Modulus for Flexible Pavement Design” National Council Highway Research Program Report 1-28A Report, Transportation Research Board of National Academies, Washington, D.C.

Witczak et al., (2004), “Laboratory Determination of Resilient Modulus for Flexible Pavement Design,” National Cooperative Highway Research Program (NCHRP) 1-28A, Research Results Digest, No. 285, Washington D.C., January 2004.

Washington State Department of Transportation (WSDOT), (2005), “WSDOT Pavement Policy.” P17. Olympia, WA.

Wisconsin Department of Transportation (WisDOT), (2011), “Facilities Development Manual: Pavement,” Madison, WI, http://roadwaystandards.dot.wi.gov/standards/fdm/14-00toc.pdf, accessed March 27, 2011

Zwick, T C., Van, V P., Tolle, D A, Arthur, M F. (1984) “Effects of Fly Ash on Microbial CO2 Evolution from an Agricultural Soil.” Water Air & Soil Pollution. 22 (2), 209.

APPENDIX A: PHOTOGRAPHS

Figure A-1: Preparing indentation in sub-base for lysimeter geomembrane.

Figure A-2: Preparing drainage pipe from lysimeter to collection tank.

Figure A-3: Installing geomembrane for lysimeter.

Figure A-4: Welding geomembrane to lysimeter drainage pipe assembly.

Figure A-5: Preparing hole for leachate collection tank and trench for drainage pipe.

Figure A-6: Assembling leachate collection tank.

Figure A-7: Installing leachate collection tank.

Figure A-8: Installing leachate collection tank.

Figure A-9: Collecting lysimeter leachate using submersible pump.

Figure A-10: Column leach test on MnROAD materials.

Figure A-11: Water leach test rotator.

Figure A-12: MnROAD water leach test samples immediately after rotation.

APPENDIX B: LYSIMETER LEACHATE CHEMICAL CONCENTRATIONS

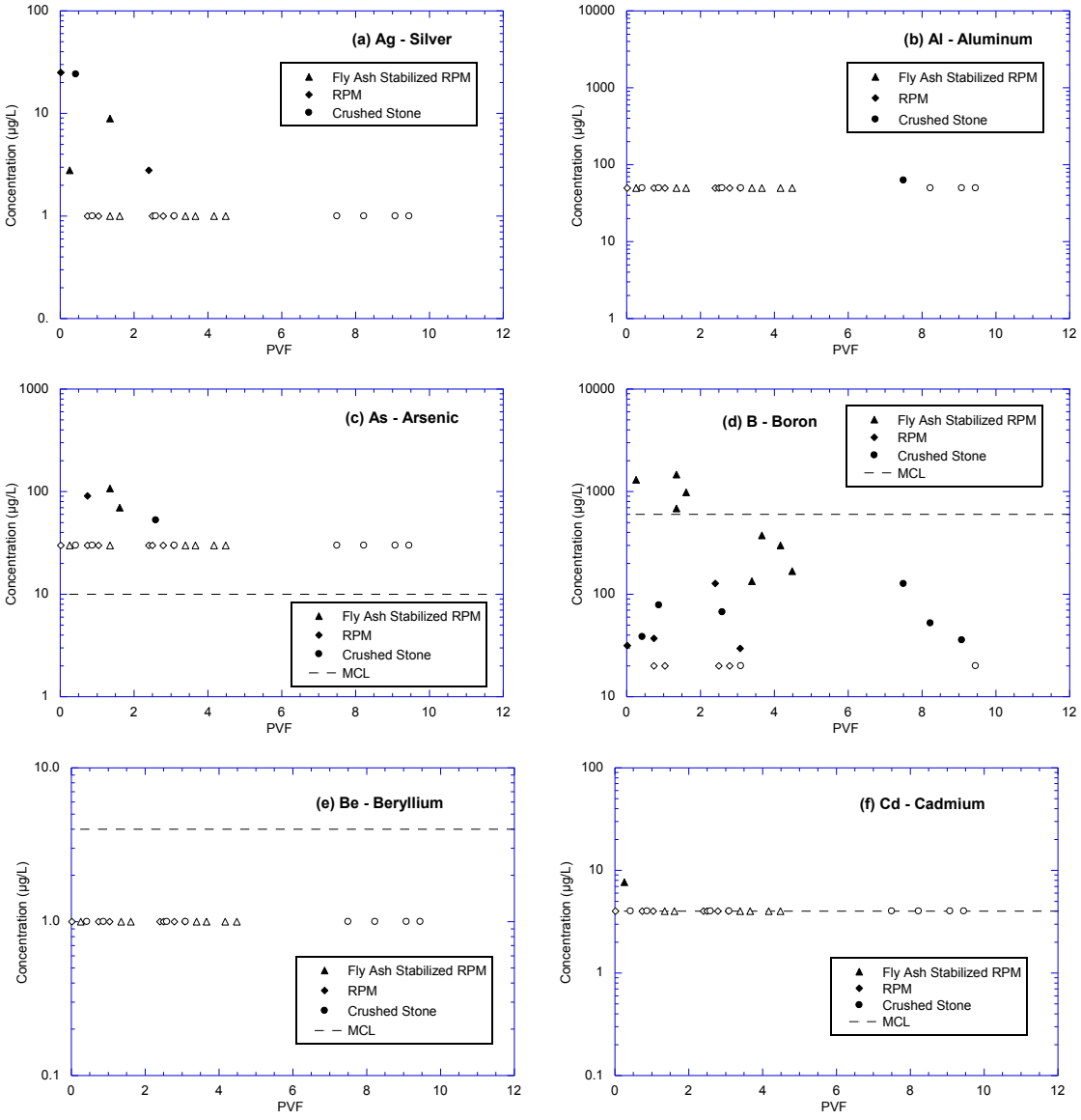

Figure B-1: (a) Silver, (b) Aluminum, (c) Arsenic, (d) Boron, (e) Beryllium, and (f) Cadmium concentrations in leachate from field lysimeters. Concentrations below minimum detection limits are plotted at the limit, and represented with an open symbol.

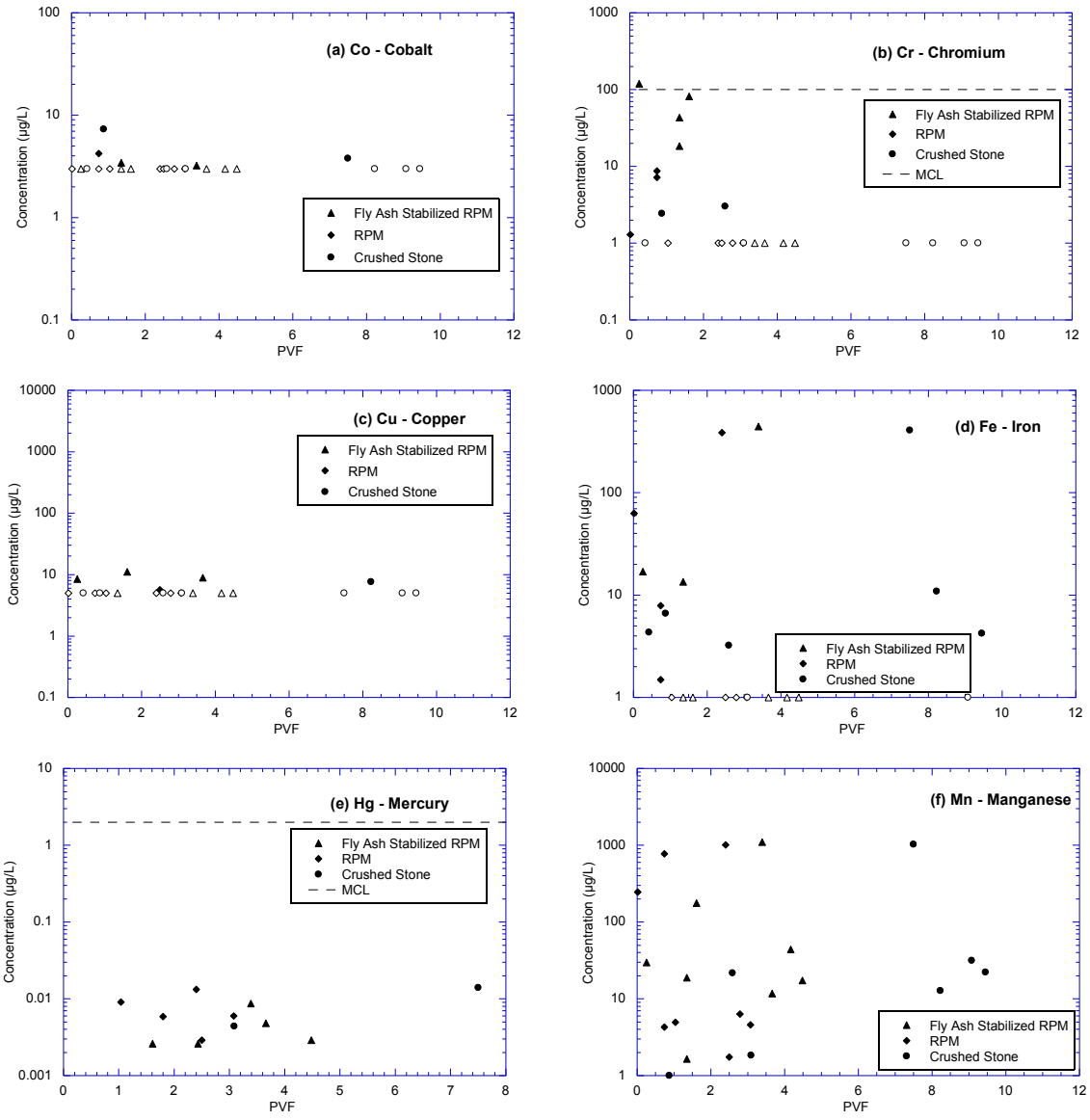

Figure B-2: (a) Cobalt, (b) Chromium, (c) Copper, (d) Iron, (e) Mercury, and (f) Manganese concentrations in leachate from field lysimeters. Concentrations below minimum detection limits are plotted at the limit, and represented with an open symbol.

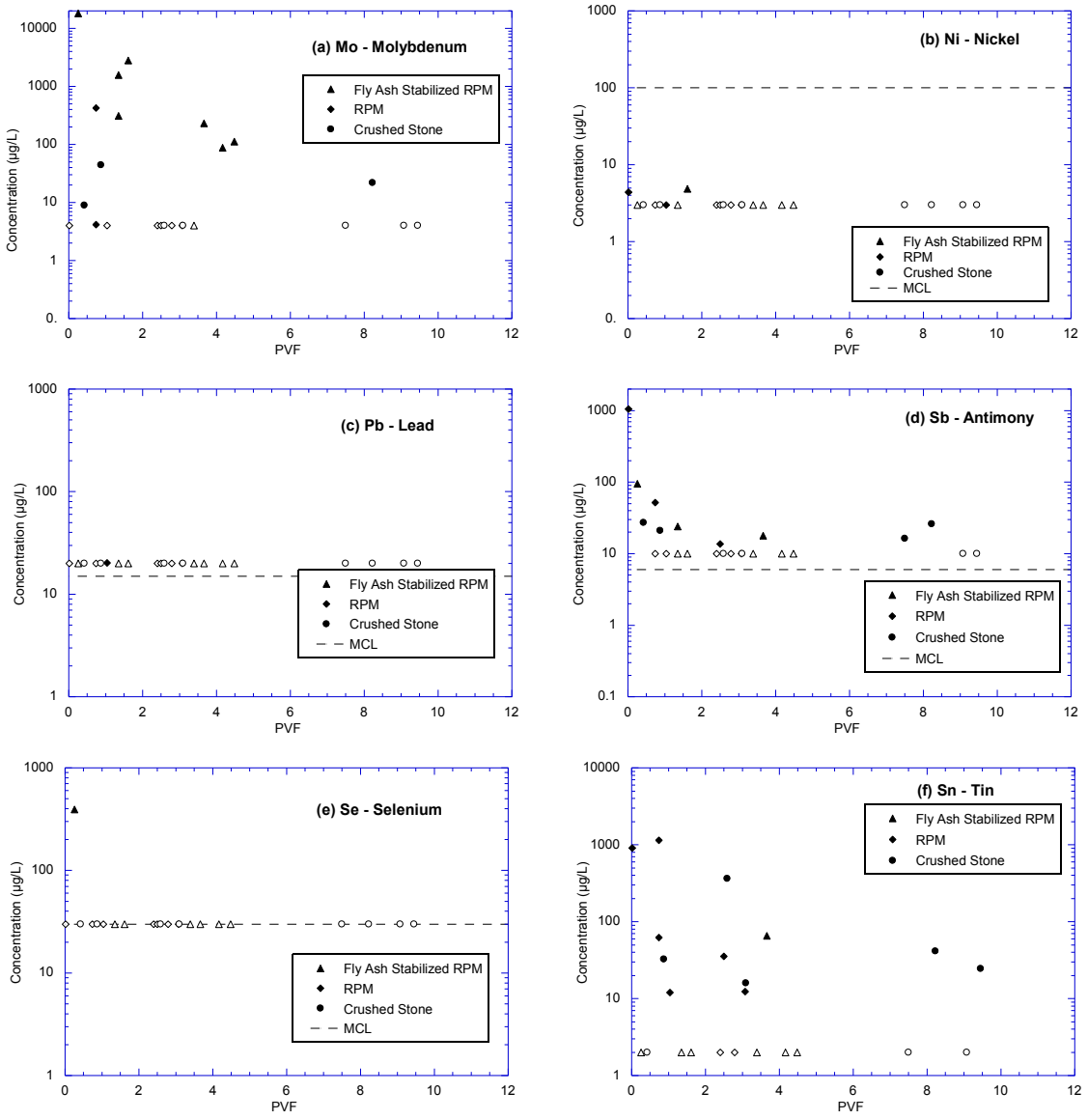

Figure B-3: (a) Molybdenum, (b) Nickel, (c) Lead, (d) Antimony, (e) Selenium, and (f) Tin concentrations in leachate from field lysimeters. Concentrations below minimum detection limits are plotted at the limit, and represented with an open symbol.

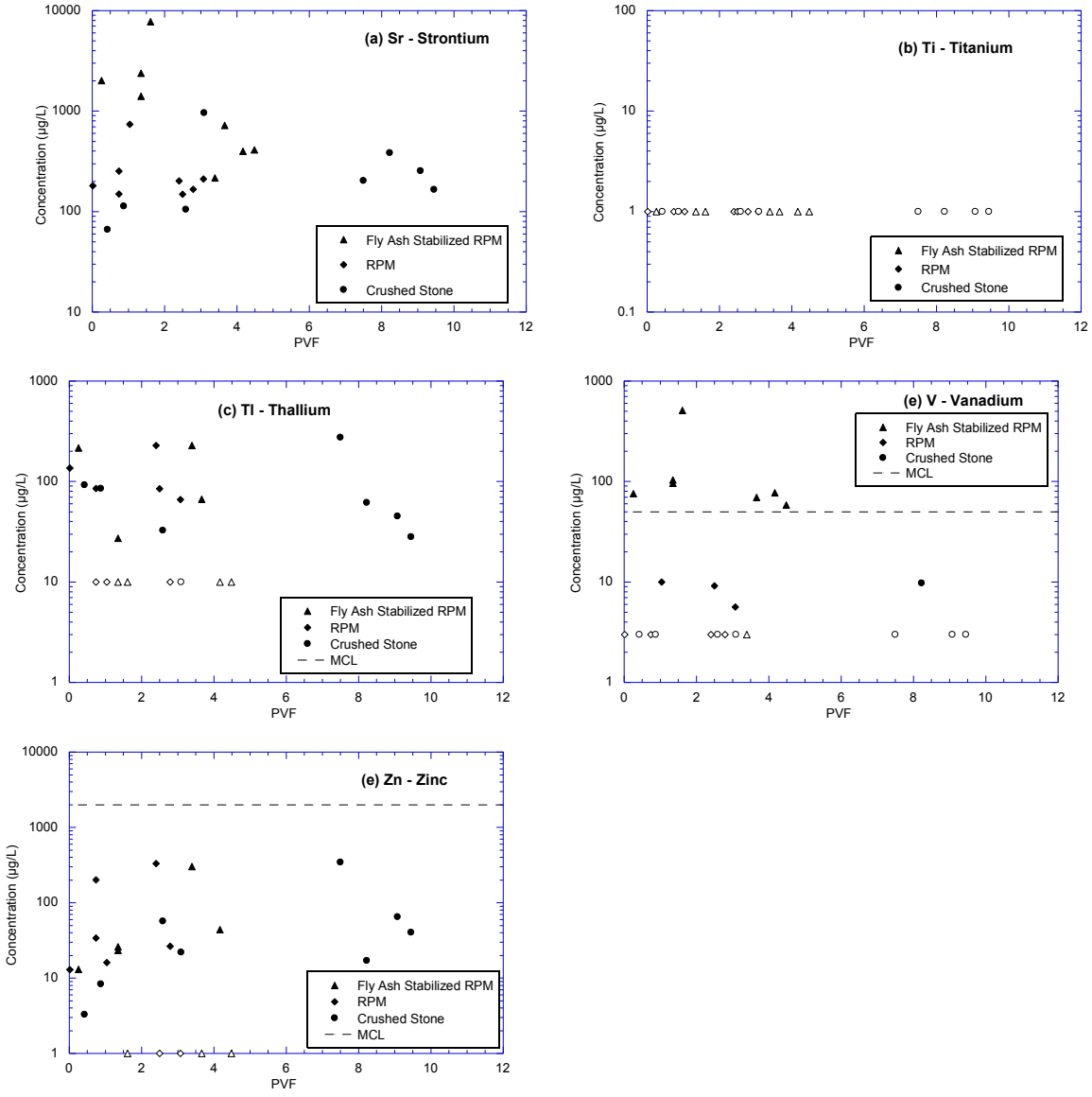

Figure B-4: (a) Strontium, (b) Titanium, (c) Thallium, (d) Vanadium, and (e) Zinc concentrations in leachate from field lysimeters. Concentrations below minimum detection limits are plotted at the limit, and represented with an open symbol.

APPENDIX C: LABORATORY CHEMICAL CONCENTRATIONS

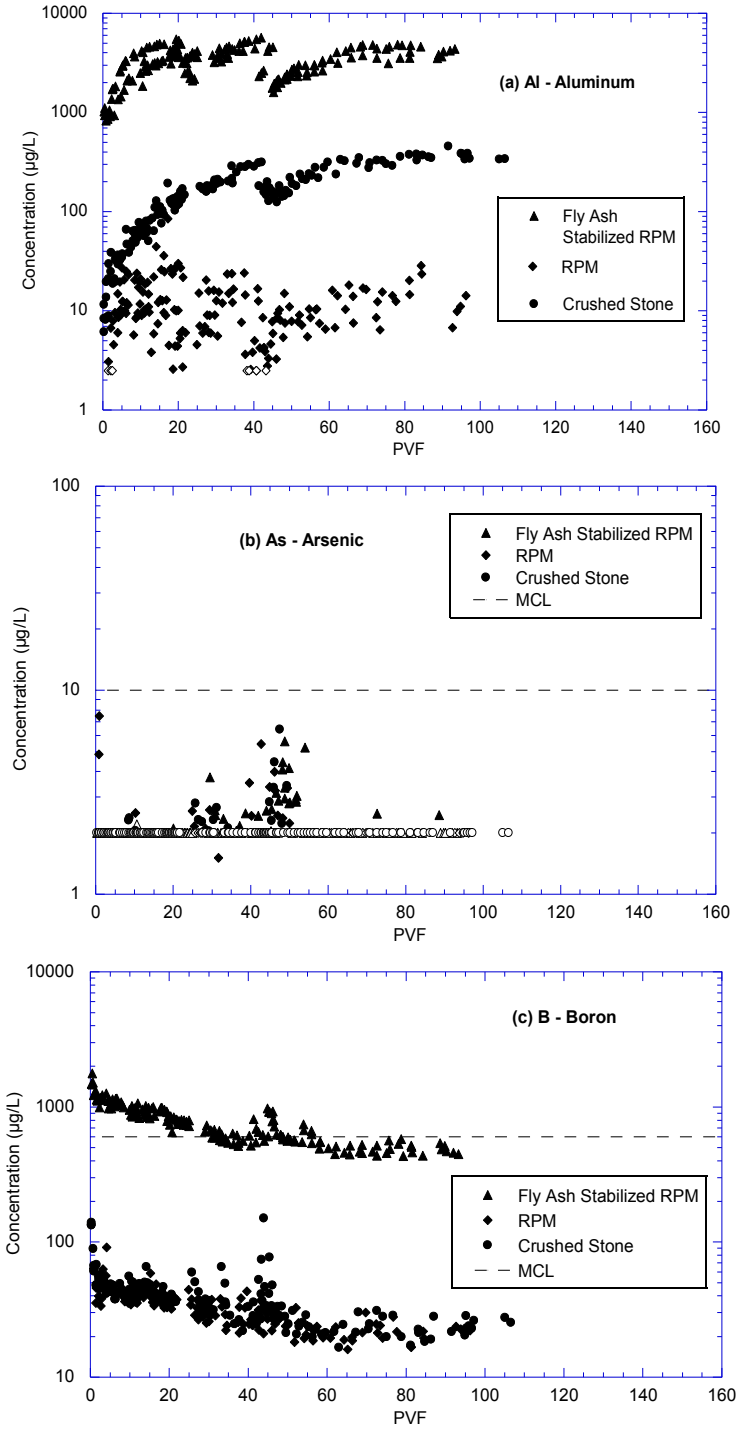

Figure C-1: (a) Aluminum, (b) Arsenic, and (c) Boron concentrations in leachate from column leach tests (CLTs). Concentrations below minimum detection limits are plotted at the limit, and represented with an open symbol. Tests stopped and restarted at approximately 45 PVF.

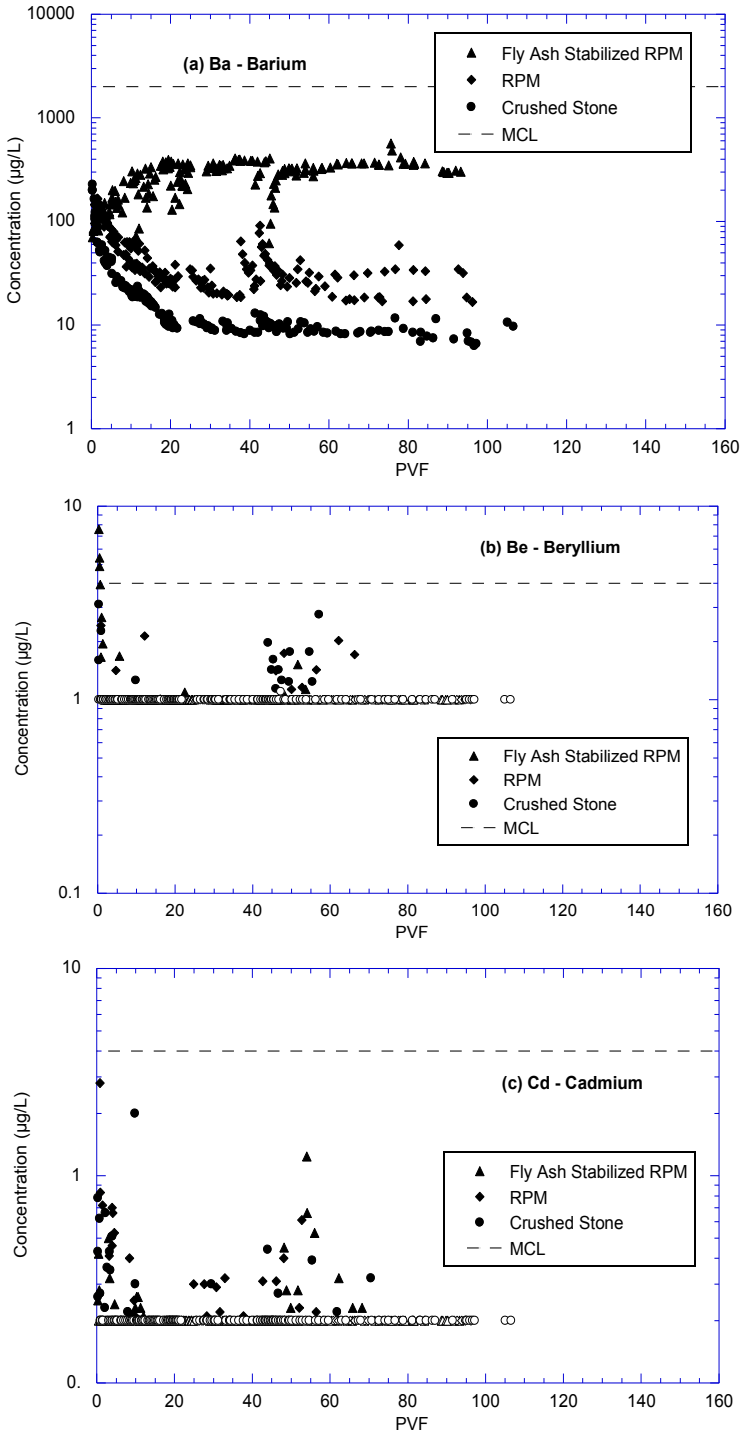

Figure C-2: (a) Barium, (b) Beryllium, and (c) Cadmium concentrations in leachate from column leach tests (CLTs). Concentrations below minimum detection limits are plotted at the limit, and represented with an open symbol. Tests stopped and restarted at approximately 45 PVF.

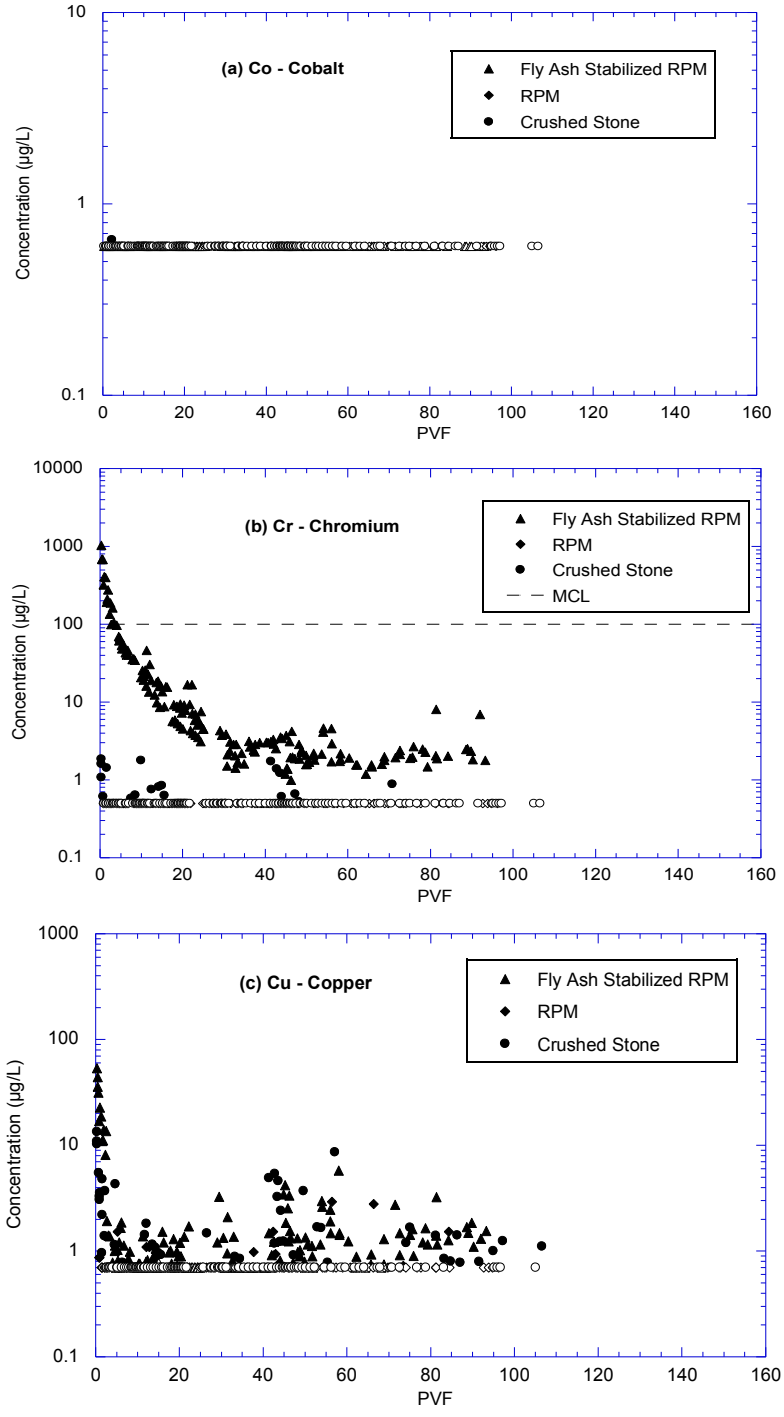

Figure C-3:(a) Cobalt, (b) Chromium, and (c) Copper concentrations in leachate from column leach tests (CLTs). Concentrations below minimum detection limits are plotted at the limit, and represented with an open symbol. Tests stopped and restarted at approximately 45 PVF.

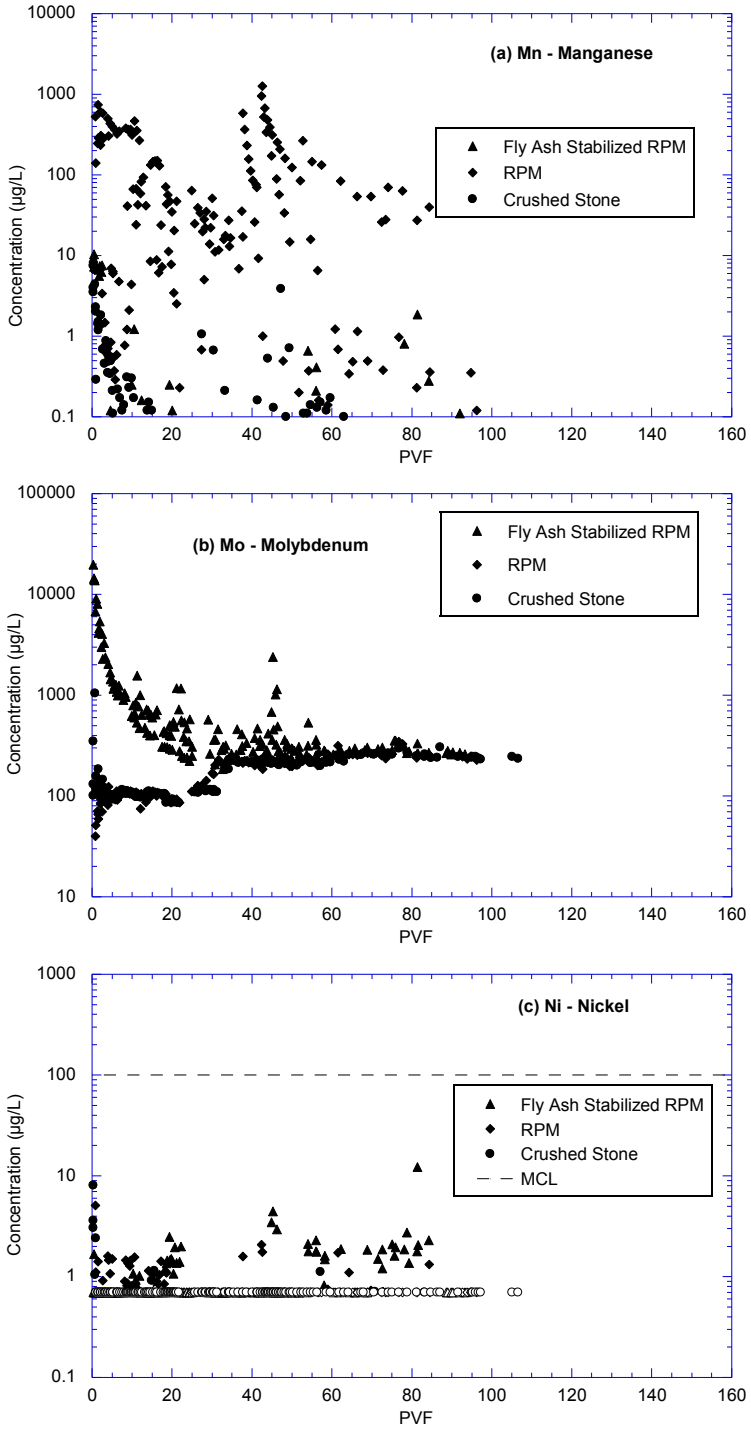

Figure C-4: (a) Manganese, (b) Molybdenum, and (c) Nickel concentrations in leachate from column leach tests (CLTs). Concentrations below minimum detection limits are plotted at the limit, and represented with an open symbol. Tests stopped and restarted at approximately 45 PVF.

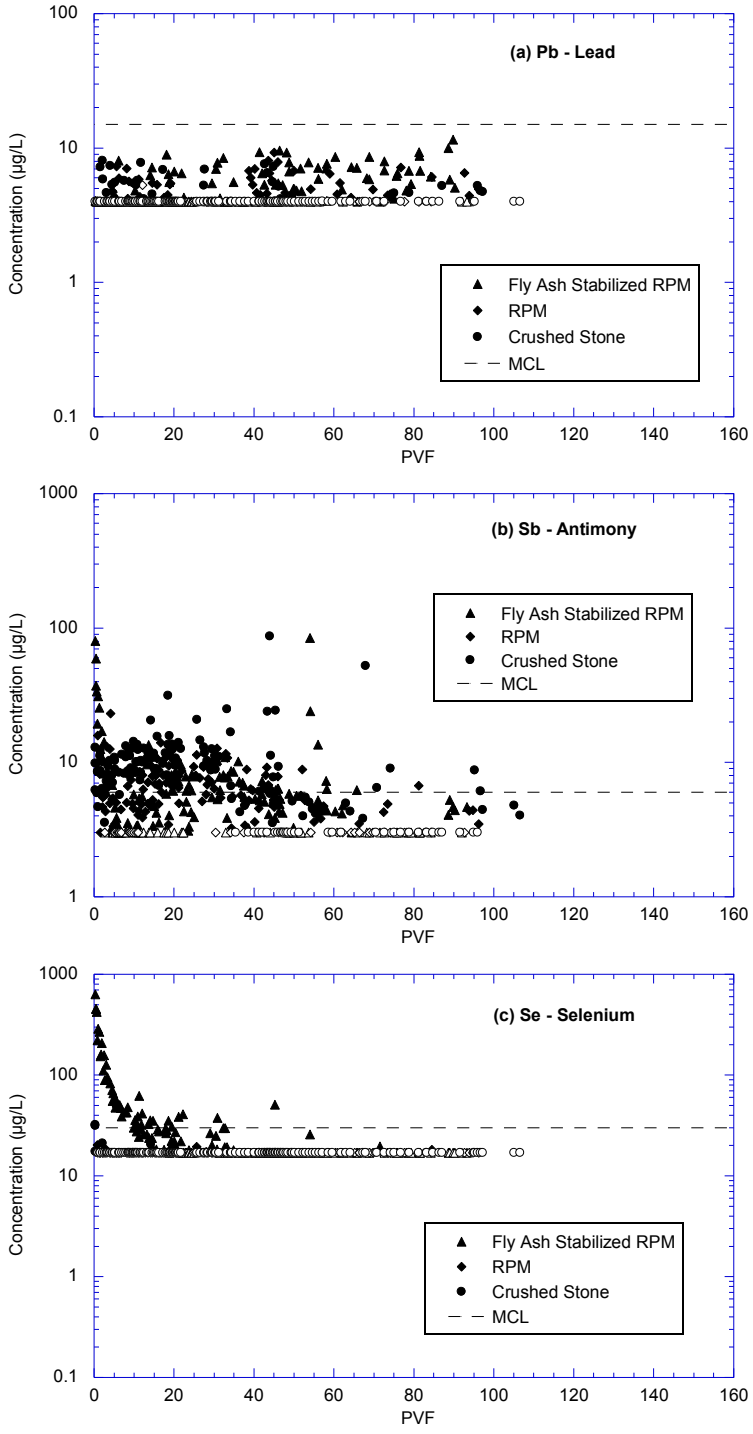

Figure C-5: (a) Lead, (b) Antimony, and (c) Selenium concentrations in leachate from column leach tests (CLTs). Concentrations below minimum detection limits are plotted at the limit, and represented with an open symbol. Tests stopped and restarted at approximately 45 PVF.

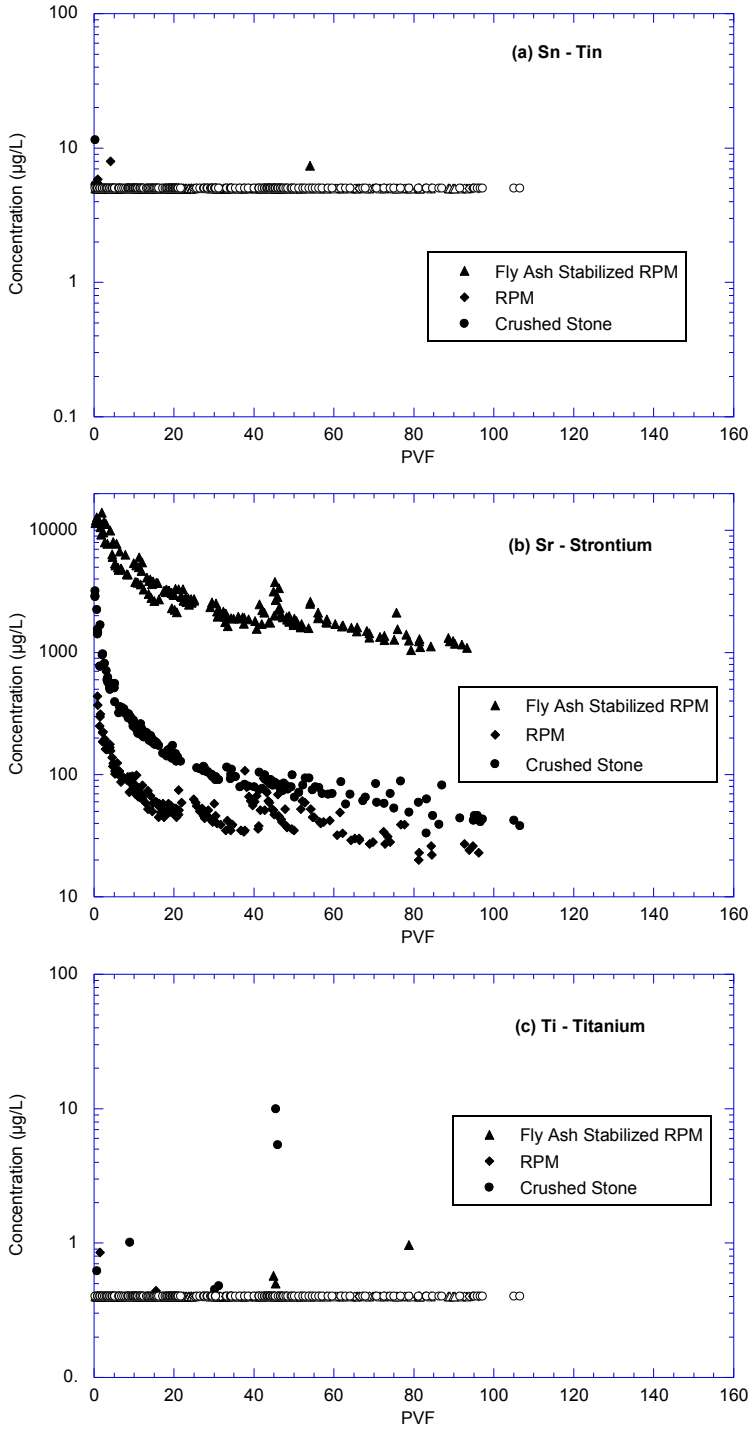

Figure C-6: (a) Tin, (b) Strontium, and (c) Titanium concentrations in leachate from column leach tests (CLTs). Concentrations below minimum detection limits are plotted at the limit, and represented with an open symbol. Tests stopped and restarted at approximately 45 PVF.

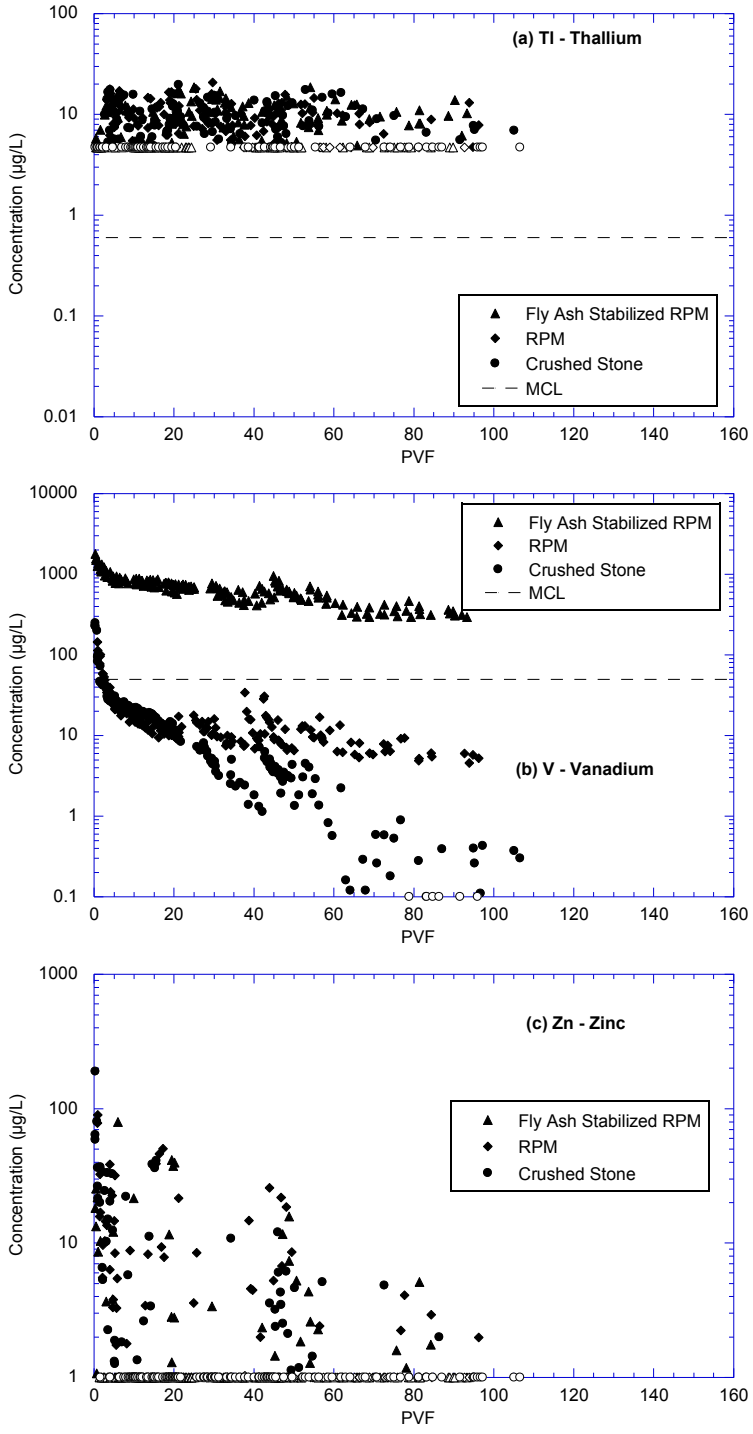

Figure C-7: (a) Thallium, (b) Vanadium, and (c) Zinc concentrations in leachate from column leach tests (CLTs). Concentrations below minimum detection limits are plotted at the limit, and represented with an open symbol. Tests stopped and restarted at approximately 45 PVF.

Table C-1: MnROAD Water Leach Test Results

Sample	Ag	Al	As	B	Be	Cd	Co	Cr	Cu	Fe	Mn	Mo
Material and L:S Ratio	ppb	ppb	ppb	ppb	ppb	ppb	ppb	ppb	ppb	ppb	ppb	ppb
Crushed Stone - 3:1	3	56.6	<30	<20	<1	<4	<3	<1	<5	230.2	2.7	<4
Crushed Stone - 5:1	<1	128.4	<30	<20	<1	<4	<3	1.1	<5	207.4	1.7	<4
Crushed Stone - 10:1	3	167.2	<30	<20	<1	<4	<3	<1	<5	52.8	0.5	<4
Crushed Stone - 20:1	<1	61.9	<30	<20	<1	<4	<3	<1	<5	<1	<1	<4
RPM - 3:1	<1	<50	<30	<20	<1	<4	<3	<1	<5	<1	2.2	<4
RPM - 5:1	<1	<50	50	<20	<1	<4	<3	1.9	<5	<1	0.6	<4
RPM - 10:1	<1	<50	<30	<20	<1	<4	<3	<1	<5	<1	5.5	<4
RPM - 20:1	<1	<50	<30	<20	<1	<4	<3	<1	<5	14.3	10.1	<4
Fly-ash-stabilized RPM - 3:1	<1	554.9	110	755.7	<1	<4	<3	127.0	6.6	<1	<1	2127.5
Fly-ash-stabilized RPM - 5:1	<1	1263.6	70	739.8	<1	<4	<3	98.4	6.6	<1	<1	1574.8
Fly-ash-stabilized RPM - 10:1	<1	3395.1	40	608.1	<1	<4	<3	42.9	<5	<1	<1	581.3
Fly-ash-stabilized RPM - 20:1	<1	7667.8	40	557.8	<1	<4	<3	20.5	<5	<1	<1	134.3

Sample	Ni	Pb	Sb	Se	Sn	Sr	Ti	Tl	V	Zn	pH
ID	ppb	ppb	ppb	ppb	ppb	ppb	ppb	ppb	ppb	ppb	
Crushed Stone - 3:1	<3	<20	<10	<30	<5	24	<1	<10	<3	5.7	7.9
Crushed Stone - 5:1	<3	24.4	<10	<30	<5	24	<1	<10	<3	5.3	7.6
Crushed Stone - 10:1	<3	<20	<10	<30	26	24	<1	<10	<3	3.2	6.9
Crushed Stone - 20:1	<3	<20	<10	<30	<5	21	<1	<10	<3	5.1	7.2
RPM - 3:1	<3	<20	<10	<30	<5	41	<1	<10	<3	3.0	7.3
RPM - 5:1	<3	<20	<10	<30	14	31	<1	<10	<3	5.9	7.2
RPM - 10:1	<3	<20	<10	<30	<5	22	<1	<10	<3	11.8	7.0
RPM - 20:1	<3	<20	<10	<30	<5	15	<1	<10	<3	44.7	7.0
Fly-ash-stabilized RPM - 3:1	5.9	<20	<10	<30	<5	10258	<1	<10	990	2.8	11.3
Fly-ash-stabilized RPM - 5:1	<3	37.8	<10	<30	<5	8293	<1	<10	900	1.1	11.2
Fly-ash-stabilized RPM - 10:1	<3	<20	<10	<30	<5	4566	<1	<10	590	1.6	10.8
Fly-ash-stabilized RPM - 20:1	<3	<20	<10	<30	<5	2978	<1	<10	410	2.6	10.4

APPENDIX D: STATE REGULATIONS REGARDING FLY ASH USE

Table D-1: Fly ash regulatory status in US states

State	Haz. Waste Status	Status	Use in PCC Specifically Authorized	Road/Soil Use Specifically Authorized	If No, Use Possible on case by case basis?
Alabama	Exempt	Special Waste	No	No	Yes
Alaska	Exempt	Indust. Solid or Inert	No	No	Yes, with TCLP and metals, meet requirements
Arizona	Exempt	None	No	No	No
Arkansas	Exempt	Recovered Materials	No	No	Yes, if not "disposal"
California	NOT Exempt	Haz. Waste unless proven not by TCLP	No	No	No
Colorado	Exempt	None	No	No	No
Connecticut	Exempt	Special or Regulated	No	No	Yes
Delaware	Exempt	Nonhaz. Indust.	No	No	Yes, TCLP required
Florida	Exempt	Solid or Indust. Byproduct	Yes	No	Yes
Georgia	Exempt	Indust. Solid	No	No	No
Hawaii	Exempt	None	No	No	Yes, with metals
Idaho	Exempt	Indust. Solid	No	No	No
Illinois	Exempt	CCW or CCB	Yes	Yes	-
Indiana	Exempt	Indust. Solid	Yes	Yes	-
Iowa	Exempt	None	Yes	Yes	-
Kansas	Exempt	Indust. Solid	No	No	No
Kentucky	Exempt	Special	Yes	Yes	-
Louisiana	Exempt	Indust. Solid	No	No	Yes

State	Haz. Waste Status	Status	Use in PCC Specifically Authorized	Road/Soil Use Specifically Authorized	If No, Use Possible on case by case basis?
Maine	Exempt	Haz. Waste unless proven not	Yes	No	No
Maryland	Exempt	Pozzolan	No	Yes	-
Massachusetts	Exempt	Solid unless beneficial reuse	Yes	Yes	-
Michigan	Exempt	Low Hazard Indust.	Yes	Yes	-
Minnesota	Exempt	None	No	No	Yes
Mississippi	Exempt	Indust. Solid	No	No	Yes
Missouri	Exempt	None	Yes	No	Yes
Montana	Exempt	Indust. Solid	Yes	No	Yes
Nebraska	Exempt	Special	Yes	Yes	-
Nevada	Exempt	None	No	No	No
New Hampshire	Exempt	waste derived product	Yes	Yes	-
New Jersey	Exempt	Solid unless beneficial reuse	Yes	Yes	-
New Mexico	Exempt	Indust. Solid	No	No	Yes
New York	Exempt	None	Yes	Yes	-
North Carolina	Exempt	None	Yes	Yes	-
North Dakota	Exempt	None	No	No	Yes
Ohio	Exempt	None	Yes	Yes	-
Oklahoma	Exempt	None	Yes	Yes	-
Oregon	Exempt	None	No	No	No
Pennsylvania	Exempt	None	Yes	Yes	-
Rhode Island	NOT Exempt	Haz. Waste unless proven not by TCLP	No	No	No
South	Exempt	Indust.	No	No	Yes

State	Haz. Waste Status	Status	Use in PCC Specifically Authorized	Road/Soil Use Specifically Authorized	If No, Use Possible on case by case basis?
Carolina		Solid			
South Dakota	Exempt	Solid or Indust. Byproduct	No	No	Yes
Tennessee	NOT Exempt	Haz. Waste unless proven not by TCLP	Yes	No	No
Texas	Exempt	Indust. Solid	Yes	Yes	-
Utah	Exempt	None	Yes	Yes	-
Vermont	Exempt	None	No	No	No
Virginia	Exempt	None	Yes	Yes	-
Washington	NOT Exempt	Haz. Waste unless proven not by TCLP	No	No	No
West Virginia	Exempt	None	Yes	Yes	-
Wisconsin	Exempt	Indust. Byproduct	Yes	Yes	-
Wyoming	Exempt	Indust. Solid	No	No	No